DEVELOPING AND DEPLOYING ENHANCED ALGORITHMS TO ENABLE OPERATIONAL STABILITY CONTROL SYSTEMS WITH EMBEDDED HIGH VOLTAGE DC LINKS

A thesis submitted for the degree of Doctor of Philosophy

by

Ronak Rabbani

Supervisor: Prof Gareth Taylor

Brunel Institute of Power Systems

Department of Electronic and Computer Engineering

College of Engineering, Design and Physical Sciences

Brunel University London

September 2015

Abstract

The increasing penetration of renewable energy resources within the Great Britain (GB) transmission system has created much greater variability of power flows within the transmission network. Consequently, modern transmission networks are presented with an ever increasing range of operating conditions. As a result, decision making in the Electricity National Control Centre (ENCC) of the GB electrical power transmission system is becoming more complex and control room actions are required for reducing timescales in the future so as to enable optimum operation of the system. To maximise utilisation of the electricity transmission system there is a requirement for fast transient and dynamic stability control. In this regard, GB electrical power transmissions system reinforcement using new technology, such as High Voltage Direct Current (HVDC) links and Thyristor-Controlled Series Compensation (TCSC), is planned to come into operation. The research aim of this PhD thesis is to fully investigate the effects of HVDC lines on power system small-disturbance stability in the presence of operational uncertainties.

The main research outcome is the comprehensive probabilistic assessment of the stability improvements that can be achieved through the use of supplementary damping control when applied to HVDC systems. In this thesis, two control schemes for small-signal dynamic stability enhancement of an embedded HVDC link are proposed: Modal Linear Quadratic Gaussian (MLQG) controller and Model Predictive Controller (MPC). Following these studies, probabilistic methodologies are developed in order to test of the robustness of HVDC based damping controllers, which involves using classification techniques to identify possible mitigation options for power system operators. The Monte Carlo (MC) and Point Estimated Method (PEM) are developed in order to identify the statistical distributions of critical modes of a power system in the presence of uncertainties. In addition, eigenvalue sensitivity analysis is devised and demonstrated to ensure accurate results when the PEM is used with test systems. Finally, the concepts and techniques introduced in the thesis are combined to investigate robustness for the widely adopted MLQG controller and the recently introduced MPC, which are designed as the supplementary controls of an embedded HVDC link for damping inter-area oscillations. Power system controllers are designed using a linearised model of the system and tuned for a nominal operating point. The assumption is made that the system will be operating within an acceptable proximity range of its nominal operating condition and that the uncertainty created by changes within each operating point can possibly have an adverse effect on the controller's performance.

Acknowledgements

Firstly I would like to express my gratitude to Prof Gareth A. Taylor for providing the opportunity to undertake this research project and for his guidance and encouragement throughout the past 4 years. I would also like to thank Dr Ahmed Zobaa for help and support. In addition I would like to express my sincerest appreciation to Dr Mohsen Mohammadi Alamuti for his valuable support and help.

And finally I would like to express my deepest gratitude to my parents, for their patience, encouragement and their support. Without their generosity, I may never have been able to survive and complete my study.

Declaration of Authorship

The work detailed in this thesis has not been previously submitted for a degree in this University or at any other and unless otherwise referenced it is the author's **own** work.

Contents

Figures

Tables

List of Abbreviations

AC	Alternating Current
ARE	Algebraic Riccati Equation
AVR	Automatic Voltage Regulator
CPU	Central Processing Unit
DC	Direct Current
FACTS	Flexible AC Transmission System
GPS	Global Positioning System
HVDC	High Voltage Direct Current
IEEE	Institute of Electrical and Electronic Engineers
IGBT	Insulated gate bipolar transistor
LCC	line commutated converter
LDS	Low Discrepancy Sequences
LMI	Linear Matrix Inequality
LQG	Linear Quadratic Gaussian
LQR	Linear Quadratic Regulator
LTR	Loop Transfer Recovery
MC	Monte Carlo
MIM	Multiple-Input-Multiple-Output
MISO	Multiple-Input-Single-Output
MLQG	Modal Linear Quadratic Gaussian
MPC	Modal Predictive Controller
MTDC	Multi-Terminal Direct Current
NGET	National Grid Electricity Transmission plc
ODIS	Offshore Development Information Statement
OPF	Optimal Power Flow
PC	Personal Computer
PDC	Phasor Data Concentrator
PDF	Probability Density Function
PEM	Point Estimated Method
PI	Proportional-Integral (Control)
PLF	Probabilistic Load Flow
PMU	Phasor Measurement Unit
POD	Power Oscillation Damping
PSS	Power System Stabiliser
PV	Power–Voltage
SISO	Single-Input-Single-Output
SSR	Sub-Synchronous Resonance
SVC	Static Var Compensator
TCSC	Thyristor Controlled Series Capacitor
TGR	Transient Gain Reduction
TPE	Two Point Estimate
UK	United Kingdom
USA	United States of America
VDCOL	Voltage Dependent Current Order Limiter
VSC	Voltage Source Converter

WAC	Wide Area Controller
WAMS	Wide Area Measurement System

List of Symbols

α	Firing angle
β	Inverter angle
Γ	Set of uncertain system parameters
γ	Extinction angle/Uncertain system parameter
δ	Generator rotor angle
ε	Error
ς	Modal damping ratio
θ	Voltage angle
λ	Complex eigenvalue
μ	Mean
σ	Modal damping (real part)/Standard deviation
τ	Signal transmission delay
φ	Power angle/Weibull scale parameter
ψ	Generator flux linkage/Left eigenvector
ω	Speed/Modal frequency (imaginary part)
Φ	Right eigenvector
a	Recursive coefficient
b	Recursive coefficient
c	Calculation constant
k	Weibull shape parameter
m	Number of power system inputs
n	Converter transformer turns ratio/Number of/Power system order
p	Number of power system outputs
r	Rank index
t	Time
u	Controller output signal (power system input)
x	System state
y	Controller input signal (power system output)
z	Modal system state
B	Susceptance
C	Capacitance
D	Generator damping constant
E	Voltage
G	Active power output from a generator
H	Generator inertia constant
I	Current
K	Controller gain
L	Inductance/Active power demand at a load
P	Active power
R	Resistance/system transfer function residue
T	Time constant
V	Voltage

X	Reactance
Y	Admittance
Z	Impedance

Subscripts

0	Initial values/equilibrium point
1, 2, 3, 4	Various controller constants
1d	Effective *d*-axis (mathematically defined parameter)
2q	Effective *q*-axis (mathematically defined parameter)
c	Complex eigenvalue pairs
comp	Compensation
conv	HVDC converter
d-axis	Machine reference frame
dc	DC system parameter
e	Generator electrical output
eq	Equivalent
ex	Excitation system
f	Excitation field
i	Index value, where i =1, 2, 3…
inv	Inverter
j	Index value, where *j* =1, 2, 3…
lk	Leakage
m	Generator mechanical input
marg	Margin
o	Open-circuit
q-axis	Machine reference frame
r	Generator rotor/real eigenvalues
rect	Rectifier
s	Generator stator
syn	Synchronous
t	Generator terminal
A, B, C, E	Various controller constants
C	Shunt capacitor (load flow)/commutating
D-axis	System reference frame
G	Generation (load flow)
I	Integral
N	Number of buses within a power system
P	Proportional
POD	Power oscillation damping controller
PSS	Power system stabiliser
Q Q-axis	System reference frame
R	Transducer delay
W	Washout

Superscripts

$\dot{}$	Derivative
$\hat{}$	Estimate
$'$	***T***ransient
$''$	Sub-transient
conv	HVDC converter
ex	Excitation system
inv	Inverter
load	Load
max	Maximum limit
min	Minimum limit
rect	Rectifier
red	Reduced
ref	Reference set-point
sys	AC power system
Idc	DC current
MLQG	Modal linear quadratic Gaussian controller
Pdc	DC active power injection
Qdc	DC reactive power injection
T	Matrix transpose
TGR	Transient gain reduction
Tx	Transformer
Vdc	DC voltage
VSC	Voltage source converter

Chapter 1

Introduction

In order to reach the EU and UK governments' targets for the decarbonisation of greenhouse gas emissions, reinforcement of Great Britain's power electricity system will be required involving some significant changes [1]. In particular, following this reinforcement, a large capacity of wind generation will have a major effect on the future operation of the GB transmission system. Consequently, there will be a requirement for additional transmission capacity to be deployed within the existing AC transmission system. Hence, more transmission technologies, such as embedded HVDC links and series compensation, will be introduced into the GB transmission system in future [2]. The flexibility and controllability of these FACTS devices will provide further benefits with respect to power system operations, including power system stability.

On the other hand, increasing the capacity of wind generation and transferring electrical power across long distances will increase the level of stress in the power system operating conditions [3], which could easily lead to the onset of stability problems. Among the stability issues in large interconnected power systems, lightly damped inter-area oscillations play the most important roll [3].

This research has been carried out in order to gain a greater understanding of the performance of embedded High Voltage Direct Current (HVDC) systems, aimed at the improvement of system stability and also greater effectiveness of the control systems in maintaining power system stability.

1.1 The GB Transmission System

The legally binding target to reduce greenhouse gas emissions is at least 80% below the 1990 level by 2050 [2] and the UK Government is dedicated to meeting it. In order to

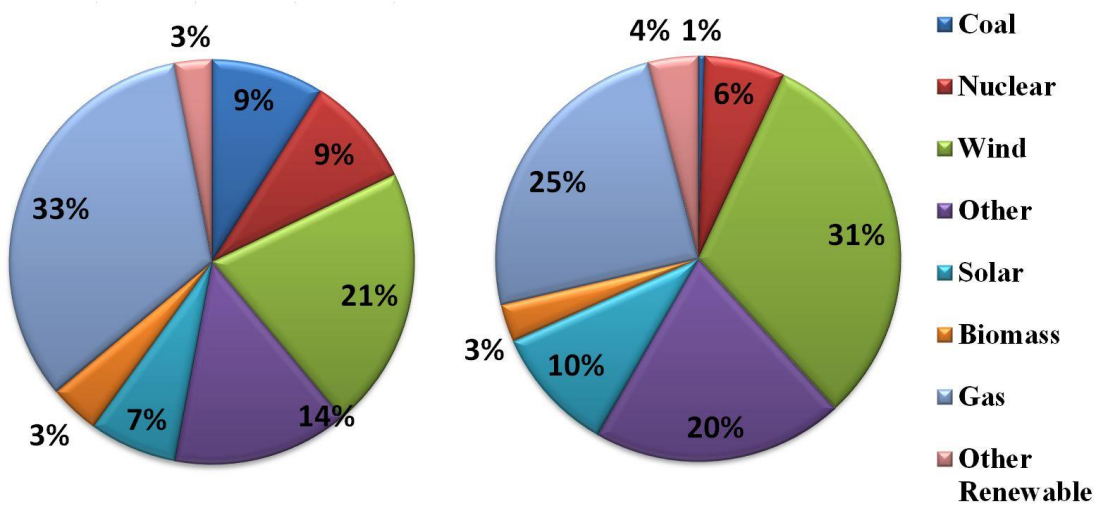

Figure 1.1 UK Energy Targets 2020 (left) and 2030 (right) [186]

do so, the government has committed itself to ensuring that 15% of the UK's energy demand will be produced by renewable sources by 2020 [2]. It is expected that wind generation will significantly increase and reach approximately 20 GW by 2020, moving up to 59.2 GW by 2035 [2], [3]. The impact of this target on the future generation mix in the UK can be seen in Figure 1.1. Also the impact of this scenario on the generation mix up to 2035 can be seen in Figure 1.2.

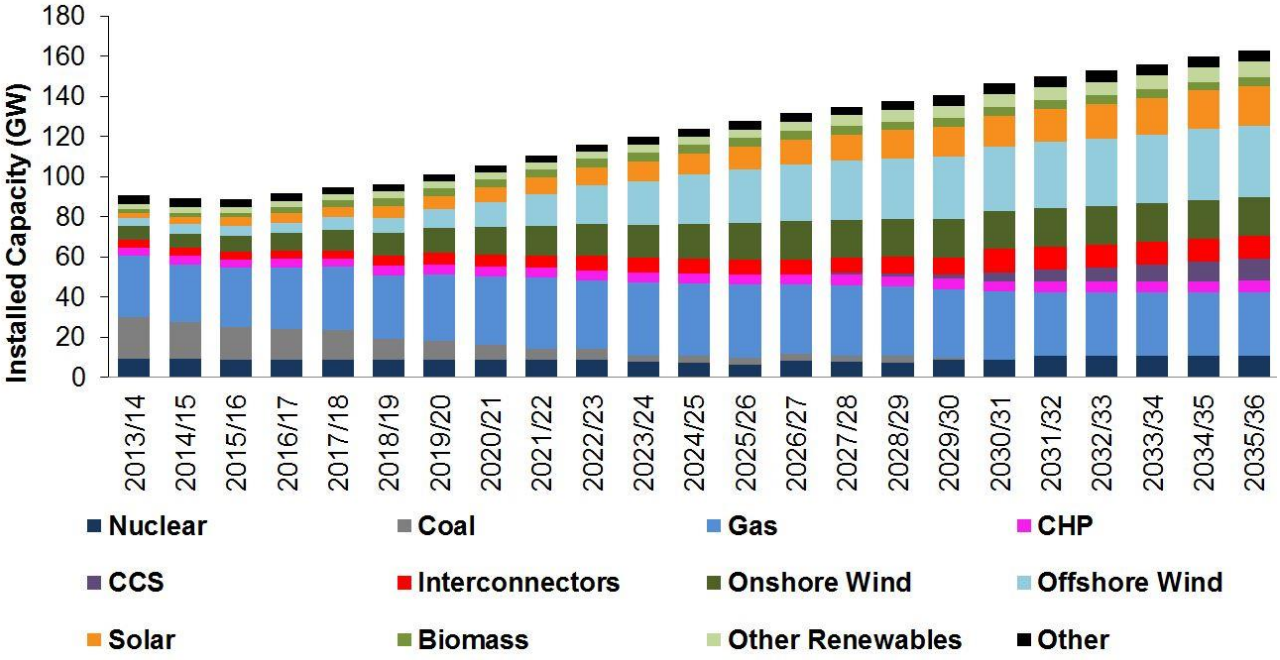

Figure 1.2 Gone Green Generation Background [186]

In order to increase the capacity of the GB transmission system, the electricity transmission network in GB (England and Wales) is connected to the Scottish Power Transmission network through two double 400 kV AC circuits. Also, there are HVDC interconnections to France, the Netherlands, Northern Ireland and Ireland [1].

Figure 1.3 summarises the proposed locations of the TCSC and the new HVDC link, which is the prototype of the GB future electric power transmission network (vision 2020/2030) [4, 5].

In this system, the majority of generation is in the North with the largest demand centre being in the South East. Consequently, this will lead to a significant increase in the power transfer capability requirement across the Anglo-Scottish boundary (B6 boundary) and make this boundary the main area of concern in terms of stability of the

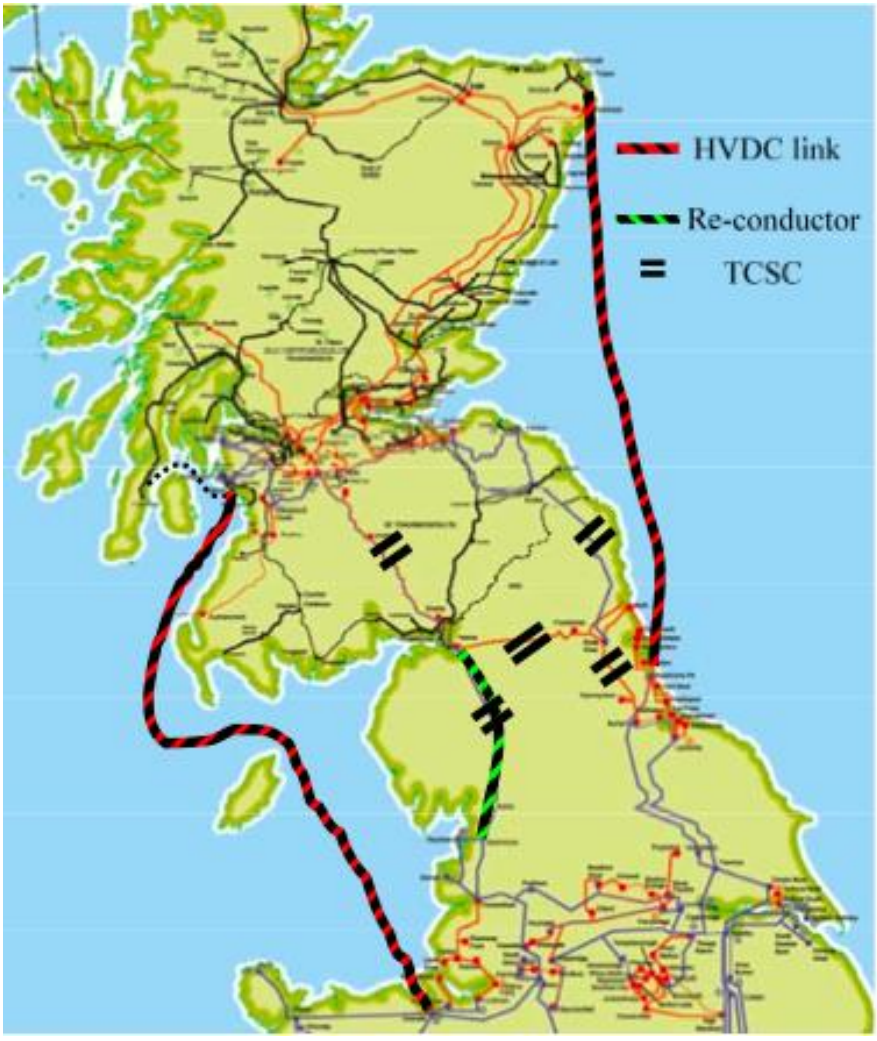

Figure 1.3 New TCSC and HVDC in the GB Transmission System [5]

system [1, 2]. The existing inter-area mode between the generators in Scotland and those of England & Wales has been identified at around 0.5 Hz [1], [6]

In increasing volumes of renewable generation and providing more connectivity between England and Scotland, the ability to manage this boundary effectively will become ever more important [1].

1.2 Power System Stability

Power system stability has been known to be an important issue for secure systems operation since the 1920s [7], [8] . Many major blackouts owing to power system instability have proved the salience of this phenomenon [7], [9].

Power system stability refers to the capability of an electrical power system to maintain stable operation during normal conditions. Also, it is necessary to have the capability to return to a suitable stable operating point with an acceptable time after disturbances have happened [10] , [11]. A large sized power system has greater risk of being subjected to large disturbances than smaller ones. These can be faults, load changes, generator outages, line outages, voltage collapse or some combination of these and the system must be capable of responding to them without failure. Under such circumstances, the remaining power system equipment should resume stable operation quickly, which is achieved by the operation of protection devices to remove the faulty component from the network [10].

Power system stability issues can be generally classified as follows [10], [11] :

- ***Rotor Angle Stability:*** the capability of the interconnected generators within the power system being at the same frequency in order to maintain synchronous operation;
- ***Voltage Stability:*** the capability of keeping acceptable voltages at all system buses [10];
- ***Frequency Stability:*** the capability of a power system to maintain steady frequency following a severe disturbance between generation and load.

It should be noted that rotor angle, voltage and frequency stability are not independent isolated events. For instance, a voltage collapse at a bus is going to lead to large trips in rotor angle and frequency. Likewise, a large frequency deviation is going to lead to large changes in voltage magnitude [11].

Each of these three stabilities can be further classified into large or small disturbances, i.e. short term or long term [11].

1.2.1 Power System Oscillations

Electro-mechanical oscillations between interconnected synchronous generators are phenomena characteristic to power systems. Generally, in a stable system, if the rotor of one machine deviates from its synchronous speed, the distribution of power generation will act to reduce this deviation [10], [12], which is associated with the remaining generators and the installed system controllers [10], [12]. In this circumstance, the retuning of the system to equilibrium is going to lead to mechanical oscillations. The effect of these can be seen as variations in the electrical output of the machine in terms of electrical power and voltage [10]. The stability of these oscillations is of fundamental concern and must be damped effectively so as to maintain secure and stable system operation.

The capability of synchronous machines of an interconnected power system to remain synchronised following small changes (small disturbances) is known as small signal stability (or small-disturbance). On the other hand, transient (or large disturbance) stability analysis is concerned with the response of the power system after large transient disturbances. The time scales can range from milliseconds (small disturbance) to a few seconds at most (large disturbance) [10], [11].

The work presented in this thesis is mainly focussed on large-disturbance stability analysis of power systems through investigating the time-varying performance of the network in the presence of HVDC links and controllers.

Electromechanical oscillations for power systems have varying reasons and these oscillatory modes can be classified as follows [10], [11].

- ***Torsional Mode***s: the frequency for these modes is between 5 and 50 Hz. These are associated with oscillations, which are caused by the rotational components in the turbine-generator shaft system [10].
- ***Control Modes:*** typically the frequency of these modes is less than 0.1 Hz. These are added to the system by installing the controllers within it.
- ***Local Modes:*** the frequency for these modes is between 1 and 2.5 Hz. These are associated with the swinging of one generator against the rest of power system.

- ***Inter-Area Modes:*** the frequency for these modes is between 0.1 and 1 Hz. These are generated when many machines within an area of the power system are oscillating against those in other areas of the network.

If any of these oscillatory modes mentioned above become unstable then this will lead to rising oscillations and finally, the disconnection of equipment or further cascading failures. Moreover, inter-area modes are traditionally harder to damp to compared with local ones [10] and hence, the former type in the power system provide the focus for this thesis.

1.2.2 Wide Area Measurement Systems

Wide Area Measurement Systems (WAMS) have the ability to collect data from various points. This ability provides greater observability of any inter-area oscillations within large interconnected system. In recent years, the development of WAMS has been very useful with regards to the design of complex controllers, which provide damping of critical inter-area modes [10]. With these measurement systems for collecting time-stamped data, the Phasor Measurement Units (PMUs) employed can significantly improve the damping of inter-area oscillations [10],[13],[14].

Phasor Measurement Units (PMU) are able to measure three phase voltages, magnitude and phase of currents as well as calculate time synchronised positive-sequence values. These calculations should be at rates equivalent to the power systems fundamental frequency, which is 50 Hz in the GB system. These accurate measurements make it possible to monitor the wide area snapshot of the power system in real-time and also, to track dynamic changes on the grid [1].

1.3 Overview of HVDC Development and Technologies

The classical application of an HVDC system is the transmission of bulk power with lower overall transmission cost and losses over long distances compared with the AC transmission lines. In fact, this system has emerged as the best power delivery solution in a number of situations [15], [16]. The main advantage of transferring the power with HVDC links is that the stability constraints associated with stability problems or control strategies, will not lead to limitations in the amounts of transmitted power on HVDC lines and the transmission and this constrains will be removed by interconnecting systems via HVDC lines [15], [16]. Another advantage of using HVDC links that

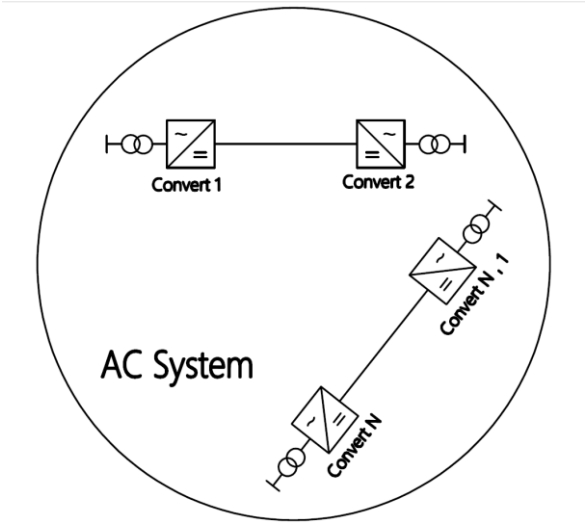

Figure 1.4 Embedded HVDC Technology in an AC Grid

should be mentioned is that this system, compared with conventional AC transmission, provides a higher degree of controllability for the operation of power systems [15], [16]. Recently, installation of HVDC links in the power system has been increasing at a pace. The installed capacity of HVDC after 47 years had become 50 GW by 2001 (first commercial installation was in 1954), with just in nine years later, in 2010, it having doubled to 100 GW and it has been planned to double again by 2016 (200 GW) [10], [17].

1.3.1 HVDC Development

An HVDC link connected between two AC systems operates regardless of the voltage and frequency conditions of the two systems. Therefore, it provides an independent control for transmitting power between systems. The same applies for an HVDC link within one AC system. HVDC technology can resolve a large number of existing AC power system steady-state and dynamic instability issues and improve the security of the system. The two systems (AC and DC) can be linked together in three configurations:embedded HVDC link, HVDC grid and DC segmentation [15].

- **Embedded HVDC System in an AC Grid**

In the first configuration, an embedded HVDC system in an AC grid, one or multiple point-to-point HVDC links are connected to the AC system buses in a single AC grid. In this configuration, the point-to-point HVDC links are used for the bulk transmission

of electrical power in a single AC grid [15]. The schematic diagram of an embedded HVDC link is shown in Figure 1.4.

Currently, The the Xiangjiaba–Shanghai is longest embedded HVDC link in the world is with 2,071 km (1,287 mi), ±800 kV, 6400 MW link connecting the Xiangjiaba Dam to Shanghai, in the People's Republic of China [15]. The longest embedded HVDC link will be the Rio Madeira link in Brazil connecting Porto Velho in the state of Rondônia to the São Paulo area. The length of this DC line will be 2,375 km (1,476 mi) [15], [17].

- **HVDC Grid**

The next configuration, which will be presented in this section, is the HVDC grid. In this configuration several AC buses are interconnected within converter stations, which are the points for sharing a common DC transmission system [15], [16]. Another approach for the combination of HVDC transmission with an AC system is the meshed HVDC grid. This configuration includes multiple DC converters that are interconnected by a meshed DC transmission network. The advantage of using this approach is that if one HVDC line is lost, another will support the partially isolated node [15].

Figure 1.5 and Figure 1.6 show a schematic diagram of a meshed HVDC grid and one

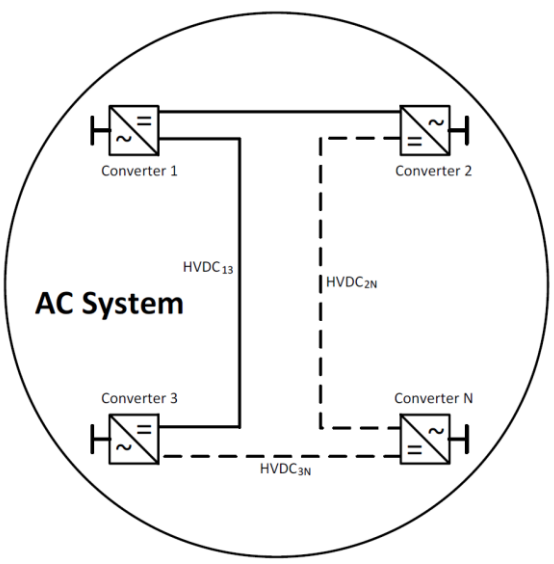

Figure 1.5 Meshed DC Grid

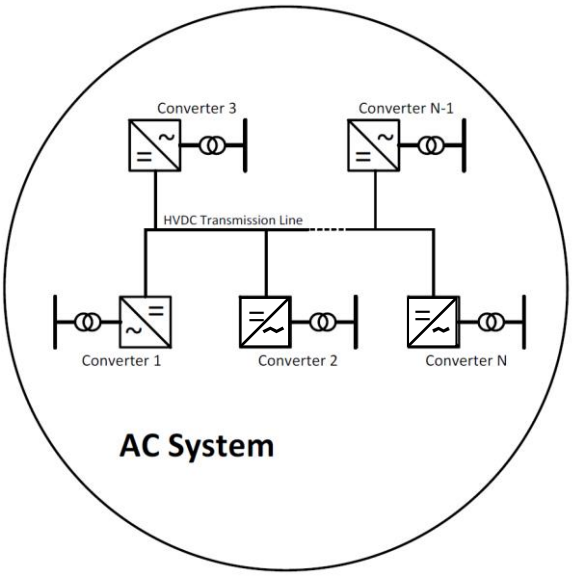

Figure 1.6 MTDC Technology

of an MTDC grid, respectively. Both line-commutated current-sourced converter (LCC) and VSC technologies can be employed in an MTDC configuration, which makes it a special type of the HVDC grid [15], [16].

- **DC segmentation**

In the third configuration, the AC grid is decomposed into sets of asynchronously operated AC segments connected through DC links [15], [18], [19] .

Figure 1.7, shows the concept of DC-segmentation. The DC links can be back-to-back (BTB) and/or PTP HVDC links [15], [19] , based on VSC and/or LCC technologies. The segments can have AC line connections as well, but these should not constitute major power corridors [15]. The size of each AC segment can be defined as a compromise between the converter cost, potential gain in reliability and power transfer capability improvement, geographical and political boundaries as well as the system operational characteristics and necessities [15] , [20].

1.3.2 HVDC Technology

There are two converter technologies available for use in HVDC transmission [10]:

- ***LCC-HVDC (Line Commutated Converter):*** LCC-HVDC was the first practical HVDC conversion technology that was developed [10] and also it is the most commonly used HVDC scheme in commercial operation today [21]. This has been seen as a great technological development, mainly in terms of its switching

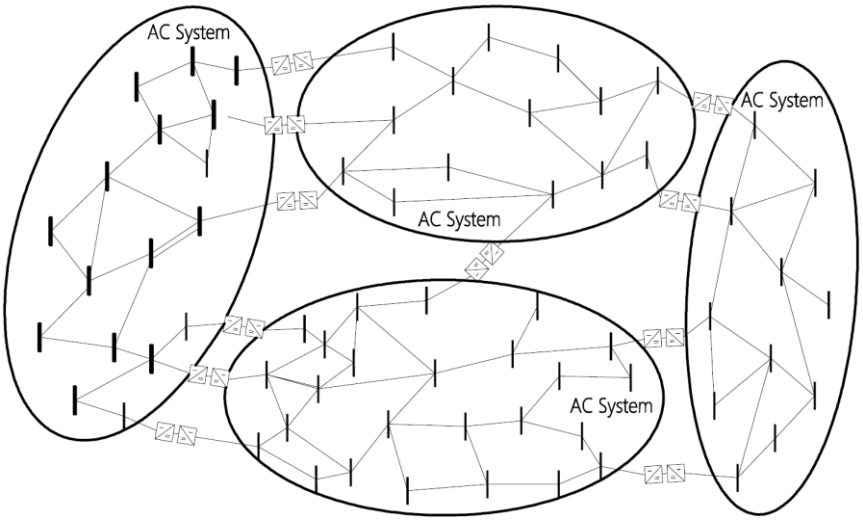

Figure 1.7 DC-Segmentation Technology

components and control systems. The thyristors that are used in LCC-HVDC technology are in a Current Source Converter (CSC) topology and when the current through a thyristor is zero it will switch off. In LCC-HVDC the current always lags the voltage due to the delayed firing of the thyristors and consequently, the LCC HVDC link absorbs the reactive power. This technology is practicable for long distance transmission and large amounts of electric power at very high voltages [21], [22].

- ***VSC-HVDC (Voltage Source Converter):*** Voltage Source Converters (VSC-HVDC) have been a known technology on an industrial basis for many years at a lower voltage scale. The VSC scheme uses Insulated Gate Bipolar Transistors (IGBT). At each power frequency cycle, IGBTs can be switched on and off several times by an external signal. For this technology, the reactive power is controlled autonomously and reactive compensation is not needed, which makes VSC-HVDC more controllable than LCC-HVDC. Also, this technology does not have inverter commutation failures and limited injection of low-order harmonic currents [21], [23]. Nevertheless, due to the numerous switching operations in VSC-HVDC, the losses in the converter are higher compared to LCC, which is a serious disadvantage in bulk power transmission and hence, makes it economically less interesting [21] . Another disadvantage of this technology is that VSC-HVDC cannot operate at the same power levels as the more mature LCC-HVDC [10].

1.4 Research Aim and Objectives

As aforementioned, to decarbonise UK electricity supply an unprecedented amount of change is required to the GB transmission system. Large volumes of various renewable generations that have been mentioned above are because of impact on the transmission network before 2020 [1]. To accommodate this, technologies currently unfamiliar to the GB system are being planned, including offshore embedded HVDC links and TCSC on the circuits of the prominent constraint boundary.

Majority of these changes will also be needed regarding the operational control procedures in order to secure such future transmission networks, especially in terms of stability and frequency constraints. All of these changes are becoming strongly dependent on increased information pertaining to the state of the power system [1].

This thesis aims to address many of the issues that have been identified within the current body of research. The main aim of this research are to undertake a thorough evaluation of the improvement in power system small-disturbance stability that HVDC based POD control can achieve, and to use probabilistic methods to produce a supplementary WAMS-based POD controller, which is more robust to the uncertainties inherent in modern power systems. In order to achieve this aim, the following research objectives have been defined:

1. To investigate thoroughly a suitable WAMS-based supplementary POD controller design for HVDC systems within meshed AC/DC power systems. Two control schemes have been proposed to achieve the main objective of this thesis aimed at improving the system stability by damping the oscillations.

2. To develop a methodology for probabilistically evaluating the robustness of WAMS-based supplementary POD controllers for HVDC systems with respect to uncertain power system conditions.

3. To develop appropriate measures that allow for the application of PEM for critical mode estimation within test system, which will result in fast and accurate calculation of system risk indices, such as the probability of instability.

1.5 Research Methodology

In order to achieve the aforementioned thesis objective, the following methodology is employed:

- Power system modelling for two test systems,
- Power system linearization for modal analysis using controllability, observability and participation factor for test system,
- Stability analysis using probabilistic small disturbance stability assessment. Two methods are used, Monte Carlo Method and Point Estimated method.
- Implementation of linearized state space model of the nonlinear system (using interfacing between DIgSILENT and MATLAB),
- Design linear control schemes for the linearized system model (using the developed MATLAB platform) and design a control scheme based on the sensitivity of the system stability margin with respect to the parameter space,
- Perform time-domain simulation: DIgSILENT/PowerFactory environment is used to evaluate the agreement between the corresponding dynamic responses of the automatically generated linearized model and the nonlinear model to small disturbances and validate the accuracy of the linearized model. The performance of the proposed control schemes (MLQG and MPC) and the dynamic behaviour of the system, including the proposed controllers, under various faults and disturbances are investigated through time domain simulations.

1.6 Main Contributions of this Research

The work in this thesis contributes to a number of areas of power systems research, specifically regarding the effects of HVDC systems on the small-disturbance stability of transmission networks. The main consequence of this research is the comprehensive probabilistic assessment of the improvement to power system small-disturbance stability that can be achieved through the use of supplementary damping control applied to HVDC systems. Assessment of the robustness of these controllers has shown the controller synthesis procedure, thus resulting in improved system performance in the presence of operational uncertainties.

To achieve the main objective of this thesis, this research work focuses on:

- Developing a small-signal dynamic model. This model has been developed based on computer-assisted linearization of AC/DC systems for control design,

time-domain simulation and also the systematic performance has been evaluated for the control scheme (The developed model can be applied for various control designs and the application of this model is not limited to the controllers designed which have been used in this thesis).

- Developing an HVDC supplementary control scheme, using a small signal dynamic model of the system. These supplementary controllers are developed to damp inter-area oscillations in an AC/DC system.
- The development of a methodology to test probabilistically the robustness of HVDC based damping controllers, using classification techniques to identify possible mitigation options for power system operators.
- The Point Estimated Method (PEM) and Monte Carlo (MC) have been developed for use in a power system to identify the statistical distributions of critical electromechanical modes in power systems in the presence of multiple operational uncertainties.
- The use of a probabilistic system representation is proposed for improving POD controller performance, yielding more robust performance when considering the effects of system uncertainties. The use of the Monte Carlo Method to establish the probabilistic system demonstration results in a rapid and robust assessment of HVDC based damping controllers.
- Developing a reduced model of the GB transmission system within a PSACD/EMTDC platform. The performance of the developed system was compared and confirmed with the DIgSILENT model, which was developed by the National Grid.

1.7 List of Publications

The work detailed in this thesis has resulted in number of refereed publications, as follows:

1.7.1 Journal Publications

1. Mohsen M. Alamuti, Ronak Rabbani, Shadi Khaleghi, Ahmen F. Zobaa and Gareth A. Taylor “Probabilistic Evaluation of Power System Stability Enhancement Using Supplementary Controller Schemes for an Embedded HVDC link “ Submitted to *IEEE Transactions on Power System, 2015.*

1.7.2 Conference Publications

- **First Author**

1. Rabbani, R.; Alamuti, M.M.; Taylor, G.A."Investigating SVC impact at the inverter side of HVDC links for Stability Analysis of the Future Great Britain Transmission System" Power System Technology (POWERCON), 2014 International Conference, China.
2. Rabbani, R.; Mohammadi, M.; Kerahroudi, S.K.; Zobaa, A.F.; Taylor, G.A." Modelling of reduced GB transmission system in PSCAD/EMTDC", International Universities' Power Engineering Conference, UPEC 2014, Cluj-Napoca, Romania.
3. Rabbani, R.; Taylor, G.A. and Zobaa, A.F., "Performance Comparison of SVC with POD and Synchronous Generator Excitation System to Investigate Oscillation Damping Control on the GB Transmission System" 48th International Universities' Power Engineering Conference, UPEC 2013, 2-5 September 2013, DIT, Dublin, Ireland.
4. Rabbani, R., Taylor, G.A. and Zobaa, A.F., "Applications of Simplified Models to Investigate Oscillation Damping Control on the GB Transmission System " The 10th International Conference on AC and DC Power Transmission (IET), ACDC 2012, 4-6 December 2012, Birmingham, UK.
5. Rabbani, R., Taylor, G.A. and Zobaa, A.F. "Critical Evaluation of Reduced Models for Stability Analysis on the GB Transmission System" 47th International Universities' Power Engineering Conference, UPEC 2012, 4-7 September 2012, Brunel University, London, UK.

- **Co-Author**

1- Alamuti, M.M.; Rabbani, R.; Kerahroudi, S.K.; Taylor, G.; Youbo Liu; Junyong Liu" A critical evaluation of the application of HVDC supplementary control for system stability improvement" Power System Technology (POWERCON), 2014 International Conference

2- Kerahroudi, S.K.; Li, F.; Bradley, M.E.; Ma, Z.; Alamuti.M.M.; Rabbani, R.; Abbod, M.; Taylor, G.A. "Critical evaluation of power system stability enhancement in the future GB transmission using an embedded HVDC link" AC

and DC Power Transmission (ACDC 2015), 11th IET International Conference on , vol., no., pp.1,6, 4-5 Feb. 2015

3- Kerahroudi, S.K.; Rabbani, R.; Fan Li; Taylor, G.; Alamuti, M.M.; Bradley, M. "Power system stability enhancement of the future GB transmission system using HVDC link", UPEC 2014, Cluj-Napoca, Romania.
4- Alamuti, M.M.; Rabbani, R.; Kerahroudi, S.K.; Taylor, G.A. "System stability improvement through HVDC supplementary Model Predictive Control", UPEC 2014, Cluj-Napoca, Romania.

1.8 Thesis Overview

Chapter2: Literature Review

This chapter provides past research on GB transmission system modelling of damping of power oscillations. Over the years, many studies have been carried out on stability analysis of power systems, controller designs and modelling of the GB system. These studies have been shown to be effective at damping power oscillations with various technologies, although very few have been implemented in real systems. Almost all studies are listed in this chapter.

Chapter 3: Power System Modelling and Analysis

This chapter briefly describes models of the main components of electrical power systems, which include synchronous generators, AVR and governors for generators' transmission lines, transformers and system loads. Also In this chapter, a reduced GB system model is presented, which is based upon a future GB transmission system model and, hence, contains different types and mix of generation. This model is also based on the reduced DIgSILENT PowerFactory model developed by the National Grid and has been designed in PSCDA/EMTDC. However, the aim of this chapter is to compare PSCAD with the more widespread simulator, DIgSILENT PowerFactory.

Chapter 4: Probabilistic Small-Disturbance Stability Assessment

In this chapter, in order to analyse power system stability and design the controllers, linearization of a power system is described mathematically in a modal analysis section. This concept is described by defining parameters, including: eigenvalues, eigenvectors, participation factors, modal controllability observability and residues. Throughout this

thesis, all modelling has been designed using the DIgSILENT PowerFactory environment (version 15).

In addition this chapter presents the MC and PEM for probabilistic small-disturbance analysis. The latter significantly reduces the number of simulations needed to complete a probabilistic system assessment, whilst still accurately producing the statistical distributions of critical system modes has been saved. The method is established on a test network where it is presented to produce the statistical distributions of critical modes precisely. Following this, techniques for a reduction in the number of considered uncertainties based on eigenvalue sensitivity are proven.

Chapter 5: Damping Controller Design

The majority of power system simulation packages do not provide a model of the system in a mathematical format to the users. Since a model of the system has to be available for MPC and LQG controller design, in this chapter, the application of a system identification method to obtain an equivalent model of the system is examined. For the next step, in order to design the damping controllers, application of the POD controller designs that have been used in this thesis is provided. Also in this chapter, signal selection, system identification and order reduction are presented, which require investigation before designing the controller. The two controllers used in this thesis are modal linear quadratic Gaussian control (MLQG) and modal predictive control (MPC).

Chapter 6: Application of Designed Controllers on a Test System

This chapter evaluates an approach for damping inter-area oscillations of power systems using HVDC supplementary control. The proposed supplementary controller is based on the model predictive control (MPC) scheme. To enhance the damping of inter-area oscillations in power systems, this research has designed and implemented an MPC scheme as an HVDC supplementary controller for improving AC system stability. The chapter also compares the performance of MPC with other HVDC supplementary controller strategies for improving AC system stability, such as modal linear quadratic Gaussian (MLQG) and state feedback (SF). These three approaches are tested on a two area four machine system incorporating parallel HVDC/AC transmission. The study results show the effective and superior performance of MPC for damping the oscillatory modes of the test system. Following this, a methodology for the robust probabilistic evaluation of damping controller performance is investigated. This method considers

the statistical uncertainty in system operating conditions based on the variability of loading and generation.

Chapter 7: Conclusion and Futures Work

In this final chapter a summary is provided on the work presented in this thesis outlining the specific contributions. In addition, proposals for future work are made.

Chapter 2

Literature Review

2.1 Introduction

Currently, the reliability of the electric power system in Great Britain is generally good. However, over the next few years the GB power system is going to experience a time of great change, which will result in the future GB transmission network being unique in many aspects. Large penetration of wind power with changing wind speed, direction and location will shift the concentration from one part of the system to another [24]. Consequently, this will cause of large variation in the power flow patterns in the network. In addition, the GB network will give rise to a power system with reasonably high concentration of FACTS devices, because of using several HVDC interconnections with external grids, internal HVDC transmission lines and offshore HVDC networks. These devices will bring various supplementary control features to improve the reliability and stability of the power system. However, they will bring new problems in the network [25]. Voltage stability is an important issue in an electrical power system. Consequently, several industrial grade power system simulator software packages have been developed in order to estimate the behaviour of the electric power system under certain conditions.

The inter area oscillation mode is used to define the perturbations associated with a group of generators in one area are swinging against a group of generators in another area. A large system usually involves several inter area oscillation modes. Most analyses of inter area oscillations are performed off line using system models that are

limited to individual power utilities, and do not consider the complete interconnected power system [26].

The need for improved inter-area mode damping has led to widespread research into the field of power oscillation damping. Over the years, many different controller designs have been shown to be effective at damping power oscillations with various technologies, though very few have been implemented in real systems. This chapter is going to review past research on the GB transmission system modelling and damping of power oscillations.

2.2 Past Research on GB Transmission System Modelling

System operators must address operational problems related to new generation and greater interconnection of systems. There is, however, a need to study the potential effect of new solutions carefully before committing to them and devoting important amounts of capital. These studies must be carried out via simulations using suitable models.

The GB network consists of an onshore transmission network, covering England, Wales and Scotland as well as an offshore one.

The installed capacity is predicted to increase up to 18-20 GW by 2020, compared to the current level of 12 GW, including 4.05 GW offshore [27], [28]. There will be key operational challenges for GB transmission networks, with increased wind penetration expected in Scotland. It is, therefore, planned to reinforce the GB electrical power transmission system between 2013 and 2022 [29], through the use of many more HVDC links operating in parallel with existing AC transmission routes, and also FACTS devices.

This will make the GB system operation unique and from an academic perspective an ideal choice to study power system operational challenges. However, obtaining a network model is not possible for academic research. There has been much research in this area using reduced model for the GB transmission system [30], [31], [32], [33].

Due to increasing levels of generation in Scotland, reinforcement of the Great Britain (GB) transmission network has been proposed in [30]. However, these could lead to sub-synchronous resonance (SSR). In addition in this study, the primary functions of bulk power transmission, a voltage source converter-based HVDC link has been used to provide damping against SSR, and this function has been modelled.

Belivanis and Bell in [31] are concerned with the coordinated operation of quadrature boosters (QB) installed on the high voltage electricity transmission network of Great Britain (GB). In this study, the simulation results have been conceded in MATLAB.

Chondrogiannis in [32] used the average time-invariant models for the representation of Doubly-Fed Induction Generators (DFIG). This study compares the steady state and dynamic behaviour of such a model with a time variant model of the frequency converter of the DFIG, where the power electronic switches are represented. The commercial software PSCAD/EMTDC is used in this study.

[33] investigates the ability of the HVDC links to act as a firewall against perturbations. To this end, two reduced dynamic equivalent transmission systems resembling that of Great Britain are developed in DIgSILENT PowerFactory.

However, there has been little research focused on modelling a reduced model of the GB system:

- Bell in [34] describes the need for new test system models to meet the needs of researchers, system planners and operators when addressing future power system requirements.
- Also, in order to provide suitable environments, which are sufficient for testing new ideas and that allow for the study of phenomena without overwhelming the researcher with excessive data or obscuring what is relevant, a new model to represent the GB transmission system has been developed to facilitate this by Belivanis and Bell in [35].

It should be noted that all the explained models have been created in a DIgSILENT PowerFactory environment.

2.3 Past Research on Damping of Power Oscillations

Due to changing generation patterns and increase in demand, power system operators will need to operate transmission systems much closer to the stability limits than was done previously. Supplementary and wide-area control of flexible AC transmission system (FACTS) devices can be employed to ensure stable operation of a power system closer to its capacity limits. When implemented correctly, supplementary controllers can change the momentary flow of active or reactive power, or the local voltage, so as to improve system stability. Two general methods of improving power system stability are installing new devices and improving the control of existing ones. In particular, the

following methods for improving power system stability have been investigated in the literature.

2.3.1 Installing New Infrastructure:

This includes adding new transmission lines to the power system or installing new generation capacity [36].

2.3.2 Installing Flexible AC Transmission System (FACTS) Controllers

There has been wide-ranging research [13, 37-51] on the use of power oscillation damping (POD) controllers installed with FACTS devices. The basis of this research lies in the use of various techniques for designing controllers that cover a wide variety of device types. These FACTS devices could be rendered more effective by connecting series-connected devices [41, 49, 52]. In this area, the effect of a designed controller on power oscillation damping for Thyristor Controlled Switched Capacitors (TCSCs) has been investigated in [39, 42, 43, 47, 50, 51, 53-55]. In [53, 56, 57], unified power flow controllers (UPFCs) have been used. The study in [57] presents a platform system for the incorporation of FACTS devices that, due to its manageable size, permits detailed electromagnetic transient simulation. This system manifests some of the common problems that FACTS devices are used to resolve: management of congestion, improvement of stability, and voltage support. Further, the platform allows for reduced order model validation (e.g. small signal or transient stability models). Using this platform, the authors showcased the development and validation of a small signal-based model with an included UPFC and they further, successfully, used the validated model to design a feedback controller for enhanced damping. A controller has been designed for thyristor controlled phase shifting transformers in [53], thyristor controlled series capacitors (TCSCs) in [53-55], static VAR compensators (SVCs) in [58-60], static phase shifters (SPSs) in [60] , and static synchronous compensators (STATCOMs) in [61] . Noroozian and Angquist in [53] investigate the enhancement of power system dynamics and analyse models appropriate for integration in dynamic simulation programs to study voltage angle stability. Deriving a control strategy for damping electromechanical power oscillations with an energy function method, the authors show that the control laws thus achieved are effective for the damping of both large-signal and small-signal disturbances. Moreover, they are also robust in respect of the loading condition, fault location and network structure. The authors also establish that the

control inputs can be derived conveniently from locally measurable variables. The effectiveness of such controls have been demonstrated for model power systems.

Arabi and Rogers in [58] discuss about the DC link and SVC model formulation and their controllers for ensuring small-signal stability in detail. The authors present several cases to demonstrate the ability and application of small-signal DC link and SVC models, and to verify small-signal results through time-domain simulation results. They establish that modes obtained by spectral analysis of the time simulation results closely approximate those obtained by small-signal stability analysis.

Iravani and Dandeno in [60] evaluated additional functions for a static phase shifter (SPS) with respect to the performance of a power system in (a) steady-state conditions, (b) small-signal dynamics and (c) large-signal dynamics. They used eigenvalue analysis as well as AC-DC transient stability and power flow programs to study four test systems exhibiting the following operational issues that are endemic to power systems: torsional oscillations, inter-area oscillations, transient instability and mechanical torques as well as the loop-flow phenomenon. The results were promising and demonstrated that, under the right conditions, an SPS could effectively function as mitigator of small-signal oscillations or an enhancer of transient stability, in addition to its usual function of steady-state power flow regulation. The results further indicated that it was feasible to achieve the most dynamic characteristics of an SPS by adding a small static power converter to a conventional phase-angle regulator.

Further, Patil and Senthil in [61] present findings from a study on the application of the static compensator (STATCOM), a recently developed FACTS device, as a torsional oscillation dampener in series-compensated AC systems, considering the IEEE first benchmark model. In the study, a STATCOM with a PI controller (for regulation of bus voltage) and a generator speed-derived auxiliary signal was utilized at the generator terminal to dampen torsional oscillations. The analyses undertaken included eigenvalue (for small value analysis) and step response analysis (to generate optimal control system parameters). Once the STATCOM controlled was thus optimized, the authors also assessed the dynamic performance of the nonlinear system under a three-phase fault. The findings were promising and indicated that an optimized STATCOM could be technically feasible as a dampener for turbine-generator torsional oscillations in series-compensated AC systems. However, in many power systems, shunt-connected devices, such as SVCs, have been installed to provide voltage support. Power oscillation

damping applications for these devices have been studied in [13, 37, 44, 46, 58, 59], whereas the combination of series- and shunt-connected devices has been investigated in [38, 40, 45, 48].

In much of the previous work into FACTS-based POD control, WAMS-based global signals have been exploited to improve system observability and modal damping [13, 37, 39, 40, 42, 50, 51] . Research has also been conducted on the most suitable signals for POD in [62-64], taking into account not only the signal content, but also the reliability and robustness of the content. In [51], the authors describe the disadvantages involved in applying the LTR (Loop Transfer Recovery) technique for reserving the robustness of the LQG damping controller. They use nonlinear power system simulation to verify the robustness of the designed controller, thereby demonstrating its effectiveness for damping power system oscillations. However, many studies cite the need for robust decentralised control, utilising only those signals that are locally available at the FACTS installation [38, 41, 43-49, 52] . In [52], the principal study objective is the identification of optimal control laws and the locations of series-connected FACTS controllers (such as TCSC and SSSC) in a unified framework for damping power swings. For the study, a circuit analogy of the electro-mechanical system is employed to identify the control laws, proposes a location index, and also posits that the signals can be synthesized with locally available measurements. The validation of the technique was undertaken on detailed models of 3-machine and 10-machine systems. The authors found that it is possible to achieve good damping factors, although performance is rendered heavily dependent on installed device location and signal availability, both of which cannot be easily controlled in practical installations, particularly where devices are not primarily installed for POD purposes.

The literature outlines a variety of controller synthesis techniques, ranging from extensions of traditional linearisation-based residue techniques that incorporate global signals [13, 50] to the novel use of fuzzy control laws [41]. There are several well-established analysis and design techniques for linear time-invariant (LTI) systems. These linear design and analysis methods cannot always be applied directly without alteration, since the inherited nature of power systems yields nonlinear dynamics for large disturbances. Lyapunov’s direct method plays a pivotal role in the stability study of nonlinear control systems. This technique is based on the existence of a scalar function of the states. This function decreases monotonically along the trajectories to

the stable equilibrium point, and the challenge is to find a suitable Lyapunov function [65-67]. This method has been used for control design in [48] and [49], resulting in robust designs that are independent of system modelling techniques. However, these designs exhibit complex formulations (particularly for large power systems) that may present challenges in practical installations. H∞ designs that attempt to guarantee robustness against system variations are proposed in [37, 45, 46] , while LMI formulations are proposed in [38, 39]. The designs so achieved are robust to a certain degree; however, controller performance has been evaluated for a small set of operating conditions only, and the practical limits of the uncertainties have not been tested at all.

Linear Quadratic Gaussian (LQG) control has been employed in [42, 47, 51] for improvement of inter-area mode damping, with improved damping continuing after a significant reduction of the final controller order. In [51], the author applies the LQG technique to the design of a robust TCSC controller for power system oscillation damping enhancement. The paper discusses in detail each step involved in the LQG design technique as applied to TCSC damping controller design. It is pertinent to note here that the requirement for participation factor analysis and complex weight tuning in LQG control implementation limits the practicality of the standard approach to large systems, especially when a large number of generating units contribute to poorly damped power oscillations.

Conversely, approaches like those employed in [40, 43, 44] make use of non-linear control theory as a means of overcoming the limitations of linearised power system models. Regarding which, complex feedback is used to create controllers that are not adversely affected by significant variations in network conditions. LQG control is also used successfully in both [63] and [64], [64], albeit effectively incorporating WAMS-based signal delays. The study in [63] pertains to power system stabilizer design for small-signal stability using phasor measurements. The authors use an optimal control system with structural constraints for achieving a two-level control mechanism, which is then augmented with order reduction to permit the following: (a) faster design algorithm convergence and (b) optimal weighting matrices choice for damping inter-area modes. The authors use two equivalent Brazilian systems as controls and discuss their control scheme as well as the modal analysis. They also assess topological changes and time delay variations. Similarly, the study in [64] presents a WAMS-based control scheme to improve power system stability that features a hierarchical structure with a

Supplementary Wide-Area Controller built on top of existing power system stabilisers (PSSs). The study also features a new LQG control design approach that targets the interarea modes directly and incorporates time delays in the transmission of the SWAC's input/output signals. The authors review three methods of selecting input/output signals for WAMS-based damping: the first, using modal observability/controllability factors; the second, based on the Sequential Orthogonalisation (SO) algorithm for optimal measurement device placement; and the third, incorporating both clustering techniques and modal factor analysis. The authors demonstrate successful enhancement of power system stability through the application of the WAMS-based control scheme on the New England Test System.

Moving on, the POD action of FACTS devices can be coordinated with that of existing power system stabilisers (PSSs) with a view to enhancing performance and robustness. In [68], the authors showcase such coordination with traditional residue-based techniques by outlining a technique for designing low-order robust controllers for power system oscillation stabilisation. Their two-stage design, which uses conic programming, results in the shifting of under-damped or unstable modes to regions of the complex plane that are sufficiently damped. This shifting of modes is achieved by a phase compensation design that works under multiple operating conditions with FACTS, PSS (stage one) and gain tuning (stage two). Thus, Simfukwe in [68] establishes that coordinated FACTS and PSS controllers can achieve oscillation damping under a variety of operating conditions with a simple, low-order control structure. Such coordination can also be demonstrated using nonlinear optimisation, as presented in studies [69-72]. In all cases, the robustness of coordinated controllers against variations and system changes must be evaluated before any pronouncement can be made as to the controller's effectiveness. However, the coordinated controllers proposed in studies [68-72] have only been assessed under a limited range of simulation scenarios and the authors of [69] accept that performance will be affected under system conditions different from those used during optimisation. That paper, i.e. [69], presents, for a multi-machine-power system, a global tuning procedure that uses a simulated parameter-constrained nonlinear algorithm for optimizing FACTS device stabilizers (FDS) and PSS. The simulation results demonstrate the success in overall power oscillation damping in the system in an optimized and coordinated manner; they also

show that the tuned FDS and PSS can provide successful damping under a variety of conditions existing in the system.

2.3.3 Modifying the Control Scheme by Adopting Power System Stabilizers (PSSs)

Typically within power systems, PSSs installed at generating units are responsible for damping power oscillations. Despite longstanding practice and experience having established the efficacy of these PSSs at damping local modes, the same cannot be said for performance with inter-area modes – it is sometimes poor and/or inadequate. This can be attributed to the complex nature of coordinated tuning and the consequent sacrifice in local mode damping that is sometimes necessary. Hence, PSSs once tuned for local modes at the time of generator installation are usually not altered with respect to settings unless there is a problem. Bomfim and Taranto in [73] discuss a technique for simultaneously tuning several power system damping controllers with genetic algorithms (GAs). For the analysis, they assume that damping controller structures consist fundamentally of lead-lag filters. The tuning method adopted in the study takes robustness into account since it ensures system stabilization for a wide (and pre-specified) range of operating conditions and it uses modified GA operators to optimise simultaneously both phase compensations and stabiliser gain settings. On a related note, [74] makes use of conic programming (as in study [68]) to resolve PSS design issues like coordinated gain tuning and coordinated phase and gain tuning. The study took into account several operating scenarios to achieve design robustness, and the design so evolved was implemented through conic programming run sequences.

Typically, optimisation-based (OB) approaches are explicitly designed to take into account a range of operating conditions. The literature refers to several methods with a variety of cost functions. For optimisation-based lead-lag (PSSs type) controllers, an objective function is minimized such that the poles of the closed loop system are properly placed under each scenario [75, 76].

Theoretically, the optimisation problem can be resolved by deploying any computational intelligence method. The number of inputs into the number of lead-lag blocks yields the total number of unknown parameters to be optimized, which in turn determines the order of the designed controller. In case further reduction in the controller order is required, model reduction can be deployed as an additional step.

Improved control of existing network generators is the preferred choice of approach when attempting to improve inter-area oscillation damping within power systems. Such efforts include coordinated tuning of existing system PSSs [73-81] and the use of advisory controllers to send supplementary control signals to appropriate generators, as in [59-64].

2.3.4 Modifying the Control Scheme by Adopting HVDC Modulation and Set-point Adjustment

Within several FACTS devices, the application of High-Voltage Direct Current (HVDC) links has been shown to be especially effective in improving the transient stability of the system, given the substantial capacity of HVDC links to perform active or reactive power modulation. Moreover, since multiple areas within the power grid are interconnected by embedded HVDC links, they can provide better inter-area oscillation damping as compared to other FACTS devices. Improving existing HVDC control schemes, i.e. adopting HVDC modulation techniques and adjusting the set-point of the HVDC links, is an attractive alternative to installing additional infrastructure. The studies reported in the literature have already established that power system stability can be enhanced by judicious control of existing HVDC connections [41].

Several research papers have addressed active power order modulation of an HVDC link for achieving effective power oscillation damping through a variety of controlling schemes. Recent studies have focused on employing local or wide area data, using centralized or de-centralized controllers and ensuring controller robustness [82-84].

Modelling techniques that display the correct level of dynamic behaviour are crucial for ensuring result accuracy. Karawita and Annakkage in [85] utilize small-signal analysis techniques to analyse multi infeed HVDC interactions. The authors demonstrate that modelling of AC network dynamics is essential for obtaining meaningful results from any small-signal stability analyses. By studying several cases, the authors conclude that interactions are possible between the HVDC terminals in an AC system. [86] presents a small-signal stability analysis for an AC/DC system with a novel discrete-time HVDC converter model based on multirate sampling. The authors develop, in a modular manner, a complete AC/DC system model in state space framework with the involvement of appropriate subsystem interfaces. The model, as proposed by the authors, is sufficiently generalized so as to allow for the inclusion of additional details

and steps. Osauskas and Wood in [87] discuss a model for evaluating stability concerns in the range of 2–200 Hz with system dynamics faster than typical electromechanical oscillations. Generalized small-disturbance HVDC models are presented in [58, 88]. In [58], the authors demonstrate that HVDC links and SVCs have controllable characteristics that could potentially influence system stability. The study included modelling of small-signal stability programs and time simulation ones to study these characteristics and thereby design controllers for better system stability. The authors addressed the formulation of DC links and SVC models and their controllers for small-signal stability through the careful study of several examples. Moreover, Cole and Belmans in [89] proposed a standardised VSC-HVDC model, based on injection modelling that allows for various levels of model complexity.

An early study on small-disturbance stability effects as a result of the location of the HVDC systems was conducted by [90]. With regard to the effects the HVDC system would have on the integrated system dynamic behaviour, Lukic and Prole in [90] deals with the question of where the HVDC system can be placed in an AC power system. As a starting point, an AC system dynamic state-space model is used. The system matrix and the sensitivity functions are then calculated in reference to the changes resulting from the flow of the direct current. The findings of the study by [90] have been improved on by [91] through the identification of the points that are optimal for connection and the preferred flow of power necessary for the improvement of the connected AC system. The study by [91] was conducted on the assumption that the installation of the HVDC system can be performed anywhere and can entirely be controlled to enhance the stability of the system. However, in practice, there are very few possible connection points besides the fact that the operation of the HVDC systems is usually based on the maximum power flow so as to maximise their economic value. It is critical to note that the studies referred to in this paper discuss the steady state operation and the altering of the converters for the enhancement of the system stability as opposed to discussing the active modulation-based controllers. It is also significant to state that many of the research studies into the utilisation of the HVDC for damping the oscillations concentrated on the use of supplementary controllers. There have also been converter controller designs that attempt to improve the inherent stabilising action of the HVDC system, such as [92] and [93], which utilise sliding mode control. Cole and Belmans in [89] discuss two distinct robust nonlinear control methodologies based on

sliding mode control with respect to enhancing the performance and stability of HVDC transmission systems. The paper outlines the development of the system's nonlinear steady state mathematical model, the formulation of appropriate feedback control signals based on sliding mode control to steer the active and reactive power towards their respective set point values, the attainment of desirable unity power factor at both sides of the DC link and finally, bringing the DC link voltage to the required value. On the other hand, [93] highlights a wide-area measurement-based robust controller (WMRC) design technique for HVDC links to improve AC/DC power system stability. To account for model impression in a conventional reduced first-order HVDC model, the WMRC proposed in the study utilizes sliding mode control; further, the area centre of inertia signals is selected as the feedback signal.

On the other hand, very few studies on the transient system stability of the hybrid HVDC-HVAC systems exist, and thus there is a potential for many studies to be conducted in this area. A study by Wang proposed a PID controller for oscillation damping of an AC system [94]. Wang later on proposed the utilisation of a controller that is based on an Adaptive Network-based Fuzzy Inference System (ANFIS) to damp the oscillations [95]. Miao *et al.* [96] also proposed the usage of a simple but efficient supplementary drop control to alter the order of the power output of an LCC converter. The performance of the controller has been presented using a wind farm connected via a HVDC system consisting of four machines. It is not a surprise that numerous researches have been published concerning the utilisation of the LCC converter for damping the oscillations given that an LCC-HVDC system has been in existence for a long time besides being used more than VSC-HVDC systems. Basically, any methodology for the modulation of active power through the use of an LCC-HVDC system could also be applied to a VSC-HVDC system since this modulation is associated with fewer concerns regarding reactive power. However, the latest studies in this area concentrate majorly on the application of VSC-HVDC

In 1976, over 35 years ago, the utilisation of controlled modulation of the active power through the use of LCC-HVDC lines was proposed for the improvement of the capacity of transmission of the parallel AC tie lines [97]. Following the standard linearization-based methods, the tuning of the traditional PSS-based controls was done using the flow of power in the AC tie as the input signal. The scheme was successful at reducing the oscillations. As such, the capacity of the AC tie-line was upgraded from 2100 MW to

2500 MW [98] . Nonetheless, due to the severe disturbances that could cause substantial oscillations, the reliance on the controller could not be assured.

Research studies into the connection of single or double-machine systems to an infinite bus via a single LCC-HVDC line have shown significant benefits in terms of the stability of the frequency [99, 100]. The improvement of the regulation of the frequency on the rectifier side of the AC system through the utilisation of a fuzzy logic controller in an HVDC system that interconnects two power systems has been discussed in The coordination of the modulation of the excitation of the generator of the rectifier side of the AC system and the DC scheme current is done by the controller in response to the frequency deviation of the rectifier side of the AC system. The fuzzy logic controller is designed using qualitative knowledge about the system rather than a precise system model. The quick stabilization of the oscillations of a transient nature through the utilisation of a simple fuzzy logical controller has also been presented in this paper; a presentation with the help of simulations of the superb performance of the simple fuzzy logic controller in suppressing the system transients is done. Similar studies to the one presented in this paper for parallel AC/DC lines have been carried out in [101, 102].

A combination of the fuzzy controller and the local generator speed or the frequency signal has been presented in [99, 100]. Similarly, in [101], the use of non-linear energy function-based techniques together with the local generator speed has been shown. The use of the methods that are based on linearization for the improvement of the small-disturbance stability of the test systems has also been presented in [102]. An analysis of the modulation of HVDC-links for the active and the reactive power for the damping of the slow oscillations is conducted in [102] with the purpose of gaining an intuitive understanding of the problem. This paper presents an analysis that demonstrates that the modulation of the active power is efficient when it is applied at a short mass-scaled electrical distance from either of the swinging machines. Additionally, the efficiency of the reactive power modulation is more when the direction of the flow of power is well defined and the modulation is conducted at a point that is close to the electrical midpoint of the swinging machines. It is demonstrated that the active and reactive power are appropriately modulated by the innately appealing feedback signal frequency and the voltage derivative respectively. The research that is presented in [99] and [100] deal with the isolated HVDC that feeds into AC power networks and thus is not related to this area of research, which is majorly concerned with AC/DC systems.

Other studies, for instance [76], show the impact that the LCC-HVDC POD based controllers can have on radial networks such as that in Australia. The comparison of the particle swarm optimisation of control parameters and the state feedback techniques that are based on LQG was done and showed that they have a similar performance. They both result in the enhancement of the post-disturbance response of the feedback signal from the network remote PMUs (Phasor Measurement Units) in Finland and in Norway, where they are utilised in damping the critical inter-area modes by means of a big SVC unit that is situated in the South-Eastern part of Norway. Additionally, the two approaches to the design of the control system, the model-based POD and the indirect adaptive POD, have been conducted.

Lately, China has the highest number of the installed LCC-HVDC lines in the world and also boasts 45 GW of operational HVDC transmission capacity. The massive investment by the Chinese in the HVDC system has attracted a lot of research in the area of POD in the Chinese grid [72, 73, 93, 103-106].Researches that have taken a broad approach in the fields of POD controllers for single lines [93, 103, 104, 106] and POD controllers for the coordinated schemes such as [72, 73, 105].

Nguyen and Gianto in [72] consider the challenge of the coordination of the proper action for control at the two ends of the link without the utilisation of a control scheme that is centralised and one that requires fast communication of the signals for control to a remote converter site. In this paper, the homotopy concept has been used to obtain a one block-diagonal controller from a controller set that is independently designed to guarantee the performance of the specific closed loop for an already established set of operating conditions. Improvements of over 10% have been displayed in low-frequency damping mode factors by studies that are based on simulations and utilise coordinated schemes. Though partly facilitated by WAMS-based global signals, it indicates a substantial increase, and makes sure that any oscillation in the power flow is settled rapidly. Many strategies for control design have been studied and include;

- Residue techniques and standard linearization by the use of local area signals [103], and wide area [104] signals,
- Sliding mode controls [93][60],
- Relative gain array [72],
- The non-linear optimisation of designs based on PSS using local signals [73], and global signals [105],

- Self-tuned adaptive controllers utilising the Prony method [106].

A good nominal performance was demonstrated by all the approaches. However, as noted by other research that made use of POD with a generator and implementations of FACTS, the assessment of the robustness of the controllers is poor and the schemes for control will often be simulated at the conditions utilised during the process of design only. Sometimes, an increase in the loading conditions is taken into consideration, but studies across a broad range of conditions are not imminent in the already existing literature.

The plans for the installations of the VSC-HVDC have recently tremendously increased a situation that has earned it an increased level of attention from researchers. Inertia is not involved in the conversion of power in VSC-HVDC and it is also possible for the settings of the VSC converters to be altered quasi-instantaneously [107]. Zhu *et al.* has taken advantage of the non-involvement of inertia to enhance the transient stability of the AC power system through the introduction of a control mechanism for emulating inertia for the VSC converters. [108] . Generally, the modulation of the active power that is transmitted can be achieved through the modulation of the frequency or from the difference of the phase angle at the two ends of the HVDC-link. Similarly, the rate at which the power flow changes can also be utilised [109]. Additionally, Liu puts into consideration a multiple infeed hybrid HVDC system that comprises both the VSC and LCC technologies [110]. The performance of the HVDC system in stabilising the AC system against faults has been enhanced by the concept of the adaptive limiters for the current controllers.

The necessity to have an enhanced damping in the inter-area mode has resulted in the extensive research in the area of power system oscillation damping. For quite a number of years, many controllers with the capability to damp power oscillations effectively have been developed. However, just a few of them have been implemented in practical power systems networks.

In assessing the POD, several factors have to be put into consideration. The degree to which the controller damps the oscillations resulting in the improvement of the power systems is critical. Additionally, the controller should be robust enough. The robustness of the controller should accommodate several variables, models, and an increase in the uncertainties of the operating conditions. The POD should remain robust and perform

desirably with changes in conditions. Further, the POD should have a simple design, and be scalable for larger power systems so as to be suitable for practical installations.

Research studies utilising small study networks have shown that several control designs can be used. Eriksson and Soder in [111] investigate the pole placement technique and presented a method for the design of a controller that is centralised and coordinated for a number of HVDC links. An estimation of the reduced order door system has been done in order to design a centralised coordinated controller. In this research, the algorithm for the Numerical Algorithms for Subspace State-Space System Identification (N4SID) has been used in the estimation of the open door system model. N4SID is a black-box identification technique. [112] has presented the non-linear strategies for control.

This article majorly contributes in the area of the coordinated control strategy for the multiple links for the HVDC system to enhance both the transient stability and the small signal stability. The mapping of the nonlinear system model to the linear system model as seen from the input to the output has been done using the input-output exact feedback linearization. This type of linearization is not a commonly employed by Taylor linearization as it cancels any nonlinearities associated with the pre-feedback loop. The representation of the internal node is then extended by the inclusion of the dynamics of the HVDC links in the non-linear differential swing equations. The extension is needed for the design of the feedback control. A lot of the difficulties experienced in [3] that include the need for the factor analysis is removed by the use of the modal formulation in [113]. Therefore, the MLQG design permits the directed control action on the inter-area modes while at the same time leaving the controlled modes unaffected and adequately damped. The simple synthesis technique of the controller as shown in [113] makes it appropriate for a number of power oscillation damping uses, though the investigation of its implementation in the generators is the only one that is currently being conducted so far.

In recent years, the attention of many researchers has been attracted by the application of the model predictive control (MPC) techniques in power systems. The introduction of the predictive control approach that is based on a wide measurement and non-linearity was done by Ford *et al.* [114] to ensure the first swing stability protection of the susceptible power system transmission line through the installation of the FACTS devices. For the higher order power system contingencies, a wide area optimal control

that utilises the MPC technique is proposed by Zweigle *et al.* [115] .The comparison of the traditional Linear Quadratic Gaussian (LQG) supplementary power system controllers and MPC for inter-area oscillation damping has also been done by Piroozazad [82]. Fuchs *et al.* [83] studied and elaborated the advantages and the disadvantages of the MPC controller's centralisation and decentralisation. Simulations indicate an improved performance with global MPC-based controllers in comparison to the damping controller that is local and de-centralised. The dynamic manipulation by means of a predictive control framework of both the active and reactive powers that is injected into the generator grid, the loads and the lines is presented in [83]. In this study, a standard example is shown by the simulations of four generators that are linked by a VSC-HVDC. Through the proposed approach, this example can be controlled by the VSC-HVDC up to an unstable point of operation while putting into consideration the system constraints while at the same time compensating for the delays in measurement. The ability of the model predictive control to deal with the constraints of the system form its key attraction feature. Similar to other parametric controllers, MPC effectiveness solely relies on the system model accuracy. An MPC that is based on the supplementary power modulation strategy for control of the HVDC system to damp the inter-area steady power oscillations, as well as the post-incident power oscillations, is proposed by the authors.

For controller design to be effected, the investigations of the energy function formulations have been done in [116]. This paper presents a VSC-HVDC in a simple model known as the injection model. Based on the simple model, the development of the energy function of the multi-machine power system including VSC-HVDC is done. Additionally, the derivation of the various control signals for the transient stability and damping of low-frequency power oscillations has been done based on Lyapunov's theory (control Lyapunov function) and small signal analysis (modal analysis). These approaches have primarily concentrated on the WAMS-based signals in the following ways:

- Specifically the measurement of the frequency of the generator [32],
- Although, frequency measurement at the VSC-HVDC connection point can also be used as a suitable input for the controller [116].

Lattore and Chandhari in [107] confirmed that the global signals are superior to the local signals through the comparison of the global and the local signals in that they can

provide high content information for the effective damping of the oscillations. However, it is realised that this level of effectiveness relies heavily on where the installed line is located. In this paper, the location of the VSC-HVDC line is based on the inter-area controllability that needs extra damping. The non-availability of this type of flexibility may see the global signal being required to make sure the POD performs optimally. The effectiveness of the POD damping has been demonstrated to be effective by studies conducted on larger multi-area testing networks.

Investigations on larger multi-area test networks have shown VSC-HVDC-based POD damping to be extremely effective such as the interconnected New England Test System and New York Power Systems (NETS-NYPS) [117]. This study highlights a robust wide-area stabilising control approach for the improvement of large power system stability, including HVDC transmission. The control system uses both wide-area measurement data and the HVDC supplementary modulation function, and it chooses appropriate feedback signals to implement a thorough, yet rapid, wide-area stabilising control against potential power oscillations. The linearised model takes the mandatory transmission time delay of the wide-area measurement signals into account for its establishment. To avoid the adverse impact of transmission delay on HVDC-WASC, the linearised model is expressed as the standard control problem of delay-dependent feedback, grounded in the robust control theory and the improved linear matrix inequalities (LMI) approach. In this study, it is suggested that a more effective use of reactive power modulation would be for the stabilisation of AC system voltages.

The option for the utilisation of the modulation of the active power is provided by the VSC-HVDC systems. Besides, the VSC-HVDC system also ensures that the injection of the reactive power is varied to make sure the power system is stable. An investigation of these benefits is done in [84] and [117] where it is established that the modulation through the active power is more efficient in damping the AC system oscillations.

In all the HVDC-based POD studies, the allowed range of deviation of the active power or the capacity for modulation varies. Early studies such as [97] and [98] utilised a variation of three percent of the rated power flow. The description of the development of the control algorithm for the modal analysis of the Pacific HVDC Intertie has been done in [97]. Based on the rate at which the AC-Intertie power changes, the application of the control signal to the current regulator at the DC Intertie sending end has been done. Moreover, a description of the implementation and operating practical knowledge

with a modulating power control system on the Pacific HVDC Intertie for damping oscillations on the parallel Pacific AC has been done. The described system has substantially improved the damping of the interconnected power system in western countries that was plagued by a long historical period of oscillations that damped negatively. The increase in the power rating from 2100 MW to 2500 MW of the Pacific AC Intertie was permitted due to the fruitful operation of DC modulation. A lot of research has been conducted with the sole purpose of attaining greater modulation capabilities due to the increased confidence in the reliability and the capacity of the converter technology. In emergency cases, the transmission of power above 20% of the rated value is permitted for long-term overload, while for short-term overload, 40% above the rated value is allowed [118]. However, no study on the impact of changing the capacity of modulation on the performance of the damping controller has been conducted.

2.4 Past Research on Probabilistic Small-Disturbance Stability Assessment

Currently, the operation of modern power systems, such as renewable energy sources and also the new type loads, increases uncertainties on the power system. Therefore the impact of this uncertainty, caused by the stochastically variable on power system small-signal stability is an issue, which has not considered by the deterministic analysis in [119-123]. Consequently the probabilistic approaches for small-disturbance stability analysis have become the topic of many researches recently. Probabilistic analysis was first introduced into studying power system small-signal stability by Burchett and Heydt (1978) in [124], but the first application of such analysis for power system load flow (PLF) study was by Borkowska in 1974 [125]. Further development on this area has been undertaken in [126] and [127].

In [128], the authors briefly explain some techniques for uncertainty and sensitivity analysis, including:

- Monte Carlo analysis;
- Differential analysis;
- Response surface methodology;
- Fourier amplitude sensitivity test;
- Sobol variance decomposition;

- Fast probability integration.

In this research, the following topics regarding Monte Carlo analysis in conjunction with Latin hypercube sampling have been described:

- Assets of random, stratified and Latin hypercube sampling;
- Comparisons between random and Latin hypercube sampling;
- Operations involving Latin hypercube sampling;
- Uncertainty analysis;
- Sensitivity analysis;
- Analyses involving stochastic

2.5 Non-Analytical Method (Numerical Method)

The numerical method involves Monte Carlo (MC) simulation of a wide range of operating scenarios, which are based on pseudo-random sampling from the pdfs of stochastic sources of system uncertainty. For each computational scenario, the standard deterministic small-disturbance stability assessment can be completed and once sufficient scenarios have been simulated, the critical mode pdf can be generated. This non-analytical method has been used in [129], [130], [123] to determine power system probabilistic stability. In [123] the MC has been applied to investigate the impact of stochastic uncertainty of grid-connected wind generation on power system small-signal stability. In this study, an example of 16-machine power system with three grid-connected wind farms is used to establish the application of the MC method. Also in [130] a Monte Carlo based probabilistic small signal stability analysis is presented to consider the influence of the uncertainty of wind generation and the case study in this research is carried out on the IEEE New England test system.

Rueda and Colome in [131] calculate probabilistic performance indexes based on a combination of the Monte Carlo method and fuzzy clustering and compare the results obtained using a 18-power plant power system with those obtained through a deterministic approach and this method has also been applied in [132] and [131]. In these studies, it is used to evaluate the stochastic effects of generation and load on inter-area mode damping for a large system. By using this simple method an accurate result can be achieved, but for large systems that have many uncertainties this might be time consuming. The reason why these systems are time consuming is that the total number

of scenarios that need to be considered to ensure that complete variation of all the parameters is taken can be extremely large.

2.6 Analytical Methods

As mentioned in the previous section, one of the most widely used approaches is Monte Carlo (MC) simulations [129], [130], [123], which model system complexities very accurately, but at a high computational cost and this characteristic may be prohibitive in a large system. Analytical methods are used for reducing the computational cost of MC simulations, whilst at the same time achieving acceptable accuracy. Specifically, these methods decrease the massive numbers of simulations by using direct calculation of the effects of the system uncertainties on the critical modes of interest [124, 133, 134]. Among various methods of probabilistic analysis, the Gram-Charlier, which is an expansion-based method (or named Cumulant-based), has been widely used in many applications of stochastic static analysis of power systems, in such as [135-140]. Bu and Du in [135] applied the Cumulant-based theory to evaluate the variances of both the complementarity of combined wind power and the probabilistic small-signal stability of power systems for the first step. At the next step, these variances have been used as two indices to explain the effect of different complementarity levels, connection topologies and DC network control schemes of offshore wind generation on the probabilistic distribution of critical eigenvalues and consequently, probabilistic small-signal stability.

Preece, in [141], compares three different efficient estimation techniques to assess their feasibility for use with probabilistic small disturbance stability analysis and their performance as illustrated on a multi-area meshed power system, which include: Estimation Methods, an Analytical Cumulant-based approach and the Probabilistic Collocation Method. Subsequently, all these techniques are compared with a traditional numerical MC approach and it is proven that the cumulant-based analytical approach is the most suitable method for such work.

In addition, some studies have compared the conventional Gram-Charlier expansion-based method and the nonlinear Monte Carlo simulation [142] . Bu and Du in [142], in order to improve the accuracy of assessment of system probabilistic stability, have applied an analytical method based on multi-point linearization.

2.7 Efficient Sampling Methods

These types of methods can be considered as a combination of both Non-analytical (numerical) and analytical techniques. One such approach for assessing probabilistic stability is the Two Point Estimate (TPE) method, which has been used in [143] and for this, 2m samples are needed for a system with m uncertain parameters. Alabduljabbar and Milanovic in [144] example of an efficient sampling method is studied, with the Low Discrepancy Sequences (LDS) method being used to tune system PSSs robustly. In [145], the author presents the use of Latin Hypercube Sampling (LHS) combined with the Cholesky Decomposition method (LHS-CD) to improve the accuracy of reduced numbers of MC runs for PLF.

2.8 Concluding Remarks

In this chapter, the extant research in the field has been reviewed and several areas that need to be addressed have been identified.

These can be summarised as follows:

- A comprehensive assessment of the robustness of LCC-HVDC POD controllers is currently lacking. Many nominally robust control schemes have been published, but these have not been thoroughly tested across the wide ranging operating conditions that are typical of modern power systems.
- The Probabilistic Collocation Method requires development for implementation on large power systems in order to assess probabilistic power system small-disturbance stability with respect to uncertain operating conditions efficiently.

Chapter 3

Power System Modelling

3.1 Introduction

The GB network consists of an onshore transmission network, covering England, Wales and Scotland as well as an offshore one. A large percentage of its installed generation capacity consists of non-renewable sources, such as gas/CHP, coal and nuclear. The proportion of generation mix is expected to reverse towards the middle of the next decade due to development of several renewable generation plants and the closure of coal and oil plants, which are either close to the end of their working life or unable to meet the emission targets [25], [24].

The installed capacity is predicted to increase up to 18-20 GW by 2020, compared to the current level of 12 GW, including 4.05 GW offshore [27], [28]. There will be key operational challenges for GB transmission networks, with increased wind penetration expected in Scotland. It is, therefore, planned to reinforce the GB electrical power transmission system between 2013 and 2022 [29], through the use of many more HVDC links operating in parallel with existing AC transmission routes, and also controllable reactive power sources, such as Static VAr Compensation (SVC) and Thyristor Controlled Series Compensation (TCSC) [24].

These changes will make the future GB transmission network unique in many aspects. Large penetration of wind power with changing wind velocity, direction and location will shift the generation concentration from one part of the system to another. Consequently, power flow patterns in the network will experience large variation. In addition, the island network, with several HVDC interconnections with external grids,

internal HVDC transmission lines and offshore HVDC networks, will give rise to a power system with reasonably high concentration of FACTS devices. These devices can offer various supplementary control features to improve the reliability and stability of the power system. However, they can cause new problems in the network [146]. Voltage stability is an important issue in an electrical power system. Consequently, several industrial grade power system simulator tools have been developed in order to estimate the behaviour of the electric power system under certain conditions.

Also, it will make the UK system operation unique and from an academic perspective an ideal choice to study power system operational challenges. However, obtaining a network model is not possible for academic research. Therefore, the system presented in this study is a reduced GB system model. The reduced model is based upon a future GB transmission system model and hence, contains different types and mix of generation. This model is also based on the reduced DIgSILENT PowerFactory model developed by the National Grid.

There are several industrial-grade power system simulation tools, which are commercially available on the market for the academic arena, but they are expensive to obtain and time-consuming to learn [147]. As a result, very few institutions (utilities, academic/research organizations) can afford to use more than one power system simulation tool [147]. The aim of this chapter is to describe models of the main components of an electrical power system, which includes synchronous generators, AVR and Governor for generator transmission lines, transformers and system loads and also to compare PSCAD with the more widespread simulator DIgSILENT PowerFactory. The most context of this chapter has been published in [24].

The tools employ different models, components as well as analytical and numerical algorithms; hence different results can be expected for the same system.

3.2 Introduction to PSCAD/EMTDC and DIgSILENT

In large-scale transmission and power systems, it is not easy to achieve field tests. Nowadays, the tools have an important role regarding planning and real-time operation. And on the other hand it is expected that the electric power systems be highly reliable [147]. Therefore, the simulation tools and software packages paly critical role regarding the accurately and reliably of the real-life systems.

These software packages are normally developed for a specific area of the power system, being aimed at improving analytical ability and computational efficiency [146]. The manufacturers of these software packages have made efforts to make them as user friendly as possible, especially those used in research and for educational purposes. PSCAD/EMTDC and DIgSILENT PowerFactory are two examples of these software packages [146].

The simulation of a power system in the time and frequency domains is the main function of PSCAD. It also can be used in harmonic research of an AC system, analysis of transient torque, the HVDC system and HVDC commutation [146]. It can simulate the electromagnetic transient process of a series or parallel multi-terminal transmission system for an AC/DC system as well as the interaction between parallel AC and DC lines on the same tower. The EMTDC program has the "snapshot" function, which means the sections at some time instants of the system can be recorded and based on this function, further study on the system's transient process can be carried out [146]. The library of the PSCAD/EMTDC includes virtually all the kinds of elements found in a power system. This software also has the capability of interfacing MATLAB, through which the visual numerical calculation function in the latter can be easily employed [148].

DIgSILENT PowerFactory is an integrated power analysis tool that combines reliable and flexible system modelling capabilities with state of the art solution algorithms and unique object oriented database management. The load flow, short circuit calculations, harmonic analysis, protection coordination, stability calculation and modal analysis have been included in this software package [149].

Generally, the quality of a simulation relies on three main parameters, as follows [147]:

- System components modelling
- Solution methodology
- System input data

These are going to be described and compared for these two software packages in the next subsection.

3.2.1 Components Modeling Comparison

1. Synchronous Generator

The following aspects relating to the generator model have been investigated.

- **Equivalent Circuit**

In power system dynamic studies, the synchronous generator is generally represented using the dq-axis. A sixth order model has been found to represent the synchronous generator sufficiently in stability studies and the equivalent circuit, which has been used to represent this model, has six electrical circuits: stator d and q-axis circuits, the field circuit, one d-axis damper winding and two q-axis damper windings [150].

In Table 3.1 the complete picture of the software capabilities with respect to generator models has been presented.

In PSCAD/EMTDC, the generator can be represented by an infinite source series with a subtransient impedance matrix. The subtransient matrix contains 3×3 sub-matrixes of the form:

$$\begin{bmatrix} \boldsymbol{X_s} & \boldsymbol{X_m} & \boldsymbol{X_m} \\ \boldsymbol{X_m} & \boldsymbol{X_s} & \boldsymbol{X_m} \\ \boldsymbol{X_m} & \boldsymbol{X_m} & \boldsymbol{X_s} \end{bmatrix} \quad \textbf{(3. 1)}$$

where, ***Xs*** is the self-reactance of each phase and ***Xm*** the mutual reactance among the three phases. As in any other three-phase network component, these self and mutual reactances are related to the positive and zero sequence values, ***X1*** and ***X0***, by [151]:

$$\mathbf{X_s} = \frac{(\mathbf{X_0} + \mathbf{2X_1})}{\mathbf{3}} \quad \textbf{(3. 2)}$$

$$\boldsymbol{X_m} = \frac{(\boldsymbol{X_0} - \boldsymbol{X_1})}{\mathbf{3}} \quad \textbf{(3. 3)}$$

- **Stator voltage equation**

Based on the dq-axis machine demonstration, the per unit stator terminal voltage (***Et***) is known by equation (3. 4).

$$\left.\begin{aligned} \tilde{E}_t &= e_d + j e_d \\ e_d &= \frac{d\psi_d}{dt} - \omega_r \psi_q - R_a i_d \\ e_d &= \frac{d\psi_d}{dt} + \omega_r \psi_d - R_a i_q \end{aligned}\right\} \qquad \textbf{(3. 4)}$$

where:

ω_r**:** Rotor angular velocity

$\psi_d \psi_q$**:** *d* , *q* axis flux linkage

$i_d i_q$ **:** *d* , *q* axis armature winding current

R_a**:** Armature resistance

It should be noted that both the investigated tools (PSCAD/EMTDC and DIgSILENT) consider the effect of speed variations.

- **Representation of mechanical input**

Regarding some studies, in which the governor set is not modelled, the generator mechanical torque input (***Tm***) has been assumed to be constant. However, if a generator is modelled with mechanical power input (***Pm***), and also rotor speed variations have been ignored, then this input and the generator mechanical torque input are equal (***Tm*** = ***Pm***). The variation of Tm with machine speed can be calculated by equation (3. 5) [147]:

$$T_m = \frac{\omega_n}{\omega_r} P_m \qquad \textbf{(3. 5)}$$

where,

ω_n: the synchronous speed

ω_r: the rotor angular speed

The DIgSILENT generator model has ***Pm*** input and the rotor speed variations are considered, whereas PSCAD/EMTDC model uses ***Tm*** as input [147].

- **Magnetic saturation**

Saturation can be assumed to affect one of the flowing parameters [147]:

i. d-axis only

ii. d-axis and q-axis

In DIgSILENT the d- axis and q-axis parameters are assumed to be saturated, whilst in PSCAD saturation is assumed to be on the d-axis only [147] .

In DIgSILENT, the user sets two saturation parameters, $S_{1.0}$ and $S_{1.2}$, which are equivalent to 1.0 and 1.2 pu terminal voltage (flux linkage), respectively [150].

The open circuit saturation curve of the generator gives these parameters and they are computed using equations (3. 6) - (3. 8) as given below [150]. It should be noted that these equations do not apply if the generator is fully saturated.

$$\psi_I = A_{sat} e^{B_{rot}(\psi_{at} - \psi_{atT1})} \quad \textbf{(3. 6)}$$

$$S_{1.0} = \frac{I_{A1.0} - I_{B1.0}}{I_{B1.0}} \quad \textbf{(3. 7)}$$

$$S_{1.2} = \frac{I_{A1.2} - I_{B1.0}}{I_{B1.2}} \quad \textbf{(3. 8)}$$

where,

Ψ_{at}: flux linkage at the point on the non-linear curve

Ψ_I: flux linkage drop due to saturation

Ψ_I**:** linear characteristic threshold flux linkage

A_{sat}**,** B_{sat}**:** constants

$I_{A1.0}$ $I_{B1.0}$ $I_{A1.2}$ $I_{B1.2}$**:** field currents

By contrast, in PSCAD the user provides data for up to ten points on the non-linear open circuit saturation curve. The first must be (0, 0) and the second must lie on the linear part of the curve, whilst the other points on the non-linear part of the curve are determined using equation (3. 6) [150].

In PSCAD, the open circuit characteristic (OCC) curve is defined through ten user defined points [147].

2. Transmission Line

Both software packages under investigation use a nominal Pi model of transmission line and PSCAD, in addition, has an equivalent Pi model.

3. Transformer

Many transformer studies, however, do require core saturation to be adequately modelled. Saturation can be represented in one of two ways: First, with a varying inductance across the winding wound closest to the core or second, with a compensating current source across this core.

In EMTDC, the current source representation is used, since it does not involve change to the subsystem matrix during saturation. A two winding, single-phase transformer saturation using a current source is shown in Figure 3.1.

The current $\boldsymbol{I_S(t)}$ is a function of winding voltage $\boldsymbol{V_L(t)}$. Winding flux $\boldsymbol{\Phi_S(t)}$ is defined by assuming that the current $\boldsymbol{I_S(t)}$ is the current in the equivalent nonlinear saturating

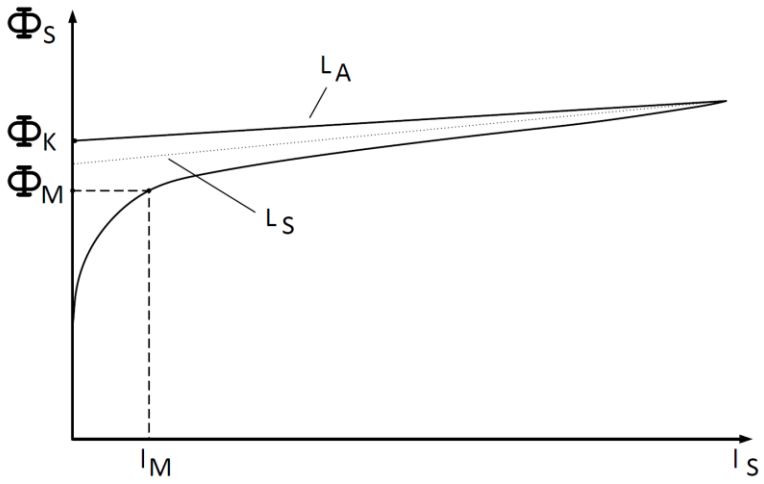

Figure 3.1 Core Saturation Characteristic of the Classical Transformer [183]

inductance $\boldsymbol{L_S(t)}$. The air core inductance L_A is represented by the straight-line characteristic, which bisects the flux axis at $\boldsymbol{\phi_K}$. The actual saturation characteristic is represented by $\boldsymbol{L_M}$ and is asymptotic to both the vertical flux axis and the air core inductance characteristic. The sharpness of the knee point is defined by $\boldsymbol{\phi_M}$ and $\boldsymbol{I_M}$, which can represent the peak magnetizing flux and current at rated volts. It is possible to define an asymptotic equation for current in the non-linear saturating inductance $\boldsymbol{L_S}$, if $\boldsymbol{L_A}$, $\boldsymbol{\phi_K}$, $\boldsymbol{\phi_M}$, and $\boldsymbol{I_M}$ are known.

This method is an approximate way of adding saturation to mutually coupled windings; however, it suffers from the disadvantage that, in most practical situations, the data are not available to make use of them and the saturation curve is rarely known much

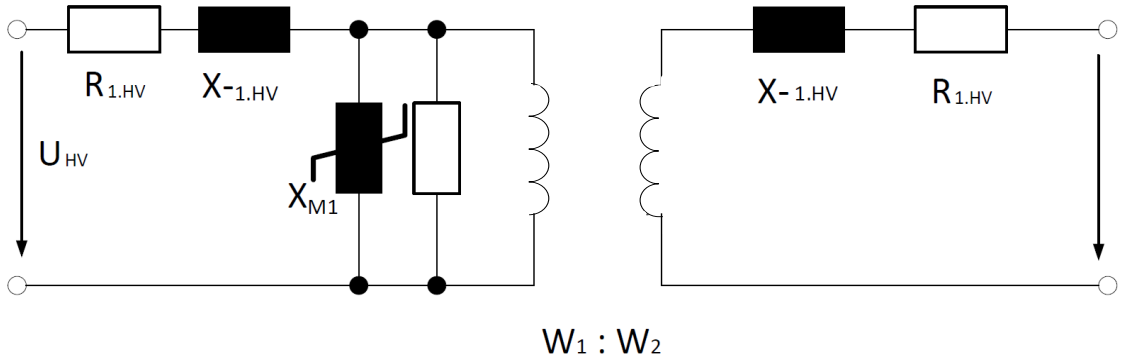

Figure 3.2 Equivalent Circuit of the 2 Winding 3-Phase for a Positive Sequence [152]

beyond the knee. Moreover, the core and winding dimensions as well as other related details cannot be easily found.

Figure 3.2 shows the equivalent model of a 2 winding 3-phase transformer for the positive sequence in DIgSILENT and for simplicity, the tap changer has been omitted from the figure [152]. To have the same system in both software tools, the automatic tab changing for the transformer has been removed from the DIgSILENT. However, the aforementioned software tools have different saturation characteristics and as a result, different data (such as distribution of leakage reactance and resistances, magnetizing impedance etc.) have to be defined for the winding transformer component.

4. Load

Load models are generally classified as static and dynamic. The static load can be modelled by either an exponential function, which is calculated by equation (3. 9) [147]:

$$\boldsymbol{P = P_0(\overline{V})^a(1 + K_{pf}\Delta f)} \qquad \textbf{(3. 9)}$$

$$\boldsymbol{Q = Q_0(\overline{V})^b(1 + K_{Qf}\Delta f)}$$

or a polynomial function (ZIP model), which is calculated using equations (3. 10) and (3. 11) [147]:

$$\boldsymbol{P = P_0[p_1\overline{V}^{\,2} + p_2\overline{V} + p_3](1 + K_{pf}\Delta f)} \qquad \textbf{(3. 10)}$$

$$\boldsymbol{P = Q_0[q_1\overline{V}^{\,2} + q_2\overline{V} + q_3](1 + K_{qf}\Delta f)} \qquad \textbf{(3. 11)}$$

where,

$$\bar{V} = {}^{V}/_{V_0} \ and \ \Delta f = f - f_0$$

P, Q: active, reactive components of load equivalent to bus voltage magnitude ***V***

F: bus voltage frequency

K_{pf} , K_{qf} : active power, reactive power frequency dependency, respectively

p_1, p_2 ,p_3: the proportion of constant impedance (***Z***), constant current (***I***) and constant power (P) components, respectively

q_1, q_2 , q_3 : the proportion of constant impedance (***Z***), constant current (***I***) and constant power (***P***) components, respectively

It should be noted that these models provide explanation for both the voltage and frequency dependency of loads [147].

3.2.2 Software Flexibility

1. Data Input

Both the focal software packages (DIgSILENT and PSCAD) have graphical user interfaces, which makes it possible for users to draw one-line diagrams (or three phase in PSCAD) of the system with data by using the pop-up windows [147].

2. Data Output

Accessibility to the system matrices is important for controller design and parameter setting purposes. The ***B*** and ***C*** matrices are of interest in the formulation of the mode controllability and observability matrices. DIgSILENT does not allow access to any of the matrices. Also, this package gives the normalized complex participation factors, but only for the machine state variables. These two parameters (the eigenvectors and participation factors) are important for the placement of power system support devices. In addition to the numerical values, the program gives a graphical representation of the participation factors [147].

PSCAD/EMTDC does not give eigenvectors or participation factors. Table 3.1 summarises the comparison of the simulation tools.

3.2.3 Interfacing with MATLAB

The standard libraries of the two software packages studied include synchronous and asynchronous machines, transmission lines, transformers, semiconductors, power electronic devices and simple processing. Nevertheless, not all the control system components required for designing a complex control system or performing specific computations, are available in one program. Consequently, a combination of the two programs in order to obtain the required features is necessary [153]. Therefore, the

Table 3.1 Summary of Software Comparison [147]

		DIgSILENT	**PSCAD**
Components Models	Generator Models	5^{th}, 6^{th}	5^{th}, 6^{th}
	Generator Saturation Parameters	$S_{1.0}$, $S_{1.2}$	Specify points on OCC curve
	Generator Mechanical Input	P_m	T_m
	Rotor Angle reference Angular Speed	ω_j	ω_n
	Transmission line	Nominal π	Nominal π and equivalent π
	Load Models	Exponential	Exponential
Solution Methodology	Linearization of System Equations	Not available	N/A
	Perturbation Size	Not available	N/A
	Eigenvalue Calculation Method	QR	N/A
Software Flexibility	Data Input	Graphical user interface with pop-up windows	Graphical user interface with pop-up windows
	Accessibility of System Matrix	Not available	N/A
	Eigenvectors	Not available	N/A
	Participation Factors	Available	N/A

majority of existing simulation software package has the capability to interface to external program to improve their abilities. Recent works in this area and transient simulation have shown that a control analysis package, such as MATLAB can be interfaced with another program. Here, this approach is investigated for the integration of two different software packages [154].

- **PSCAD/EMTDC**

Data input for PSCAD/EMTDC software is supported by using a GUI interface called DRAFT [154]. After drawing the circuit diagram and entering values via pop-up menus that are selected by clicking on the component's icon, the resulting schematic diagram is translated into a data and FORTRAN file called DSDYN that contains dynamic models, such as a control block. This interface is a powerful feature as it allows users to develop their own model in FORTRAN and add these to the PSCAD/EMTDC component repertoire. It has been used to establish communication between the two programs [154].

MATLAB, on the other hand, is an interpreted language containing a large number of mathematical functions and a control system block. These are invoked using statements entered directly onto the command line or directly called through an "m.file". One feature available in MATLAB is that the engine can be started from a user written FORTRAN or C program, which allows for communication with PSCAD/EMTDC to be established [154].

In Figure 3.3, the structure of the interfacing between PSCAD/EMTDC and MATLAB

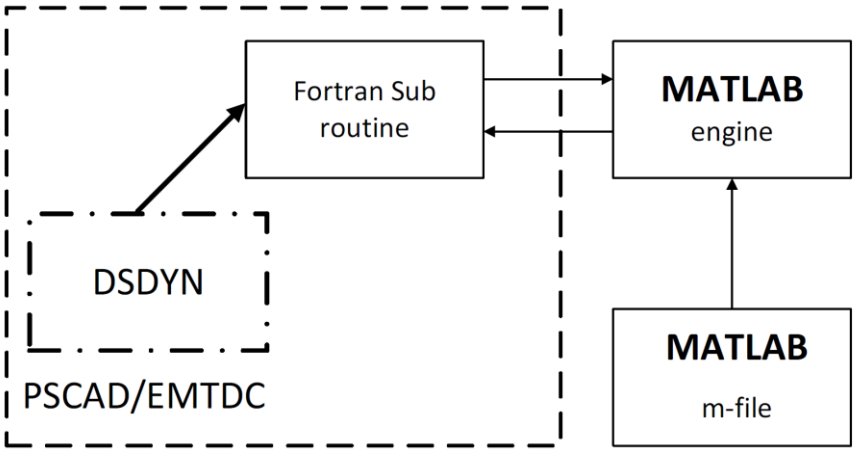

Figure 3.3 Structure of PSCAD/EMTDC- MATLAB Interface [154]

is shown. It can be seen that PSCAD/EMTDC has a DSDYN, which is the FORTRAN file and can be called as external FORTRAN subroutines. This subroutine should be written to set up the data communication pipe between the subroutine and the MATLAB engine. It should be noted that this subroutine is automatically generated by using a program developed by the authors. Also, the MATLAB part of the simulation has been written independently as an m.file [154]. There is, in principal, no time-step delay in the solution as both the MATLAB and PSCAD/EMTDC blocks are concurrently solved.

A new MATLAB block can be developed by using a program written by the authors. The name of the new component as well as the number of inputs and outputs with their name should be defined by the user. After this step, the graphical icon of the block is automatically generated with an empty m.file and the appropriate MATLAB statement should be written into it by the user [154].

- **DIgSILET/ PowerFactory**

The overall structure of the interface is illustrated in Figure 3.4. In the process of linking Matlab/Simulink to PF the following programs interact during the simulation time [155].

• PowerFctory.

• Matlab data and data models in the form of m.files(.m)

• Matlab/Simulink model (.mdl)

The m.files and Matlab/Simulink models present the model and algorithms of the external controllers. Also the PF model presents the power system. In order to interface MATLAB with PowerFactory, the MATLAB algorithm needs to be included in a frame similar to the dynamic simulation language (DSL) model definition as shown inFigure 3.4 . The first step is to create a ‘slot’ inside a composite frame (ElmComp) in the PowerFactory project and the algorithm should be implanted in this created frame. A block definition (BlkDef) is also required to be created in the ‘type’ library [156]. This performance allows definition of the MATLAB code to be imported by ticking the MATLAB m.file check box in the classification section and providing the address of the m.file [156].

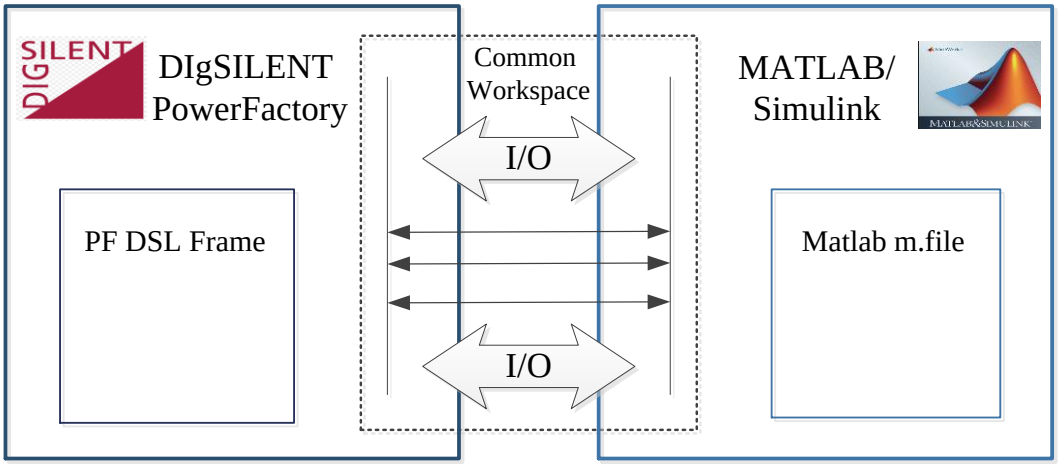

Figure 3.4 Structure of DIgSILENT and MATLAB Interface [155]

In the block definition (BlkDef) of this composite frame all of the following parameters should be defined properly in the m.file [156]:

- all of the required inputs from PowerFactory
- the outputs obtained from MATLAB
- the state variables all the defined inputs
- outputs and state variables check

3.3 Modelling of the Component

The important part when modelling the system is obtaining the same result for active and reactive power flow from the generators in PSCAD/EMTDC and DIgSILENT. In order to achieve the same ***P*** and ***Q*** for both systems, for the first step, each generator in PSCAD/EMTDC is modelled as a voltage source with a defined voltage angle and magnitude to obtain the specific ***P*** and ***Q***. In the next step, the voltage source is replaced by a generator and exactly the same voltage angle and magnitude is used for the generator in order to have an exact ***P*** and ***Q*** [24].

The real and reactive power are decided by three factors: the generator terminal voltage (magnitude and angle), the source voltage (magnitude and angle) and the impedance between the generator and source.

In PSCAD/EMTDC, the generator starts as a source at T=0s and after a period of time, the exciter is put into operation. Then after a further time period set by the user in the "lock rotor-normal mode transition" part of the "Variable Initialization Data" window, the governor is put into operation. Finally, the generator is put into operation. This

performance of PSCAD/EMTDC makes it possible for users to model the generator as a voltage source so as to obtain the voltage magnitude and angle [24].

During the transition from source to generator, the initial voltage and angle is important for a smooth transition. If the initial condition is far from the required final state, it takes a long time to reach to the steady state. Usually the initial conditions can be obtained from power flow programs (such as PSSE or DIgSILEN), or for a very simple case they can be calculated manually. In this case, the initial conditions are obtained from the load flow solution from DIgSILENT (P and Q for each generator).

In PSCAD/EMTDC, there are two ways to let the generator output real power as the required final result [24]:

1- Selecting “control source ***P*** out” as "No" in the "configuration-advanced" window. Then, the generator will finally output the power specified in the “initializing real power” of the “variable initialization data”,
2- Selecting “control source ***P*** out” as "Yes" in the "configuration-advanced” window. Then, the generator will finally output the voltage magnitude and angle specified in the “initial conditions”. The real and reactive power is thereby decided by the voltage magnitude and angle.

In this study the second method has been applied.

As a last step, since the transformer used for this system has a D-Y connection, there is a 30 degree difference for voltage angle, which has to take into account for the initial voltage angle [24]. The used algorithm for this method can be summarized as shown in Figure 3.5.

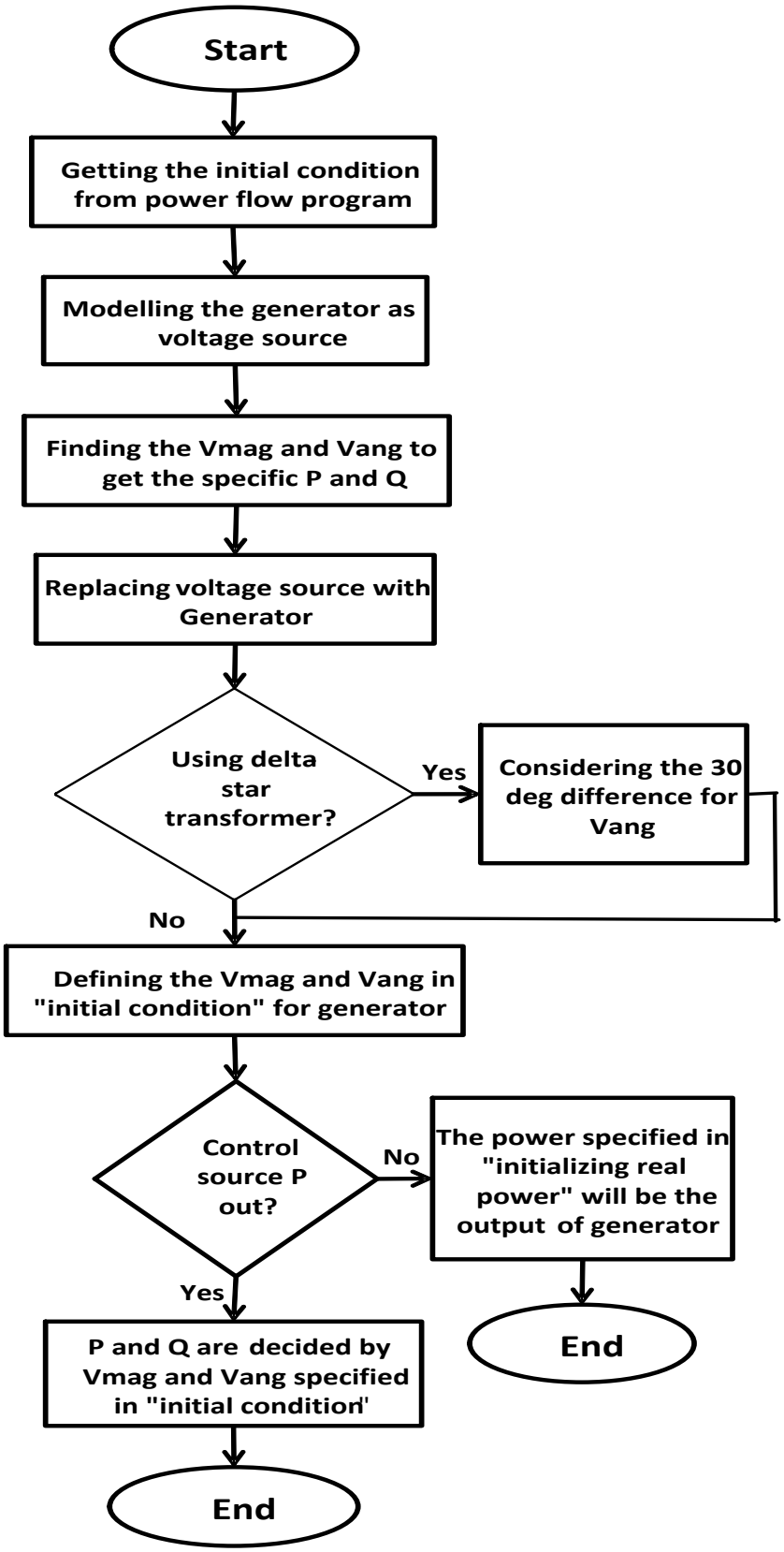

Figure 3.5 Algorithm for Modelling the Generator in PSCAD

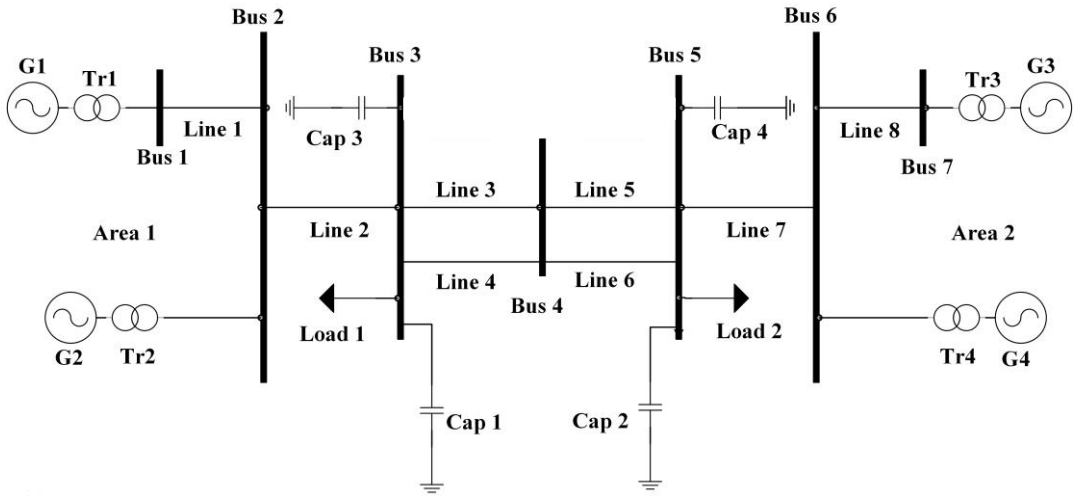

Figure 3.6 Two-area Test Network

3.4 Case Study

3.4.1 Small Test System

The small test system which has been used in this study is the four-machine two area network, taken from Kundur [11] as shown in Figure 3.6. This system not only is an appropriate case study for investigating the physical nature of low frequency electromechanical power oscillations in the time domain, but also can be considered as a useful tool for the study of electromechanical oscillations in the GB power system. Area 1 and area 2 can be presented as the Scottish and the English power systems respectively.

In this study, the synchronous generator model is the full order one as presented in [152] . Figure 3.7, Figure 3.8 and Figure 3.9 show the AVR block diagram, DC exciter of generators block diagram and governor block diagram respectively which are used in this work. All details for this are included in Appendix A.

As described by Vittal in [157], the DC exciters that are used as a part of excitation, a DC current generator and a commutator, typically respond more slowly than static systems.

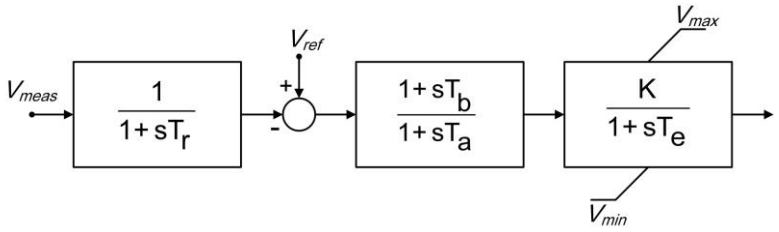

Figure 3.7 AVR Block Diagram [11]

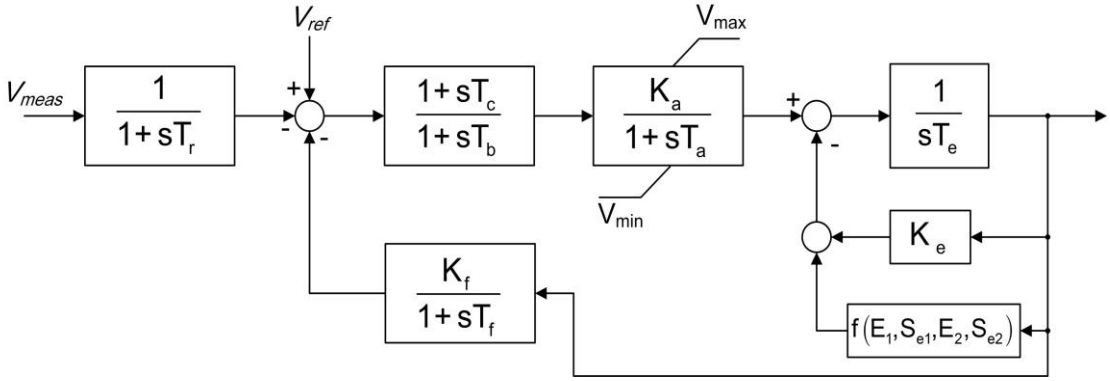

Figure 3.8 Block Diagram of a DC Exciter of Generators

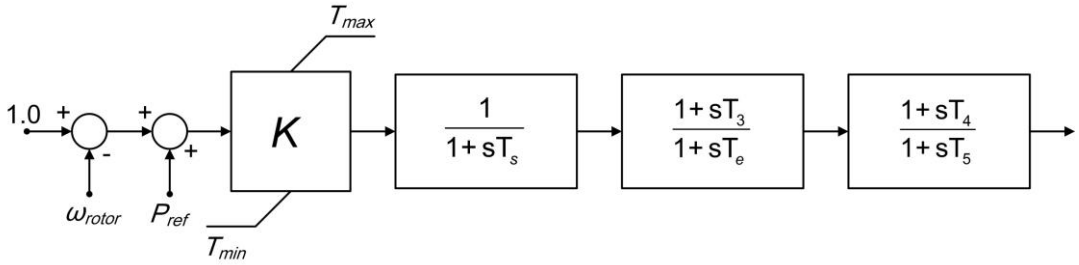

Figure 3.9 Governor Block Diagram

Throughout the work presented in this research, transmission lines are modelled using a lumped parameter model. All the parameters for AC transmission regarding the rated voltage, length, resistance, reactance and susceptance are listed in Appendix A.

In this thesis for small test system, two-winding transformers with Y_N connection on both sides of high and low voltage have been modelled. Also the active loads are modelled as 50% dynamic and 50% constant impedance. Also, the reactive loads are modelled as constant impedance. More details can be found in Appendix A.

- **Simulation Results**

As aforementioned, both programs have a graphical user interface. In the graphics environment, the user can draw the system as a one-line diagram (or three phase in PSCAD) and populate it with data using the pop-up windows. The one distinct advantage of the graphical user interface is that the user is able to modify the network topology and input data quickly.

In PSCAD, the user has online access to input variables, i.e. the user can change parameters during a simulation. Switches, push buttons, sliders and ammeters are examples of the control and meter interfaces available in the program.

In DIgSILENT, the user is able to run a load flow before the dynamic simulation. PSCAD does not perform load flow calculations and hence, the user should have pre-calculated initial conditions for all elements in the power system. The lack of an algorithm for the calculation of the initial condition is a weakness of using this software for the modelling of a large system. The user starts a simulation without a disturbance and brings the system to steady state operation, after which the disturbance can be applied [150].

A. Steady-state Characteristic

To compare the modelled system in PSCAD/EMTDC and DIgSILENT, the models must be verified. The active, reactive power and voltage magnitude for each zone in PSCAD/EMTC and DIgSILENT are shown in Figure 3.10, Figure 3.11 and Figure 3.12. As can be seen, the results for active and reactive power flow for each busbar are very close together. The slightly difference between result is because of different saturation characteristics of the transformer and the generator, as was expected. In terms of voltage magnitude, the system follows exactly the same pattern for increasing and decreasing each busbar for both software tools.

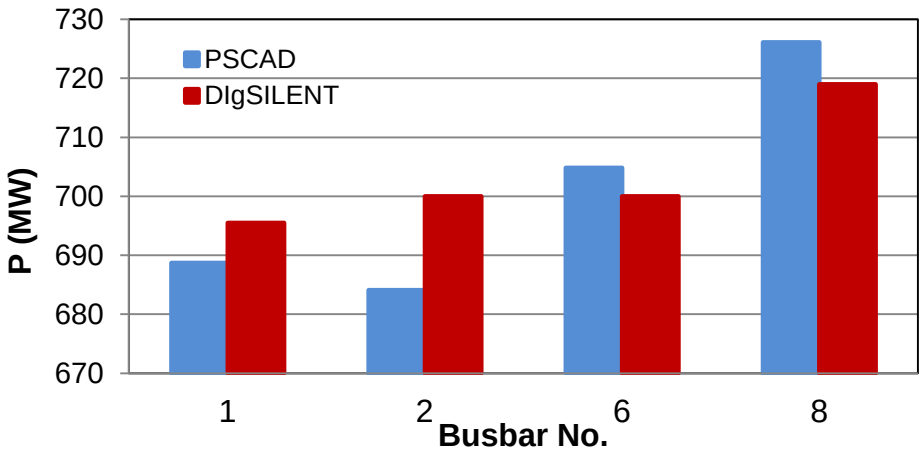

Figure 3.10 Active Power Flow Results in PSCAD/EMTDC and DIgSILENT

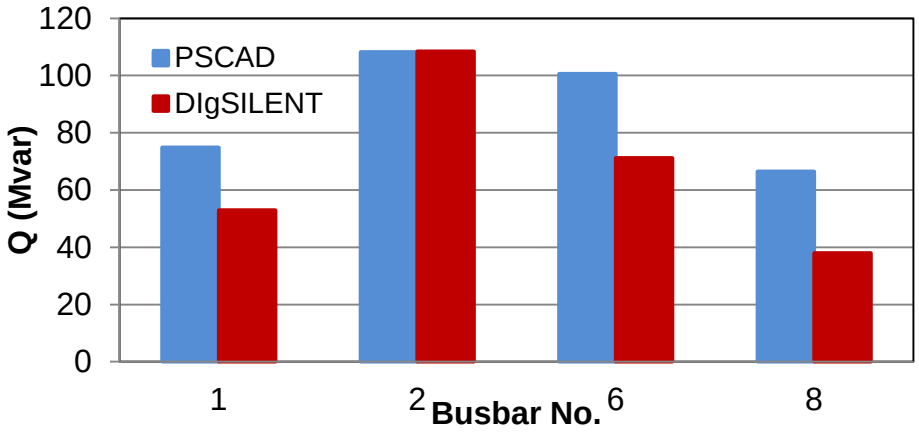

Figure 3.11 Reactive Power Flow Results in PSCAD/EMTDC and DIgSILENT

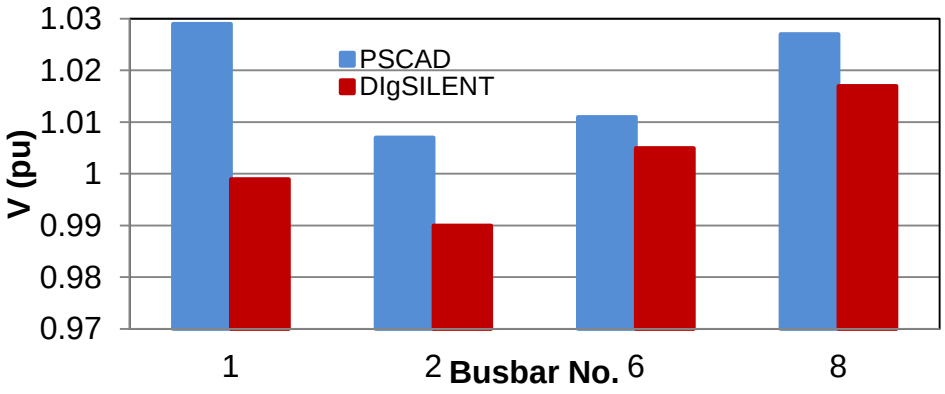

Figure 3.12 Voltage Magnitude Results in PSCAD/EMTDC and DIgSILENT

B. Dynamic Characteristic

To investigate and compare the transient stability, the three-phase fault has been applied at Line 6 and the behaviour of the voltage and active power flow at Line 3 has been monitored as shown in Figure 3.13 and Figure 3.14.The fault is cleared after 100 ms. The aim of this -study was to assess the two aforementioned software tools. It should be noted that some of the data required to reproduce the case was not available. Moreover, the modelling and data of the AVR, governor and saturation curve for the transformer and generator were not given, hence matching the absolute values of the results was difficult. The simulation results for the voltage magnitude for busbar 3 using the two tools are shown in Figure 3.14. It can be observed that the results obtained using

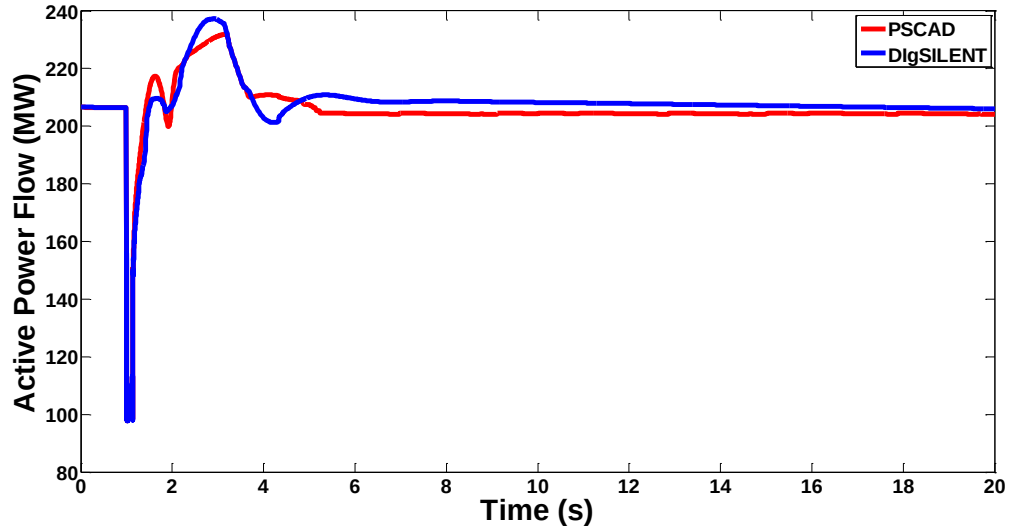

Figure 3.13 Active Power Flow at Line 3

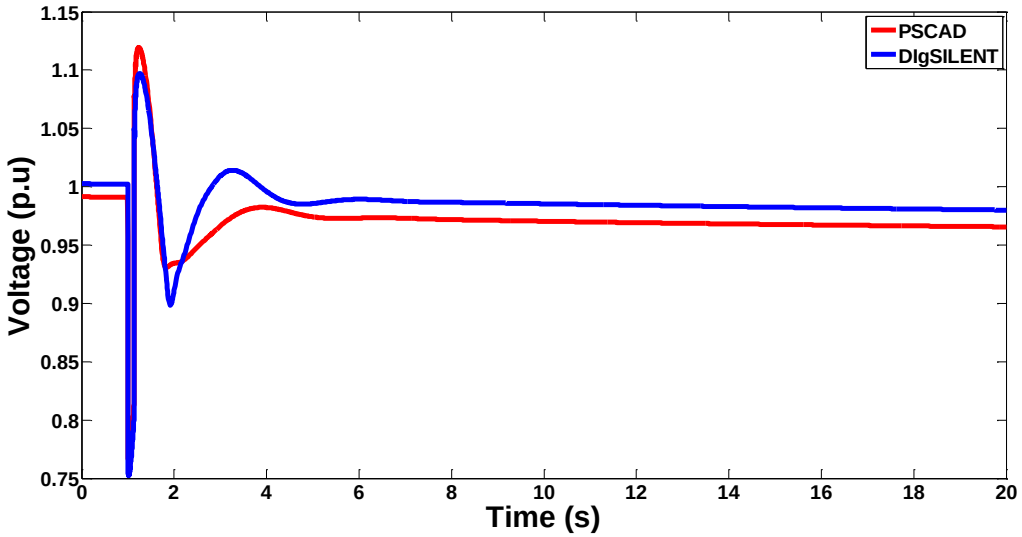

Figure 3.14 Voltage Magnitude at Busbar3

DIgSILENT and PSCAD are similar, but, in post-fault, those for PSCAD exhibited better damping than the other tool.

3.4.2 Large Test System

Figure 3.15 shows a single line diagram of the model consisting of 37 substations, inter connected through 64 transmission lines. It contains 67 generators of various

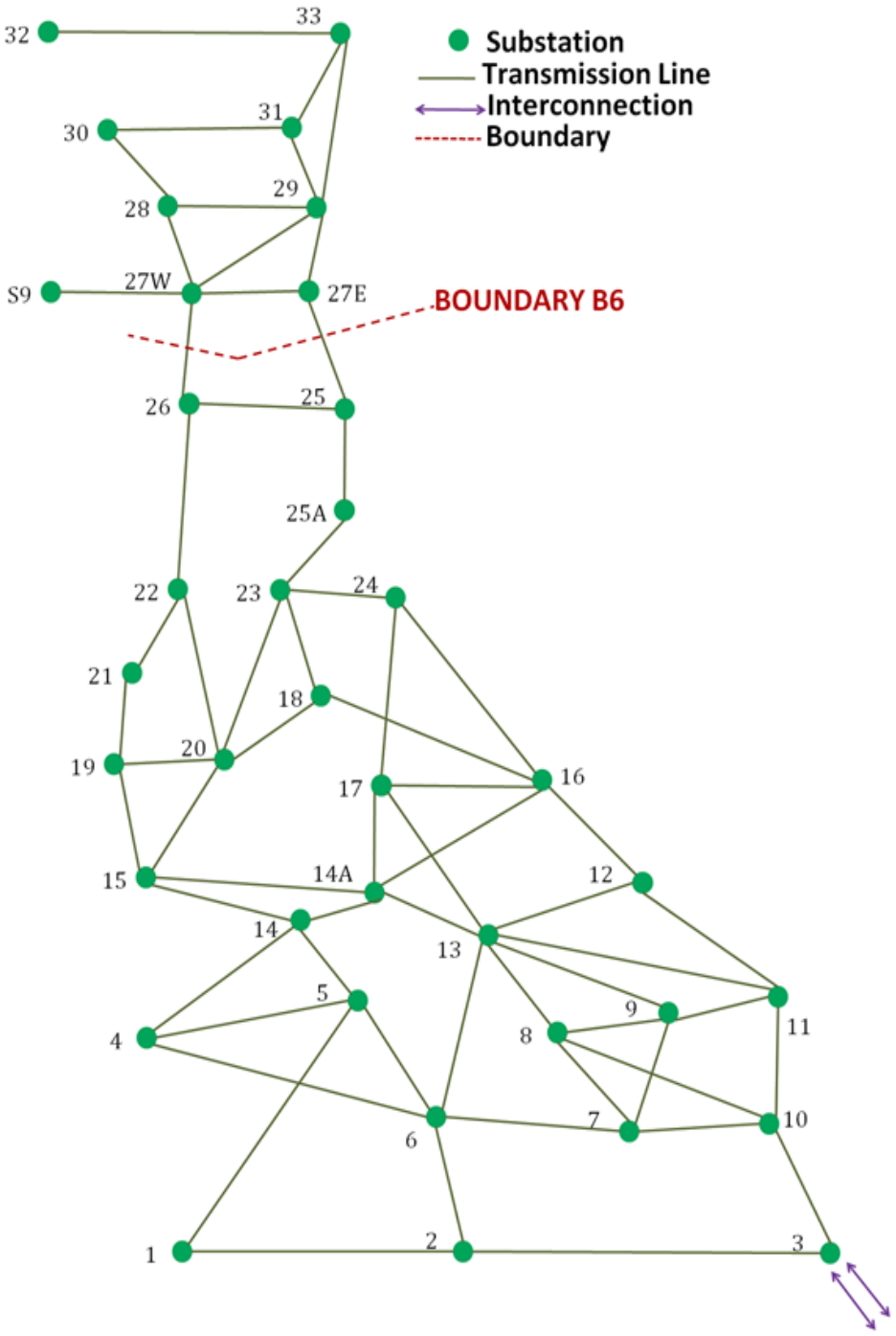

Figure 3.15 Representative GB Transmission Network

generation types, 23 SVCs and 36 loads. These network branches are intended to represent the main routes on which power flows across the GB transmission system [24].

- **Synchronous Generator**

A fifth order generator model is used to represent salient pole machines, which is similar to the sixth order model, but has only one damper winding on the q-axis. These two models are available in both DIgSILENT and PSCAD software and both tools have fifth and sixth order degrees of complexity [150].

- **Excitation**

Static excitation systems supply direct current to the generator field winding through the rectifiers, which are fed by either transformers or auxiliary machine windings. A simplified version of this consists of a voltage transducer delay, an exciter and Transient Gain Reduction (TGR). The signal EPSS is a stabilising signal from the PSS, if one is used in conjunction with the exciter.

The exciter model used in PSCAD/EMTDC is an IEEE type STlA excitation one and the schematic in PowerFactory that defines the AVR model is presented in Figure 3.16.

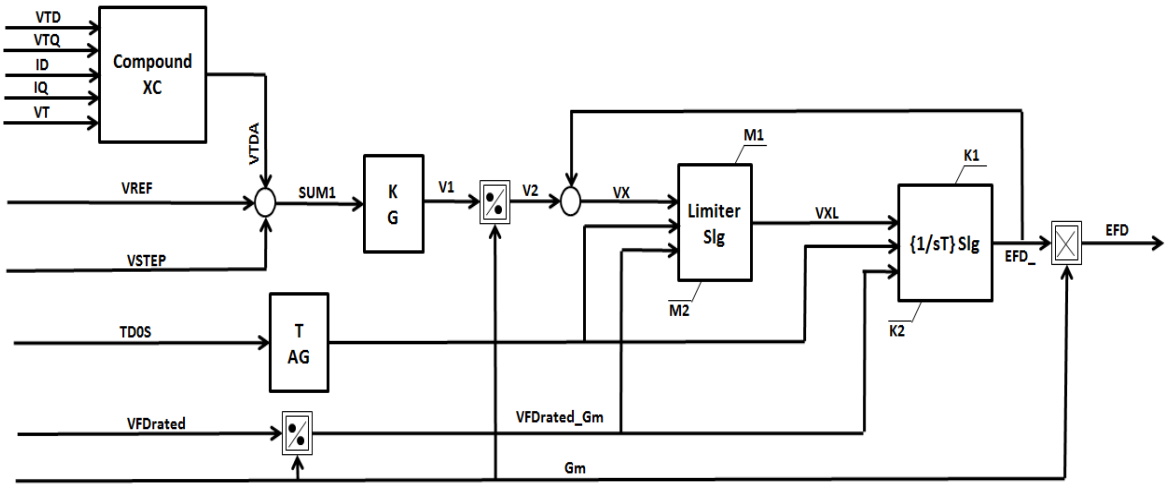

Figure 3.16 The AVR Model in DIgSILENT

- **Transmission**

Throughout the work presented in this chapter, for large test system, in both PSCAD/EMTDC and DIgSILENT PowerFactory transmission lines are modelled using a lumped parameter model and common representation.

A simple Pi section model will give the correct fundamental impedance, but cannot accurately represent other frequencies unless many sections are used (which is inefficient). It also cannot accurately represent the frequency dependent parameters of a (such as the skin effect) [151].

- **Simulation Result**

A reduced model of the GB transmission system has been modelled for this research and is presented in Figure 3.15. The effort has been made to inter similar data as two software tools allow. However, for some components, such as generators and transformers, because of their different characteristics, different information was needed.

A. Steady-state Characteristic

In order to compare the modelled system in PSCAD/EMTDC and DIgSILENT, the active, reactive power and voltage magnitude for each zone in PSCAD/EMTC and DIgSILENT are shown in Figure 3.17, Figure 3.18 and Figure 3.19. As can be seen, the results for active and reactive power flow for some zones are very close together, and for some others the difference is up to 20%. This is because of the different saturation characteristics of the transformer and the generator, as was expected (Figure 3.17 and Figure 3.18). In terms of voltage magnitude, the system follows exactly the same pattern for increasing and decreasing each zone for both software tools, as shown in Figure 3.19. The largest difference is for Zone number 32, which is 5%.

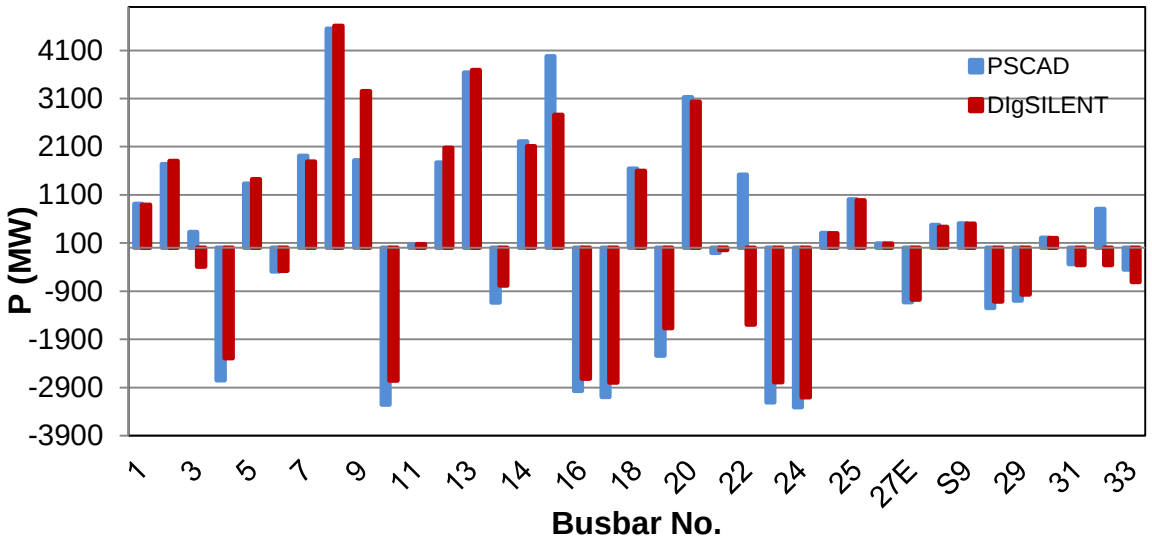

Figure 3.17 Active Power Flow Results in PSCAD/EMTDC and DIgSILENT

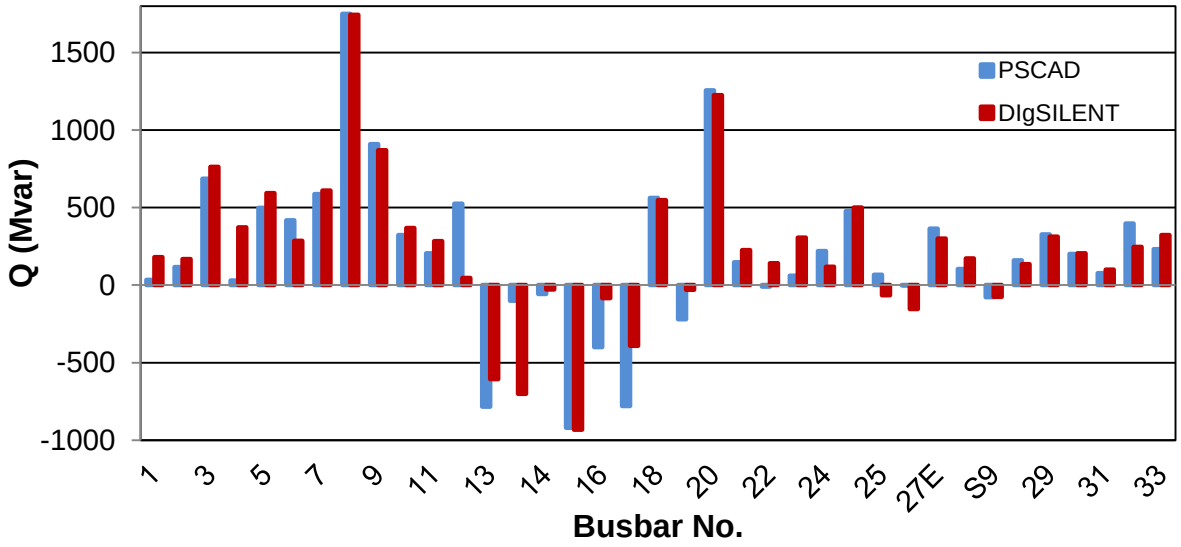

Figure 3.18 Reactive Power Flow Results in PSCAD/EMTDC and DIgSILENT

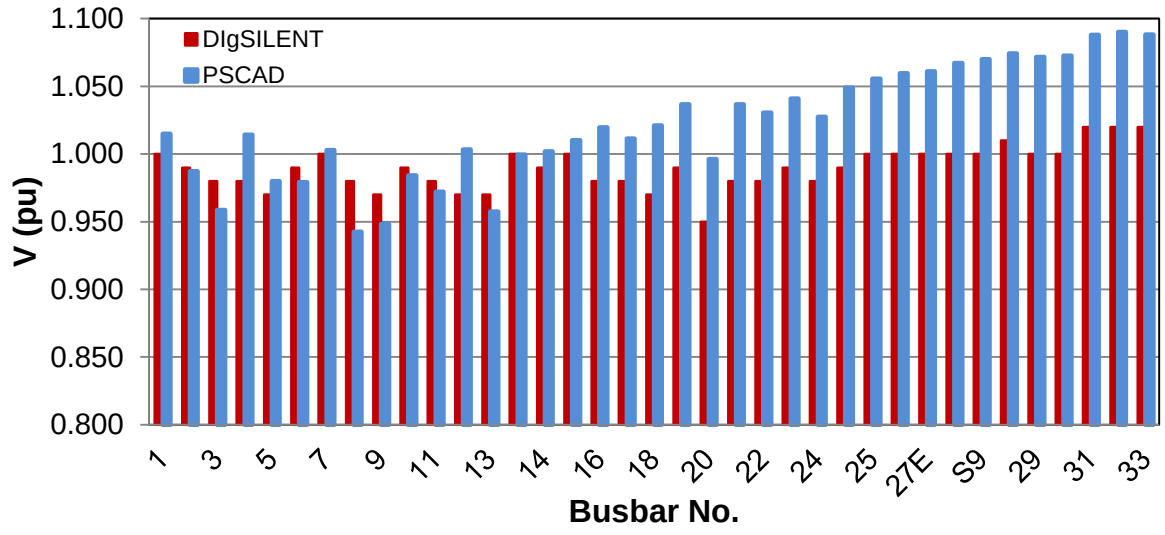

Figure 3.19 Voltage Magnitude Results in PSCAD/EMTDC and DIgSILENT

B. Dynamic Characteristic

To investigate and compare the transient stability, the three-phase fault has been applied at Zone 1 and the behaviour of the G2 (nuclear generator) at this busbar, in terms of voltage and active power flow, has been monitored as shown in Figure 3.20 and Figure 3.21.

The pre-fault system condition base is:

DIgSILENT: P = 1026 MW and V= 0.998 p.u.

PSCAD/EMTDC: P = 1056 MW and V= 0.96 p.u.

The fault is cleared after 50 ms, which is the critical fault clearing time for this model in PSCAD/EMTDC.

The aim of this study was to assess the two aforementioned software tools. It should be noted that some of the data required to reproduce the case was not available. Moreover, the modelling and data of the AVR, governor and saturation curve for the transformer and generator were not given, hence matching the absolute values of the results was difficult.

The simulation results for the voltage magnitude for Zone 1 using the two tools are shown in Figure 3.20. It can be observed that the results obtained using DIgSILENT and PSCAD are similar, but, in post-fault, those for PSCAD exhibited better damping than the other tool. In terms of voltage stability, both software tools agreed well when

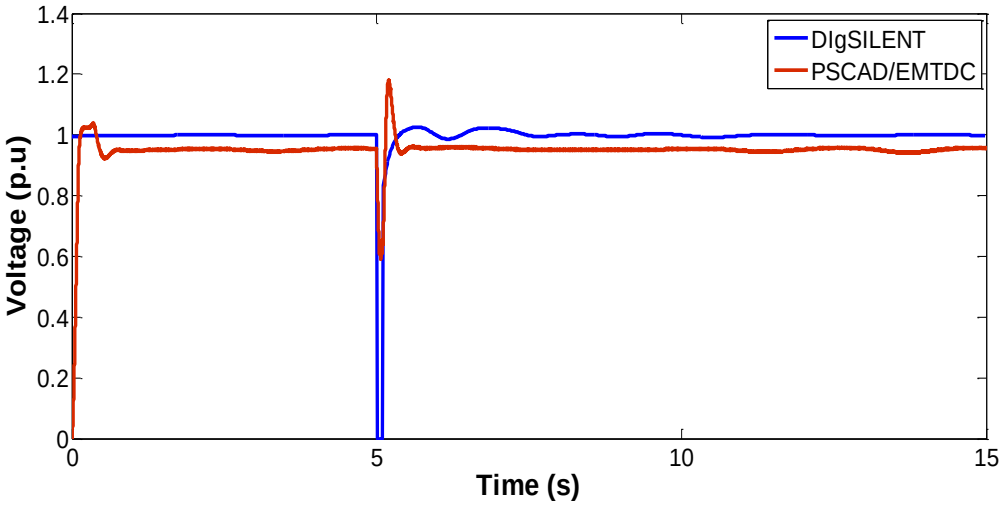

Figure 3.20 Voltage Magnitude at Zone 1

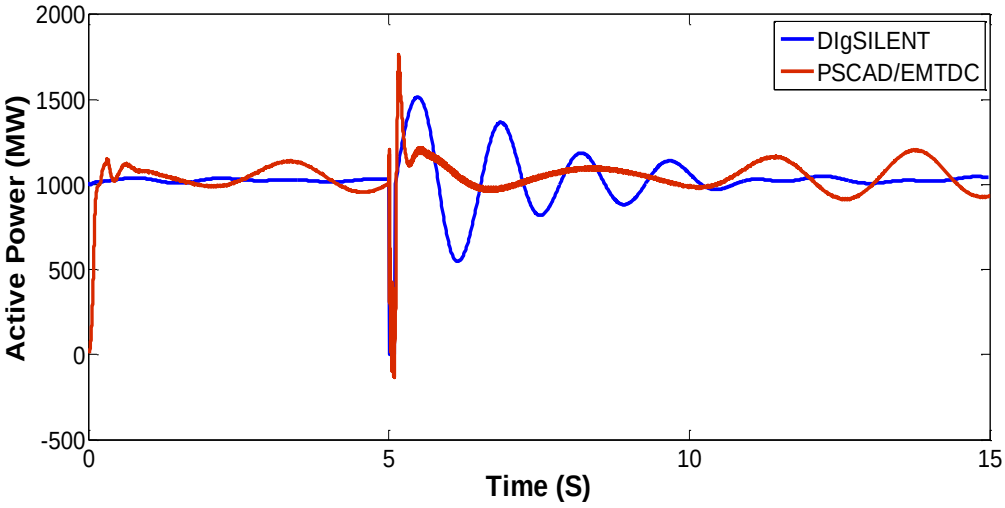

Figure 3.21 Active Power Flow for G2 (Nuclear Generator) at Zone 1

both the AVR and PSS were modelled, which might be attributed to the presence of the PSS, which damps the oscillations.

Figure 3.21 shows the results for active power flow in DIgSILENT and PSCAD, where it can be seen that, for both software tools, the active power flow is not quite settled. The period of this oscillation in PSCAD is more than DIgSILENT, but the overshot in the latter is bigger than for the former. This can be associated with the action of a governor, which improves the recovery of the power flow after disturbance. In sum, this system for stability analysis study needs further improvement and a different type of governor should be tested for this model.

3.5 Concluding Remarks

In this chapter, two area Kondure model and a reduced model of the GB transmission system were developed within a PSACD/EMTDC platform. The performance of the developed systems were compared and confirmed with the DIgSILENT model. The results show that both models respond similarly to three phase to ground fault, although there are slight differences in the transient period and post-fault, which might be due to numerical solving issues in the control system that relate to the different solvers used in the two software tools. Nevertheless, the results show, in terms of active and reactive power flow, that both software tools provide similar results. The difference between the active and reactive power flow for some zones was expected, because the tools employ different models, components as well as analytical and numerical algorithms.

Chapter 4

Probabilistic Small-Disturbance Stability Assessment

4.1 Introduction

One of the most important requirements for the operation of a power system is knowing all the forms of security constraints under different operating conditions. Specifically, this refers to determining the assessment of limits associated with both static and dynamic constraints, including rotor angle stability, voltage stability and frequency stability, for if these are exceeded it could result in system failures and also severe consequences such as system blackouts [158],[159], Regarding system stability assessment ,voltage and frequency stability are the main parts to consider for dynamic constraints [160]. The small signal stability (SSS) problem is usually because of unsatisfactory damping for oscillations in the power system [161].

Traditionally, to evaluate SSS only the worst case scenario or a few scenarios have been considered. These studies, generally, have been based on established techniques, such as modal or Prony analysis [131]. However, significant disadvantages of using this method are that it is that not possible to have the stochastic nature of power system behaviour and not all the information regarding the instability risk of the system can be obtained [131], [124], [162].

At first step, in order to analyse the power system stability and design the controllers, linearization of the power system is described mathematically in this chapter, through modal analysis section. The modal analysis includes eigenvalues, eigenvectors, participation factors, modal controllability and observability as well as residues.

Throughout this thesis, the DIgSILENT PowerFactory environment (version 15) has been used for modelling of component

4.2 Power System Analysis

4.2.1 Modal Analysis

For the study of the electromechanical oscillations of the power system, the linearized model around the steady state point is needed [163]. Modal analysis not only is used to determine the oscillatory modes and the sources of the oscillatory modes, but also, the achieved parameters from this analysis tool are needed for designing oscillation controllers.

The modal analysis will be introduced in this section and tool will then be used to explain the physical phenomenon of inter-area oscillations of the test system.

1. Power System Linearization for Modal Analysis

The power system can be modelled using a group of first order nonlinear differential equations with the following form [11]:

$$\dot{\boldsymbol{x}} = \boldsymbol{f}(\boldsymbol{x}, \boldsymbol{u}) \qquad \textbf{(4. 1)}$$

where:

$$\boldsymbol{x} = \begin{bmatrix} \boldsymbol{x_1} \\ \boldsymbol{x_2} \\ \dots \\ \boldsymbol{x_n} \end{bmatrix}, \boldsymbol{u} = \begin{bmatrix} \boldsymbol{u_1} \\ \boldsymbol{u_2} \\ \dots \\ \boldsymbol{u_r} \end{bmatrix}, \boldsymbol{f} = \begin{bmatrix} \boldsymbol{f_1} \\ \boldsymbol{f_2} \\ \dots \\ \boldsymbol{f_n} \end{bmatrix}$$

$\boldsymbol{x}$: the state vector.

$\boldsymbol{x_i}$: the elements of the state variables.

$\boldsymbol{n}$: the number of system states.

$\boldsymbol{u}$: the vector of inputs to the system,

$\boldsymbol{r}$: the number of inputs.

$\boldsymbol{f}$: the vector of the differential equations.

The outputs of the system, in terms of the state variables and the input variables, can be written as:

$$\boldsymbol{y = g(x, u)} \qquad \textbf{(4. 2)}$$

where:

$$\boldsymbol{y} = \begin{bmatrix} \boldsymbol{y_1} \\ \boldsymbol{y_2} \\ \dots \\ \boldsymbol{y_m} \end{bmatrix} \; and \; \boldsymbol{g} = \begin{bmatrix} \boldsymbol{g_1} \\ \boldsymbol{g_2} \\ \dots \\ \boldsymbol{g_m} \end{bmatrix}$$

y: the vector of outputs

g: the vector of nonlinear functions for calculating the system outputs

m: the number of system outputs

All the derivatives $\boldsymbol{\dot{x}_1, \dot{x}_2, \dots, \dot{x}_n}$ are simultaneously zero at equilibrium points where all the variables are unvarying with time and are constant. Which means in this case, the system is in steady state and can be represented by the equation (4. 3):

$$\boldsymbol{\dot{x}_0 = f(x_0, u_0) = 0} \qquad \textbf{(4. 3)}$$

where,

$\boldsymbol{x}$: the state vector at the equilibrium point

$\boldsymbol{u}$: the input vector at the equilibrium point.

By assuming the system is disturbed from its equilibrium point by small deviations ($\boldsymbol{x = x_0 + \Delta x}$, $\boldsymbol{u = u_0 + \Delta u}$) , equation (4. 1) can be written as following form:

$$\boldsymbol{\dot{x} = f[\,(x_0 + \Delta x\,), (u_0 + \Delta u)]} \qquad \textbf{(4. 4)}$$

As the prefix Δ denotes a small deviation, the nonlinear equation (4. 4**)** can be approximated using a Taylor series expansion in terms of $\Delta \mathbf{x}$ and $\Delta \mathbf{u}$**.** It should be mentioned that the first order term of this expansion has been considered. As a result:

$$\dot{\boldsymbol{x}}_{\boldsymbol{i}} = \dot{\boldsymbol{x}}_{\boldsymbol{io}} + \Delta\,\dot{\boldsymbol{x}}_{\boldsymbol{i}} = \boldsymbol{f}_{\boldsymbol{i}}[(\boldsymbol{x_0} + \Delta\boldsymbol{x}), (\boldsymbol{u_0} + \Delta\boldsymbol{u})]$$
$$= \boldsymbol{f}_{\boldsymbol{i}}(\boldsymbol{x_0}, \boldsymbol{u_0}) + \left(\frac{\boldsymbol{\partial f_i}}{\boldsymbol{\partial x_1}}\Delta\boldsymbol{x_1} + \cdots + \frac{\boldsymbol{\partial f_i}}{\boldsymbol{\partial x_n}}\Delta\boldsymbol{x_n}\right) \quad \textbf{(4. 5)}$$
$$+ \left(\frac{\boldsymbol{\partial f_i}}{\boldsymbol{\partial u_1}}\Delta\boldsymbol{u_1} + \cdots + \frac{\boldsymbol{\partial f_i}}{\boldsymbol{\partial u_m}}\Delta\boldsymbol{u_m}\right)$$

As $\dot{\boldsymbol{x}}_{\boldsymbol{io}} = \boldsymbol{f}_{\boldsymbol{i}}(\boldsymbol{x_0}, \boldsymbol{u_0})$, equation (4. 5) can be written as:

$$\Delta\dot{\boldsymbol{x}}_{\boldsymbol{i}} = \frac{\boldsymbol{\partial f_i}}{\boldsymbol{\partial x_1}}\Delta\boldsymbol{x_1} + \cdots + \frac{\boldsymbol{\partial f_i}}{\boldsymbol{\partial x_n}}\Delta\boldsymbol{x_n} + \frac{\boldsymbol{\partial f_i}}{\boldsymbol{\partial u_1}}\Delta\boldsymbol{u_1} + \cdots + \frac{\boldsymbol{\partial f_i}}{\boldsymbol{\partial u_m}}\Delta\boldsymbol{u_m} \quad \textbf{(4. 6)}$$

where, i=1,2,…,n.

And similarly, based on equation (4. 2):

$$\Delta\boldsymbol{y_j} = \frac{\boldsymbol{\partial g_j}}{\boldsymbol{\partial x_1}}\Delta\boldsymbol{x_1} + \cdots + \frac{\boldsymbol{\partial g_j}}{\boldsymbol{\partial x_n}}\Delta\boldsymbol{x_n} + \frac{\boldsymbol{\partial g_j}}{\boldsymbol{\partial u_1}}\Delta\boldsymbol{u_1} + \cdots + \frac{\boldsymbol{\partial g_j}}{\boldsymbol{\partial u_r}}\Delta\boldsymbol{u_r} \quad \textbf{(4. 7)}$$

where, j=1,2,…,m.

Therefore, the linearised form of state equation around the equilibrium point is expressed as:

$$\Delta\dot{\boldsymbol{x}} = \boldsymbol{A}\Delta\boldsymbol{x} + \boldsymbol{B}\Delta\boldsymbol{u} \quad \textbf{(4. 8)}$$

$$\Delta\boldsymbol{y} = \boldsymbol{C}\Delta\boldsymbol{x} + \boldsymbol{D}\Delta\boldsymbol{u} \quad \textbf{(4. 9)}$$

where:

$$\boldsymbol{A} = \begin{bmatrix} \frac{\boldsymbol{\partial f_1}}{\boldsymbol{\partial x_1}} & \cdots & \frac{\boldsymbol{\partial f_1}}{\boldsymbol{\partial x_n}} \\ \vdots & \ddots & \vdots \\ \frac{\boldsymbol{\partial f_n}}{\boldsymbol{\partial x_1}} & \cdots & \frac{\boldsymbol{\partial f_n}}{\boldsymbol{\partial x_n}} \end{bmatrix}, \quad \mathbf{B} = \begin{bmatrix} \frac{\boldsymbol{\partial f_1}}{\boldsymbol{\partial u_1}} & \cdots & \frac{\boldsymbol{\partial f_1}}{\boldsymbol{\partial u_r}} \\ \vdots & \ddots & \vdots \\ \frac{\boldsymbol{\partial f_n}}{\boldsymbol{\partial u_1}} & \cdots & \frac{\boldsymbol{\partial f_n}}{\boldsymbol{\partial u_r}} \end{bmatrix}$$

$$\boldsymbol{C} = \begin{bmatrix} \frac{\boldsymbol{\partial g_1}}{\boldsymbol{\partial x_1}} & \cdots & \frac{\boldsymbol{\partial g_1}}{\boldsymbol{\partial x_n}} \\ \vdots & \ddots & \vdots \\ \frac{\boldsymbol{\partial g_m}}{\boldsymbol{\partial x_1}} & \cdots & \frac{\boldsymbol{\partial g_m}}{\boldsymbol{\partial x_n}} \end{bmatrix}, \quad \mathbf{D} = \begin{bmatrix} \frac{\boldsymbol{\partial g_1}}{\boldsymbol{\partial u_1}} & \cdots & \frac{\boldsymbol{\partial g_1}}{\boldsymbol{\partial u_r}} \\ \vdots & \ddots & \vdots \\ \frac{\boldsymbol{\partial g_m}}{\boldsymbol{\partial u_1}} & \cdots & \frac{\boldsymbol{\partial g_m}}{\boldsymbol{\partial u_r}} \end{bmatrix}$$

$\boldsymbol{\Delta x}$: the state vector of length n

$\boldsymbol{\Delta u}$: input disturbance vector of length r

$\boldsymbol{\Delta y}$: the output vector of length *m*

$\boldsymbol{A}$: the state matrix of size $n \times n$

$\boldsymbol{B}$: the input matrix of size $n \times r$

$\boldsymbol{C}$: the output matrix of size $m \times n$

$\boldsymbol{D}$: a matrix of size $m \times r$. this matrix defines the part of the input that directly affects the output $\boldsymbol{\Delta y}$

2. Eigenvalues and Eigenvectors

Equation (4. 10) is defined as the characteristic equation of matrix **A** [11], and the *n* roots of this equation ($\boldsymbol{\lambda = [\lambda_1, \lambda_2, \dots, \lambda_n]}$) are the eigenvalues of the system (A).

$$\mathbf{det}(\boldsymbol{\lambda I - A}) = \mathbf{0} \qquad \textbf{(4. 10)}$$

For any eigenvalue, $\boldsymbol{\lambda_i}$ there is $\boldsymbol{\varphi_i}$ which is an *n*-column vector and can be calculated by:

$$\mathbf{A\varphi_i = \lambda_i \varphi_i} \qquad \textbf{(4. 11)}$$

where: *i=1,…,n*

and:

$$\boldsymbol{\varphi_i} = \begin{bmatrix} \boldsymbol{\varphi_{1i}} \\ \boldsymbol{\varphi_{2i}} \\ \dots \\ \boldsymbol{\varphi_{ni}} \end{bmatrix}$$

This achieved matrix (the right eigenvector) is indicated on which system variables the mode is more observable [164]. This means that information about the observability of the associated mode in the state variable corresponding to each component is included in the right eigenvector of that component and hence, this eigenvector is called the mode shape .The associated magnitudes for each element of $\boldsymbol{\varphi_i}$ show the amount of the behaviours of the *n* state variables in the $\boldsymbol{i^{th}}$ mode and the achieved angles of the elements show the phase movements of the state variables with regards to the associated mode.

Likewise, the left eigenvalue of the system (A) associated with the eigenvalue $\boldsymbol{\lambda_i}$ can be calculated using equation (4. 12) and the form of this matrix has been presented in equation (4. 13):

$$\boldsymbol{\psi_i A = \lambda_i \psi_i} \qquad \textbf{(4. 12)}$$

where: $i=1,\ldots,n$

$$\boldsymbol{\psi_i = [\psi_{i1} \quad \psi_{i2} \quad \ldots \quad \psi_{in}]} \qquad \textbf{(4. 13)}$$

The achieved matrix ($\boldsymbol{\psi_i}$) is associated with a mode provides the distribution of the states within a mode, which means that the information about the controllability of the mode for each component can be found in the left eigenvector.

3. Participation Factors

One problem in using the both right and left eigenvectors independently for identifying the relationship between the states and the modes is that their elements are dependent on the units and scaling related to the state variables. A solution for this problem is a participation matrix ($\boldsymbol{P}$). This Matrix combines the right and left eigenvectors and is used as the measure of the association between the state variables and the modes. The concept of participation factor was developed in [165] initially to measure the degree of participation of a state variable in a mode [3].

$$\boldsymbol{P = [p_1 \quad p_2 \quad \ldots \quad p_n]} \qquad \textbf{(4. 14)}$$

$$\boldsymbol{P_i = \begin{bmatrix} p_{1i} \\ p_{2i} \\ \ldots \\ p_{ni} \end{bmatrix} = \begin{bmatrix} \phi_{1i}\psi_{1i} \\ \phi_{2i}\psi_{2i} \\ \ldots \\ \phi_{ni}\psi_{ni} \end{bmatrix}} \qquad \textbf{(4. 15)}$$

where,

$\boldsymbol{\phi_{ki}}$: the kth entry of the right eigenvector $\boldsymbol{\varphi_i}$

$\boldsymbol{\psi_{ik}}$: the kth entry of the left eigenvector $\boldsymbol{\psi_i}$

The element $\boldsymbol{P_{ik}}$ presents the participation factor ($\boldsymbol{P_{ik} = \varphi_{ki} \cdot \psi_{ik}}$). In this calculation $\boldsymbol{\varphi_{ki}}$ measures the activity of $\boldsymbol{x_k}$ in the $\boldsymbol{i^{th}}$ mode and $\boldsymbol{\psi_{ik}}$ weights the impact of this activity to the mode. Therefore, the net participation $\boldsymbol{P_{ik}}$ of the $\boldsymbol{k^{th}}$ state to $\boldsymbol{i^{th}}$ mode can be calculated by multiplying the right and left eigenvalues. As a result of using this method for calculation of the participation factors, the source of an oscillatory mode can be identified for each state.

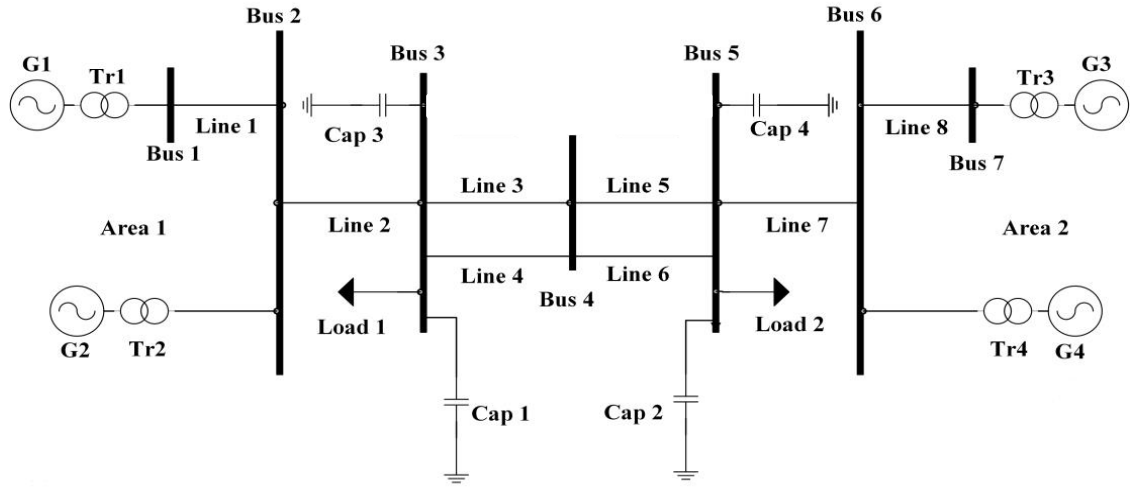

Figure 4.1 Schematic of the Two-Area Four-Machine System

4.3 Test Networks

The test system which has been presented in this study is the four-machine two area network, taken from Kundur [11]. This system not only is an appropriate case study for investigating the physical nature of low frequency electromechanical power oscillations in the time domain, but also can be considered as a useful tool for the study of electromechanical oscillations in the GB power system. Area 1 and area 2 can be presented as the Scottish and the English power systems respectively. In this research, this system is studied with and without HVDC.

4.3.1 System without HVDC

The four-machine two area network is shown in Figure 4.1. In this study, each generator is equipped with an AVR and governor. However, no PSS is installed for better

Table 4.1 Power Flow and Voltage Magnitude for System without HVDC

Line No.	From Bus	To Bus	Active Power (MW)	Reactive Power (MVAr)	Voltage (p.u)
1	1	2	695.5	52.9	1.015
2	2	3	1383.7	-34.4	0.999
3	3	4	198.7	-0.5	0.998
4	3	4	198.7	-0.5	0.998
5	4	5	194.2	-25	0.99
6	4	5	194.5	-25.1	0.99
7	6	5	1406.5	-92.5	1.01
8	7	6	719	38	1.005

illustration of the inter-area oscillation between two areas of the system. The full set of the system parameters, i.e. the generator, transformer and transmission line parameters, as well as the controller settings of the Automatic Voltage Regulator (AVR) and Turbine Governor (TG) are presented in Appendix A.

The active and reactive power flow and voltage for each line are presented inTable 4.1. This simple model shows the electromechanical oscillations that are inherent in the two area system and there are three possible modes in this system.

Containing two local modes, one is related to generator 1 swinging against generator 2, and another is associated to generator 3 swinging against generator 4. In addition, there is also one inter-area mode, in which the generators in area 1 swing against the generators in area 2. The oscillatory modes and their information are presented in Table 4.2. There are three electromechanical oscillatory modes, two of which have a damping factor around 0.46 (mode 2 and 3), and a third that is unstable (mode 1). The other five oscillatory modes are the excitation and governor control modes. As shown in Table 4.2, the frequency of the two local modes is 1 Hz, and that of the inter-area mode is 0.55 Hz.

Table 4.2 Eigenvalues of Test System without HVDC

No.	Real Part	Imaginary Part	Damped Frequency (Hz)	Damping Factor (1/s)	No.	Real Part	Imaginary Part	Damped Frequency (Hz)	Damping Factor (1/s)
1	0.02	3.44	0.55	-0.02	21	-0.97	-1.07	0.17	0.97
2	-0.46	6.28	1.00	0.46	22	-1.65	-1.66	0.26	1.65
3	-0.46	6.49	1.03	0.46	23	0.02	-3.44	0.55	-0.02
4	-1.65	1.66	0.26	1.65	24	-5.62	0.00	0.00	5.62
5	-0.97	1.07	0.17	0.97	25	-5.67	0.00	0.00	5.67
6	-0.33	1.02	0.16	0.33	26	-0.46	-6.28	1.00	0.46
7	-0.41	0.64	0.10	0.41	27	-0.46	-6.49	1.03	0.46
8	-0.39	0.63	0.10	0.39	28	-10.22	0.00	0.00	10.22
9	-3.45	0.00	0.00	3.45	29	-10.21	0.00	0.00	10.21
10	-1.11	0.00	0.00	1.11	30	-10.15	0.00	0.00	10.15
11	-1.59	0.00	0.00	1.59	31	-10.16	0.00	0.00	10.16
12	-1.82	0.00	0.00	1.82	32	-16.42	0.00	0.00	16.42
13	-1.94	0.00	0.00	1.94	33	-17.36	0.00	0.00	17.36
14	-1.94	0.00	0.00	1.94	34	-18.77	0.00	0.00	18.77
15	-0.19	0.00	0.00	0.19	35	-18.82	0.00	0.00	18.82
16	-0.20	0.00	0.00	0.20	36	-25.16	0.00	0.00	25.16
17	-0.20	0.00	0.00	0.20	37	-26.21	0.00	0.00	26.21
18	-0.33	-1.02	0.16	0.33	38	-32.28	0.00	0.00	32.28
19	-0.41	-0.64	0.10	0.41	39	-32.38	0.00	0.00	32.38
20	-0.39	-0.63	0.10	0.39	40	-34.32	0.00	0.00	34.32

The eigenvalues and the system state matrix are used to calculate the eigenvectors and participation factors that correspond to the inter-area oscillatory mode. The elements of the right eigenvector corresponding to the 1st eigenvalue, which is associated with the inter-area mode, are given in Table 4.3. Also the elements of the controllability factor corresponding to the 1st eigenvalue, are given in Table 4.4.

To obtain more information about the inter-area oscillatory mode, the participation factors are calculated, as shown in Table 4.5. The states associated with the rotor speed and phase angle of the generators dominate the inter-area oscillatory mode. The participation factors associated with the rotor angles and generator speeds are much

Table 4.3 Observability Factor for Eigenvalue 1 (Inter-area Mode)

Mode No.	Object	State Variables	Observability Mag.	Observability Angle (deg)
1	G2	avr	1	160.9178
1	G1	avr	0.8050	163.1535
1	G2	phi	0.4895	-4.6276
1	G1	phi	0.4486	-5.0980

Table 4.4 Controllability Factor for Eigenvalue 1 (Inter-area Mode)

Mode No.	Object	State Variables	Controllability Mag.	Controllability Angle (deg)
1	G3	speed	1	0
1	G1	speed	0.9837	-179.5797
1	G2	speed	0.700	-177.1394
1	G4	speed	0.6943	3.090

Table 4.5 Participation Factor for Eigenvalue1 (Inter-area Mode)

Mode No.	Object	State Variables	Participation Mag.	Participation Angle (deg)
1	G3	speed	1	0
1	G3	phi	0.9915	177.326
1	G4	phi	0.6354	-179.5859
1	G4	speed	0.6280	3.101

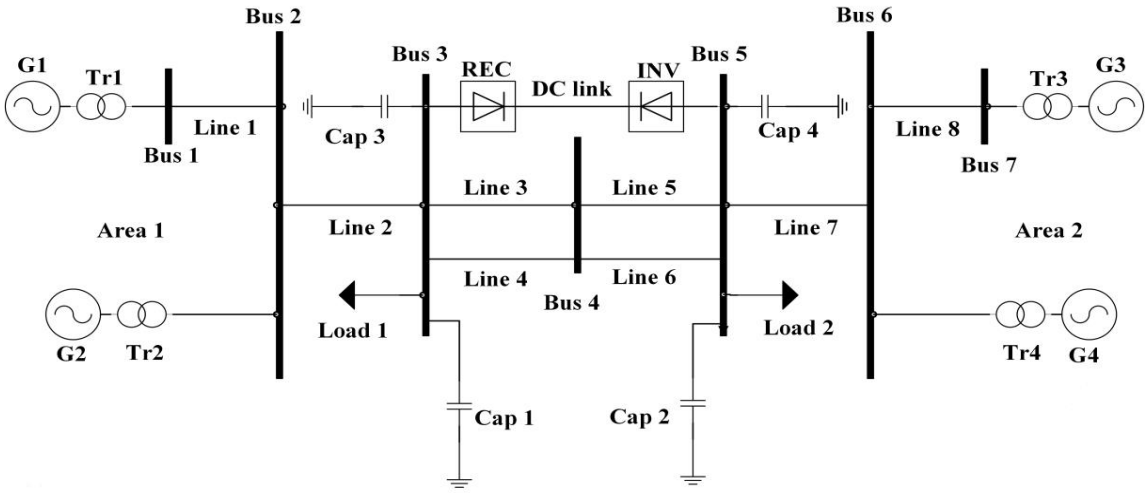

Figure 4.2 Schematic of the Two-Area Four-Machine System Connected with an HVDC Transmission Link.

higher than those relating to the other state variables. These have all been normalized, so that the largest element is 1.00 as this allows for the source of the oscillatory mode to be identified.

4.3.2 System with HVDC

In order to test the system with HVDC link, the four-machine two area network, taken from Kundur [11] incorporated with an LCC-HVDC model as shown in Figure 4.2. In the modified Kundur system, an HVDC link has been added in parallel with an AC transmission corridor between two areas. 100 MW of active power is transferred by LCC-HVDC link that connects two areas of the network in a steady state operating condition. The active and reactive power flow and voltage for each line are presented in Table 4.6. It can be seen this system is contained two local modes, one is related to

Table 4.6 Power Flow and Voltage Magnitude for System with HVDC

Line No.	From Bus	To Bus	Active Power (MW)	Reactive Power (MVAr)	Voltage (p.u)
1	1	2	693.9	84.6	0.986
2	2	3	1381.9	71.6	0.986
3	3	4	144.8	-14.5	0.974
4	3	4	144.8	-14.5	0.974
5	4	5	142.5	-20.5	0.978
6	4	5	142.5	-20.5	0.978
7	6	5	-1386.2	192.5	0.988
8	7	6	-700	-62.2	0.993
HVDC	3	5	105.7	0	1.048

Table 4.7 Eigenvalues of Test System with HVDC

No.	Real Part	Imaginary Part	Damped Frequency (Hz)	Damping Factor (1/s)	No.	Real Part	Imaginary Part	Damped Frequency (Hz)	Damping Factor (1/s)
1	-0.54	6.12	0.97	0.54	21	-0.54	-6.12	0.97	0.54
2	-0.54	6.35	1.01	0.54	22	-16.87	2.15	0.34	16.87
3	0.04	2.95	0.47	-0.04	23	-16.56	0.00	0.00	16.56
4	-1.75	1.60	0.25	1.75	24	-16.87	-2.15	0.34	16.87
5	-0.97	1.03	0.16	0.97	25	-18.69	0.00	0.00	18.69
6	-0.42	0.65	0.10	0.42	26	-18.77	0.00	0.00	18.77
7	-0.42	0.65	0.10	0.42	27	-1013.9	0.00	0.00	1013.95
8	-3.56	0.00	0.00	3.56	28	-999.68	0.00	0.00	999.68
9	-1.33	0.00	0.00	1.33	29	-25.17	0.00	0.00	25.17
10	-0.23	0.00	0.00	0.23	30	-26.43	0.00	0.00	26.43
11	-0.14	0.00	0.00	0.14	31	-32.23	0.00	0.00	32.23
12	0.00	0.00	0.00	0.00	32	-32.38	0.00	0.00	32.38
13	-0.42	-0.65	0.10	0.42	33	-34.44	0.00	0.00	34.44
14	-0.42	-0.65	0.10	0.42	34	-35.03	0.00	0.00	35.03
15	-0.97	-1.03	0.16	0.97	35	-37.04	0.00	0.00	37.04
16	-1.75	-1.60	0.25	1.75	36	-37.07	0.00	0.00	37.07
17	0.04	-2.95	0.47	-0.04	37	-100.09	0.00	0.00	100.09
18	-5.56	0.02	0.00	5.56	38	-100.07	0.00	0.00	100.07
19	-5.56	-0.02	0.00	5.56	39	-100.04	0.00	0.00	100.04
20	-0.54	-6.35	1.01	0.54	40	-100.04	0.00	0.00	100.04

generator 1 swinging against generator 2, and another is associated to generator 3 swinging against generator 4.

In addition, there is also one inter-area mode, in which the generators in area 1 swing against the generators in area 2. The oscillatory modes and their information are presented in Table 4.7.There are three electromechanical oscillatory modes, two of which have a satisfactory damping ratio (1 and 2) (>5%), and a third that is unstable (shaded). The other five oscillatory modes are the excitation and governor control modes. As shown in Table 4.7, the frequency of the two local modes is 1 Hz, and that of the inter-area mode is 0.47 Hz. The eigenvalues and the system state matrix are now

Table 4.8 Observability Factor for Eigenvalue 3 (Inter-area Mode)

Mode No.	Object	State Variables	Observability Mag.	Observability Angle (deg)
3	G3	phi	1	-1.190
3	G4	phi	0.9422	-1.155
3	G2	avr	0.9067	169.6816
3	G1	avr	0.7583	172.076

used to calculate the eigenvectors and participation factors that correspond to the inter-area oscillatory modes. The elements of the right eigenvector corresponding to the 3th eigenvalue, which is associated with the inter-area mode, are given in Table 4.8. Also the elements of the controllability factor corresponding to the 3th eigenvalue are given in Table 4.9.

To obtain more information about the inter-area oscillatory mode, the participation factors are calculated, as shown in Table 4.10. The states associated with the rotor speed and phase angle of the generators dominate the inter-area oscillatory mode. The participation factors associated with the rotor angles and generator speeds are much higher than those relating to the other state variables. These have all been normalized, so that the largest element is 1.00 as this allows for the source of the oscillatory mode to be identified. In order to compare the performance of system with and without HVDC, the associated eigenvalues layouts regarding the oscillatory modes for two systems, are presented in Figure 4.3. As it can be seen in this figure, the eigenvalues which have positive real part are associated with inter-area mode.

Table 4.9 Controllability Factor for Eigenvalue 3 (Inter-area Mode)

Mode No.	Object	State Variables	Controllability Mag.	Controllability Angle (deg)
3	G3	speed	1	0
3	G1	speed	0.9896	-179.2265
3	G2	speed	0.6639	-175.9410
3	G4	speed	0.6487	5.0413

Table 4.10 Participation Factor for Eigenvalue 3 (Inter-area Mode)

Mode No.	Object	State Variables	Participation Mag.	Participation Angle (deg)
3	G3	phi	1	0
3	G4	phi	0.6196	5.8935
3	G3	speed	0.5585	-178.8663
3	G1	speed	0.4196	171.9864

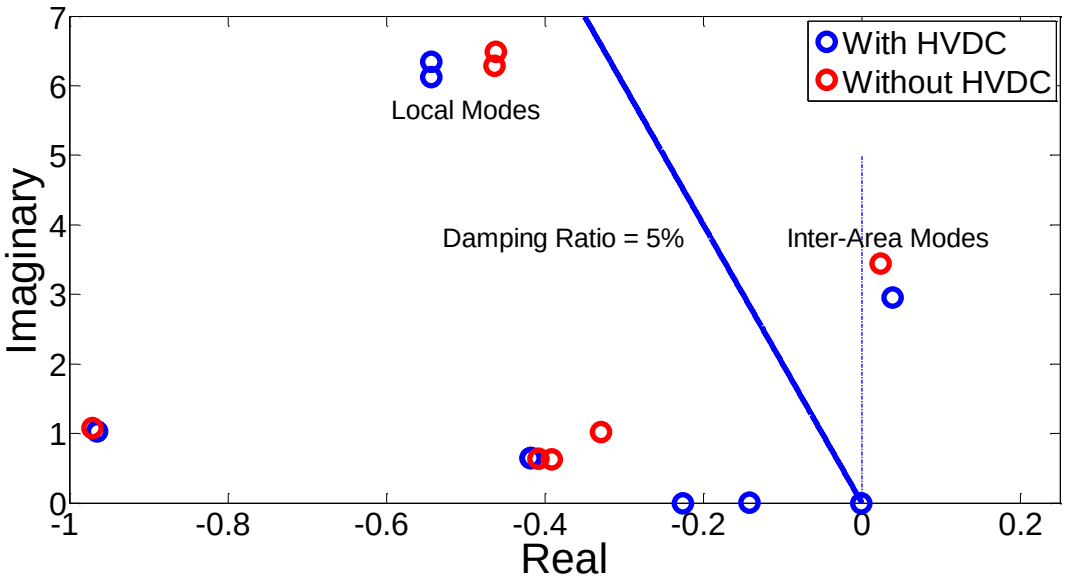

Figure 4.3 Comparison of Oscillatory Modes in the Test Systems with and without HVDC.

4.4 Stability Analysis

4.4.1 Uncertainty Analysis

For analysing a complex system, the effect of uncertainty on a power system should be considered [128], [166]. Uncertainty analysis is associated with the study of functions of the form [128].

$$\boldsymbol{v} = \boldsymbol{h}(\boldsymbol{z}) \qquad \textbf{(4. 16)}$$

where:

$\boldsymbol{h}$: a vector to describe the behaviour of the model

$\boldsymbol{z}$: a vector of input variables

$\boldsymbol{v}$: a vector of output variables

The main aim of uncertainty analysis is to define the uncertainty in the elements of vector $\boldsymbol{v}$ that results from uncertainty in the elements of vector $\boldsymbol{z}$ [131] , [128]. Sensitivity analysis is a typical adjunct to uncertainty analysis, which aims to establish how the uncertainty in individual elements of $\boldsymbol{z}$ has an effect the uncertainty in the elements of $\boldsymbol{v}$ [128].

h, practically, can be a set of complex functions, which in the power system, can be defined as an equation of power system dynamics, and the vectors of input and output variables (***z*** and ***v***) are contain a large amount of elements [128],[131].

The uncertainty analysis of probability theory can be achieved by determining of the probability distribution function (PDF) of the output variables (***v***). The acquired results the function and the PDFs describe the probability space of the input variables (***z***) [131].

4.4.2 Probabilistic Techniques for Small-disturbance Stability Analysis

Small-disturbance stability relates to the ability of a power system to maintain synchronous operation when it is subjected to small disturbances occurring continuously throughout the operation process [167],[11]. When the power system model is linearized and the eigenvalues of the state matrix are calculated, it is possible to identify the system modes of oscillation. Naturally, in large power systems, inter-area, low-frequency and electromechanical oscillations are typically the least damped, most persistent modes, which dominate post-disturbance system behaviour and therefore represent the critical modes in the system. Deterministic, conventional, small-disturbance stability analysis illustrates and characterizes these modes. Probabilistic small-disturbance stability analysis incorporates system uncertainties, for instance, in system loading or power generation from renewable energy sources in small-disturbance stability assessment for the production of statistical distributions of critical modes which describe the behaviour of uncertain power systems more accurately [167].

Probabilistic small-disturbance stability analysis has various efficient estimation methods [167], [168], [10]. A short theoretical background to several of the efficient and frequently used methods is presented in this section, which are explored further and their application demonstrated in successive sections. It is assumed that in all cases the uncertain parameter set is known and that probability density functions are completely detailed for each uncertain input parameter.

For raw moments, standardized moments and central moments of distributions reference is made all through this section [167].

The definitions below relate to a random variable containing a PDF [167], [169].

The n^{th} order raw moment $\propto_n^x$ is represented as:

$$\propto_n^x = \int_{-\infty}^{\infty} x^n f(x) dx \quad \textbf{(4. 17)}$$

The first raw moment is the mean [167].

While the nth order central moment $\boldsymbol{\beta_n^x}$ is represented as:

$$\boldsymbol{\beta_n^x} = \int_{-\infty}^{\infty} (x - \mu_x)^n f(x) dx \quad \textbf{(4. 18)}$$

The second central moment is the variance.

The nth order standardized moment $\boldsymbol{\psi_n^x}$ is represented as:

$$\boldsymbol{\psi_n^x} = \frac{\boldsymbol{\beta_n^x}}{\boldsymbol{\sigma_x^n}} \quad \textbf{(4. 19)}$$

While the third and fourth standardized moments are the measures of skewness and kurtosis of the distribution, in that order.

4.4.3 The Monte Carlo Method

The use of Latin hypercube sampling constitutes part of a procedure, which is often called a Monte Carlo procedure for the propagation of uncertainty. The effectiveness of Monte Carlo method in the assessment of uncertainties has been determined in different engineering fields [131], [128] and it is suitable for studying complex large-scale power systems with high dimensional space of input random variables, this is a suitable procedure. The most important idea here is to draw random samples of system states for the approximation of the arithmetical properties of the system eigenvalues.

For each input set, they are generated at random by applying the MC approach, there is performance of deterministic study which has a, modal identification, load flow, system linearization and eigenvalue analysis, for the calculation of the particulars of critical system modes [167]. By increasing the number of samples, this increases the probability that the distribution of output variation is an accurate representation of the true variation. Consequently, it is necessary to run large numbers of full deterministic studies, which can limit the application of the MC method when performing probabilistic studies on large uncertain power systems. For, many sample data a huge

computational effort may be required in order to obtain reliable estimates. As a result, Monte Carlo method may become prohibitively time consuming [167].

The overall structure of the MC based small signal stability analysis is presented in Figure 4.4. The initial stage of the scheme is the generation of a random number and then a loop of random input variables, load flow and calculation of the system eigenvalues, which is followed by the last stage of analysis of eigenvalues [130].

A random number is required for the first stage in order to provide uniform distribution. The probabilistic models of input variables for subsequent power system analysis must be built as realistic as possible in order to guarantee the accurateness of MC simulation. This process repeats for a particular number (***n***) of cycles. This number is usually determined as no significant statistical variations of the results can be observed [140, 170].

Finally, the statistics of the system parameters, including the damping ratios and eigenvalues, are calculated with the outcomes stored from the preceding stage. Further studies of topics related to stability can be performed based on the consequential statistics [130].

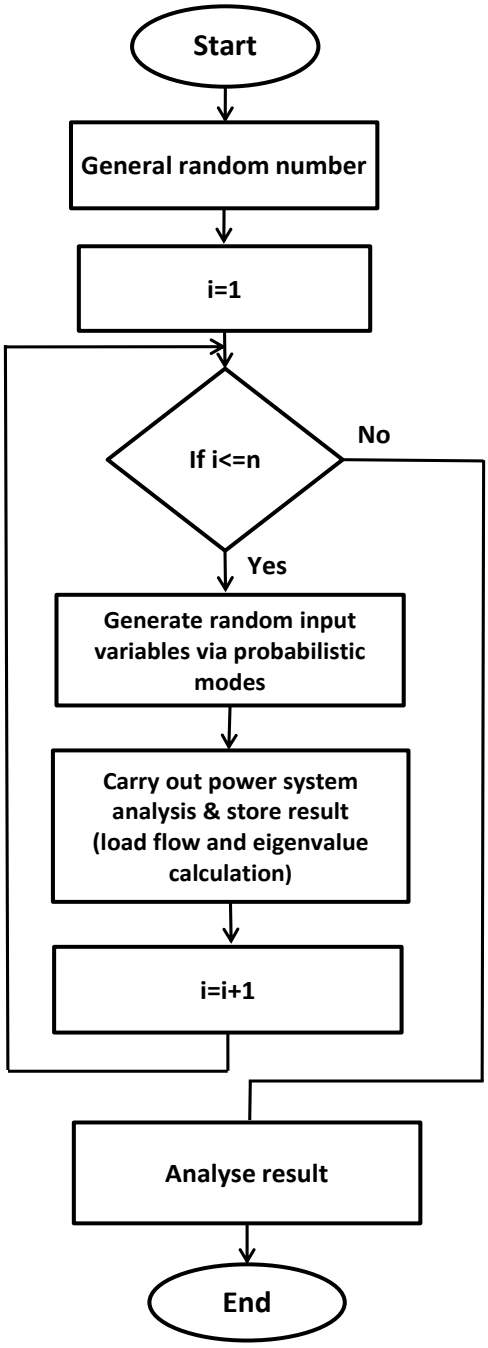

Figure 4.4 Flowchart of Monte Carlo Based Small Signal Analysis [130]

4.4.4 Point Estimated Method

There are several point estimated methods (PEMs) that have been developed, which provide a variety of levels of application regarding probabilistic power system research [167], [168].

All PEMS have the purpose of computing the moments of the system output that is a function of uncertain input variables and with the application of diverse expansion techniques, the distribution can consequently be established.

The PEM techniques applied in this study are taken from [167], [171] and have been shown to be effective when it comes to probabilistic load flow studies in [172]. These approaches cannot be used with correlated system uncertainties but rather, with symmetric or asymmetric variables. There are other PEM approaches and given that input correlation is required, diverse PEM methods like [173], [174] might be more appropriate although they can sacrifice the efficiency and accuracy. PEM variants have been established in [171], where there is the necessity of $\boldsymbol{km}$ or $\boldsymbol{km+1}$ full deterministic study (and $\boldsymbol{k}$ is a positive integer) and they rely on the allocation of input uncertainties. Taking into consideration the input uncertainties with Gaussian distributions in this study, the $\boldsymbol{4m+1}$ PEM variants is examined. The brief details of PEM are presented below, and full details are given in [171] and [172].

There is a requirement of deterministic studies at $\boldsymbol{km}$ or $\boldsymbol{km+1}$ for separate operating points, termed concentrations. The $\boldsymbol{k^{th}}$ concentration is a pair with a location $\boldsymbol{\gamma_{j,k}}$ and an associated weight value $\boldsymbol{w_{j,k}}$. This location represents for the $\boldsymbol{k^{th}}$ value that the variable $\boldsymbol{\gamma_j}$ will take during full deterministic studies.

Only one input variable is varied at a time for PEM deterministic studies, and the remaining uncertainties in $\boldsymbol{\Gamma}$ take their mean values $\boldsymbol{\mu_{\gamma_j}}$. For this reason, only one $\boldsymbol{km}$ deterministic study needed, i.e. $\boldsymbol{k}$ variations of each $\boldsymbol{m}$ uncertain inputs. For the $\boldsymbol{km+1}$ PEM variants, a further deterministic study is completed with all uncertainties at their mean values [167] .

The locations are determined by:

$$\boldsymbol{\gamma_{j,k} = \mu_{\gamma_j} + \zeta_{j,k}\sigma_{\gamma_j}} \qquad \textbf{(4. 20)}$$

where, $\boldsymbol{\mu_{\gamma_j}}$ and $\boldsymbol{\sigma_{\gamma_j}}$ are the mean and standard deviation of the $\boldsymbol{j^{th}}$ uncertain parameter $\boldsymbol{\gamma_{j,k}}$, and $\boldsymbol{\zeta_{j,k}}$ is the standard location [167].

For the determination of the weights and the standard locations the following nonlinear equation must be solved [171].

$$\sum_{k=1}^{K} w_{j,k} = \frac{1}{m}$$

$$\sum_{k=1}^{K} w_{j,k} (\zeta_{j,k})^n = \psi_{j,j}^{\gamma} \quad n = 1, \dots, (2k-1) \tag{4. 21}$$

In Equation (4. 21), $\psi_{j,j}^{\gamma}$ is the nth standardized moment of the nth uncertain parameter γ_j [171]. Based on standard definitions $\psi_{j,1}^{\gamma}$**=0,** $\psi_{j,2}^{\gamma}$**=1,** $\psi_{j,3}^{\gamma}$ is the skewness, and $\psi_{j,4}^{\gamma}$ is the kurtosis of γ_j.

Equation (4. 21) can only be analytically solved where $k=2$. For $k > 2$, numerical solutions are needed. Full deterministic studies are performed for each concentration at the operating point to obtain the value of the system output $Y(j,k)$. These values are subsequently combined with the previously determined weight factors by applying:

$$\alpha_n^Y = E[Y^n] \cong \sum_{j=1}^{m} \sum_{k=1}^{K} w_{j,k} (Y(j,k))^n \tag{4. 22}$$

When determining the n^{th} raw moment α_n^Y of the system output Y, the raw moments α_n^Y are applied to establish the central moment β_n^x of the system output. If sufficient moments are approximated, The PDF of Y can be approximated with the application of a suitable expansion. The problem is that as the order of the estimated raw moment increases, the accuracy of PEM approaches usually deteriorates [172].

- ***2m*** Variant: If principally described by low order moments, distributions generated using this approach will in that case be more accurate ***2m*** Variant. When it comes to the ***2m*** PEM variant, only the first three standardized moments ψ^{γ} of every uncertain input are necessary. The weights and standard locations of the uncertain input γ are calculated using [171]:

$$\zeta_{j,k} = \frac{\psi_{j,3}^{\gamma}}{2} + (-1)^{k+1} \sqrt{m + \left(\frac{\psi_{j,3}^{\gamma}}{2}\right)^2} \tag{4. 23}$$

$$w_{j,1} = \frac{-\zeta_{j,2}}{m(\zeta_{j,1} - \zeta_{j,2})} \quad w_{j,2} = \frac{\zeta_{j,1}}{m(\zeta_{j,1} - \zeta_{j,2})} \tag{4. 24}$$

- ***4m+1*** Variant: For the PEM variant, the standard locations are calculated as the roots of the polynomial (4. 25), where the coefficients are found by solving the linear equations in [171]:

$$f(\zeta) = \zeta^4 + C_3\zeta^3 + C_2\zeta^2 + C_1\zeta + C_0 \tag{4. 25}$$

$$\begin{pmatrix} 0 & 1 & \psi_{j,3}^{\gamma} & \psi_{j,4}^{\gamma} \\ 1 & \psi_{j,3}^{\gamma} & \psi_{j,4}^{\gamma} & \psi_{j,5}^{\gamma} \\ \psi_{j,3}^{\gamma} & \psi_{j,4}^{\gamma} & \psi_{j,5}^{\gamma} & \psi_{j,6}^{\gamma} \\ \psi_{j,4}^{\gamma} & \psi_{j,5}^{\gamma} & \psi_{j,6}^{\gamma} & \psi_{j,7}^{\gamma} \end{pmatrix} \begin{pmatrix} C_0 \\ C_1 \\ C_2 \\ C_3 \end{pmatrix} = - \begin{pmatrix} \psi_{j,5}^{\gamma} \\ \psi_{j,6}^{\gamma} \\ \psi_{j,7}^{\gamma} \\ \psi_{j,8}^{\gamma} \end{pmatrix} \tag{4. 26}$$

The weights of which can be determined by solving:

$$\begin{pmatrix} \zeta_{j,1} & \zeta_{j,2} & \zeta_{j,3} & \zeta_{j,4} \\ \zeta_{j,1}^2 & \zeta_{j,2}^2 & \zeta_{j,3}^2 & \zeta_{j,4}^2 \\ \zeta_{j,1}^3 & \zeta_{j,2}^3 & \zeta_{j,3}^3 & \zeta_{j,4}^3 \\ \zeta_{j,1}^4 & \zeta_{j,2}^4 & \zeta_{j,3}^4 & \zeta_{j,4}^4 \end{pmatrix} \begin{pmatrix} w_{j,1} \\ w_{j,2} \\ w_{j,3} \\ w_{j,4} \end{pmatrix} = - \begin{pmatrix} 0 \\ 1 \\ \psi_{j,3}^{\gamma} \\ \psi_{j,4}^{\gamma} \end{pmatrix} \tag{4. 27}$$

The weight value of w_0 can be calculating by:

$$w_0 = 1 - \sum_{j}^{m} \sum_{k=1}^{K} w_{j,k} \tag{4. 28}$$

Applied in the "+" operating point where all uncertainties take their mean values.

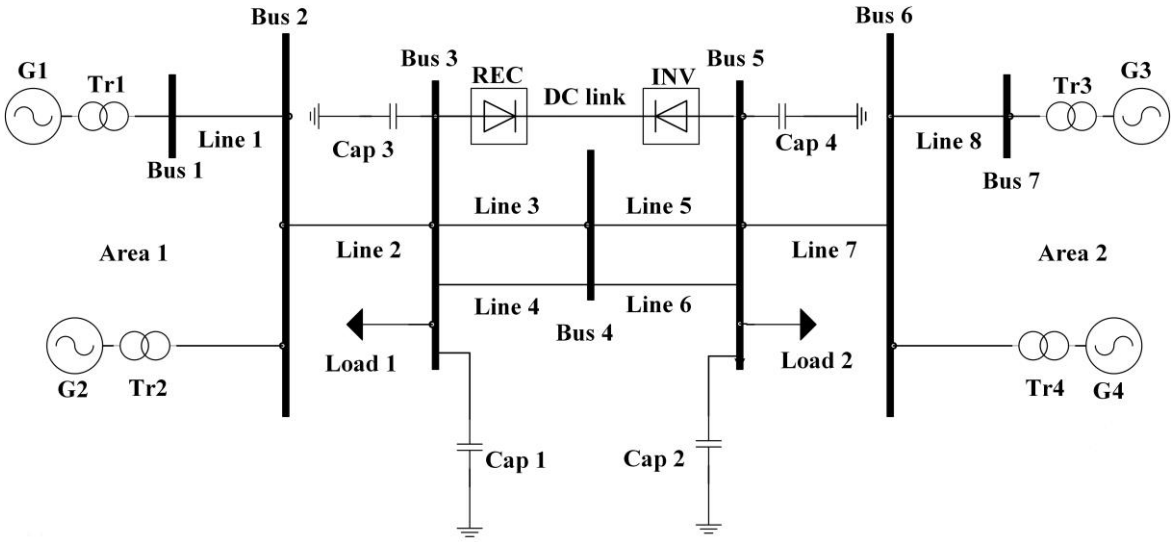

Figure 4.5 Two-area Test Network Including Embedded VSC-HVDC Line

4.4.5 Test System

The efficient estimation methods described in this thesis are illustrated using the four-machine two area network, taken from Kundur [11], as described in Chapter 3, incorporated with an LCC-HVDC model as shown in Figure 4.5 In the modified Kundur system, an HVDC link has been added in parallel with an AC transmission

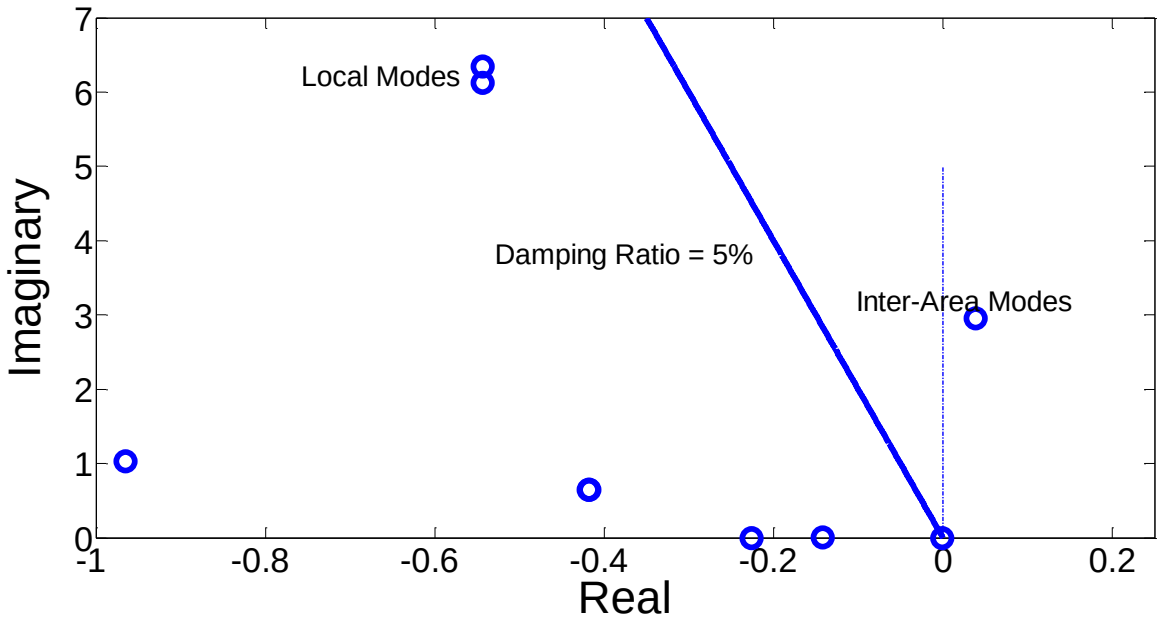

Figure 4.6 Oscillatory Modes in the Test System.

corridor between two areas. All methods and deterministic system studies are performed in the MATLAB/Simulink environment and DIgSILENT/Powerfactory. In this study, each generator is equipped with an AVR and governor. However, no PSS is installed so as to provide better illustration of the inter-area oscillation between the two areas of the system. 100MW of active power is transferred by the LCC-HVDC link that connects the two areas of the network in a steady state operating condition and all generators are represented by full sixth-order models, with system loads being modelled as constant impedance Appendix 1.

The associated eigenvalues layouts regarding the oscillatory modes of this test system are presented in a Figure 4.6. This figure shows the electromechanical oscillations that are inherent in the two area system and there are three possible modes in this system. As it can be seen in this figure, the eigenvalue which has positive real part is associated with inter-area mode. The oscillatory modes and their information are presented in Table 4.11.

To implement above described methods, the probabilistic distribution of the system operating points must be defined. The considered uncertainties are composed for all generator outputs (G_2,G_3,G_4), loads (L_1, L_2) and HVDC active power (P_{dc}). Since all the outputs for the generators have been calculated by the Optimal Power Flow (OPF) method, there are a total of three uncertain parameters (L_1, L_2 and P_{dc}) in the test system being investigated. Loads follow a normal distribution with the nominal operating point assumed to represent 80% of maximum system loading. The full loading represents a $+3\sigma$ increase from the mean nominal values μ [10]. The active power of the HVDC is uniformly distributed between 100 to 300 MW for this case study. Since in practical power systems the behaviour of various loads and generators can be correlated, an OPF determines the generators' output [189].

Table 4.11 Oscillatory Modes in Test System

No.	Real Part	Imaginary Part	Damped Frequency (Hz)	Damping (1/s)
1	-0.54	6.12	0.97	0.54
2	-0.54	6.35	1.01	0.54
3	0.04	2.95	0.47	-0.04

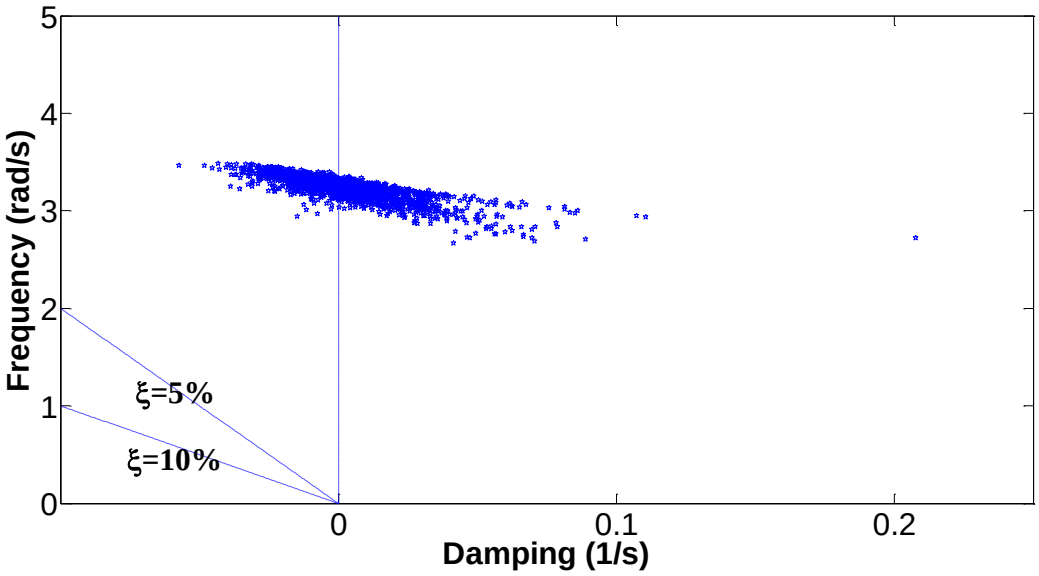

Figure 4.7 Probabilistic Inter-area Mode Locations for the Test System

4.4.6 Simulation and Results

In the first effort probabilistic small signal stability analysis, the sensitivities of the eigenvalues from known statistics of some parameters of the system were determined [124], [132]. It can be assumed that a multivariable normal PDF can be defined to represent the joint PDF of the real parts of the system eigenvalues. According of the assumption the probability when all the real parts of the critical eigenvalues lie on the left half complex plane is computed using the generalized tetrachoric series [132].

The test network displays one inter-area mode and two local modes with damping lower than 0.6 as shown in Figure 4.6. The analysis presented here focusses on these three modes, which are the critical ones for the system. Specifically, the purpose of the simulations is to produce the moments of the damping of this critical electromechanical oscillation.

- **Monte Carlo Method**

The Probabilistic Small-disturbance Stability analysis was evaluated by creating 10,000 distinct operating points using the Monte Carlo (MC) method and Figure 4.7 shows the locations of the inter-area mode for the system without WAC.

The distribution of data values across the data range in terms of damping and the real part of the poles are shown in Figure 4.8. Here, histograms a and d relate to the local

mode 1 (mode number1 as shown in Table 4.11), whilst b and e are associated with local mode 2 (mode number 2) and figures c and f are related to the inter-area mode (mode number 3).

- **Point Estimate Method**

For PEM variants, owing to the large inaccuracy in the estimation of moments above only the mean and st.d. are used to generate pdfs for σ_{crit} [167]. Consequently, a Gaussian distribution has been used for considered PEM variants [167].

It should be noted that the ***4m+1*** PEM variant also provides results with low error [167] and therefore this method has been used in this study. While the PEM method does not impose a parametric distribution for the output, it was found that the estimated moments above second order were too erroneous to be included [167]. The modelling of output distributions was therefore effectively controlled to Gaussian [167].

The Probabilistic Small-Disturbance Stability analysis was evaluated by creating 13 distinct operating points using the Point Estimated Method (PEM).

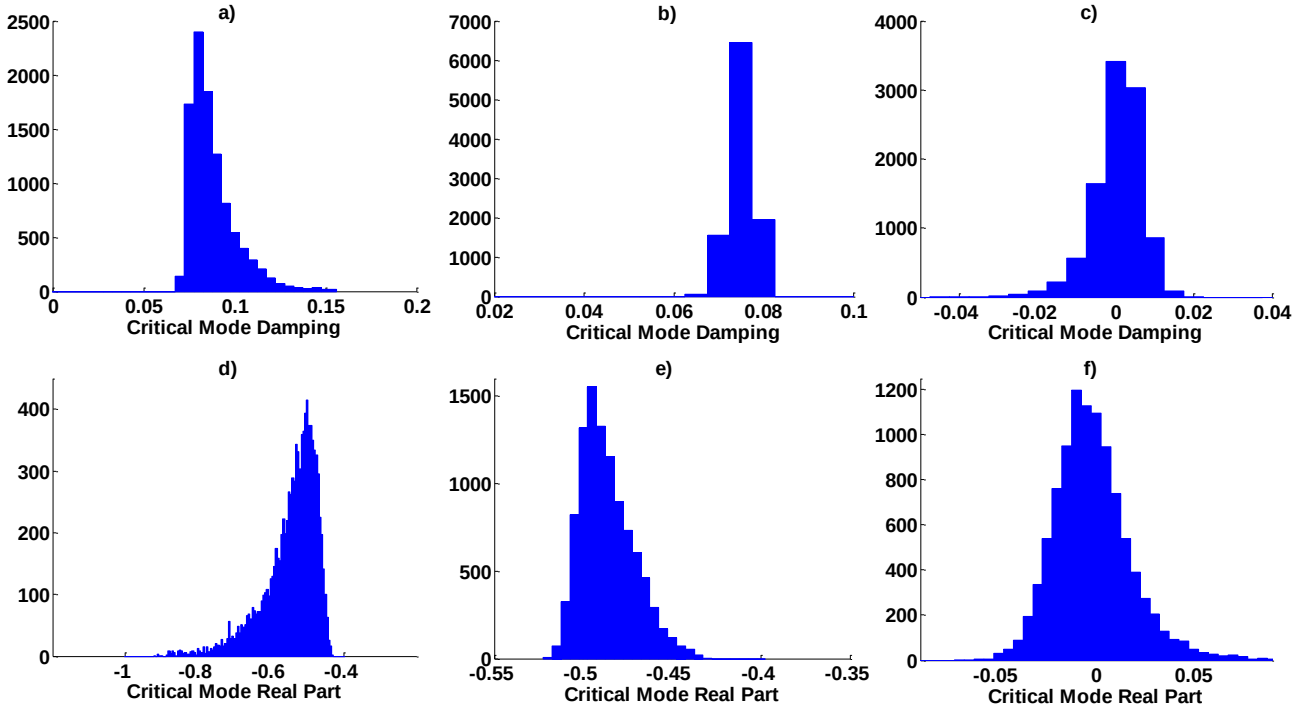

Figure 4.8 Histogram of the Distribution for Critical Modes Damping (Upper) and the Real Part (Lower) for Modes Numbers 1, 2 and 3 using MC

A. Accuracy of Moment Estimation

The results from the PEM for the calculated selected moments (mean, st.d, skewness, and kurtosis) are shown in Table 4.12 and Table 4.13 associated with critical mod damping and critical mode real part for two local mods and one inter-area mode, respectively. In this table, the bold text relates to the inter-area mode, whereas the other two modes refer to the local modes for each area. For this study, a variation for a level of input are equal to 24% at (i.e. 99.7% of input variation is found within 24% of the nominal mean values).

Furthermore from the results collated in Table 4.12 and Table 4.13 it can be observed that the PEM is very accurate at estimating the mean value. Regarding the estimation of the st.d, it can be seen that this parameter is more variable. The estimation skewness is near zero and a similar trend for this has been observed in a previous study [167]

B. Comparison of the Probability Density Function Estimations

In order to evaluate the estimated moments of σ_{crit}, the probability density functions (PDF) is also calculated (Figure 4.9).

The Probability distributions Function (pdfs) and cumulative probability density functions (cdfs) using Monte Carlo and the PEM are shown in Figure 4.9 and Figure 4.10. when uncertain input variation is equal to 24% in the case. In these figures, the charts a and d relate to the local mode 1 (mode number1 as a shown in Table 4.11), whilst b and e are associated with local mode 2 (mode number 2) and figures c and f

Table 4.12 Moment of Mode Damping

Method	Critical Mode Real Part Moments			
	Mean(s^{-1}) $\mu_{\sigma_{crit}}$	**St.d.(s^{-1})** $\sigma_{\sigma_{crit}}$	**Skewness** $\psi_3^{\sigma_{crit}}$	**Kurtosis** $\psi_4^{\sigma_{crit}}$
	-0.0018	**0.0202**	**1.0880**	**7.1980**
Monte Carlo	-0.5464	0.0753	-1.4423	5.5061
	-0.4866	0.0149	0.7174	3.2221
	-0.0073	**0.0190**	**0.0034**	**2.3125**
PEM (4m+1)	-0.5127	0.0484	-0.0548	5.7063
	-0.4761	0.0143	-0.0010	2.5402

Table 4.13 Moment of Mode Damping Ratio

Method	Critical Mode Damping Moments			
	Mean(s^{-1}) $\mu_{\zeta_{crit}}$	**St.d.(s^{-1})** $\sigma_{\zeta_{crit}}$	**Skewness** $\psi_3^{\zeta_{cri}}$	**Kurtosis** $\psi_4^{\zeta_{crit}}$
	0.0004	**0.0065**	**-1.4618**	**9.2447**
Monte Carlo	0.0879	0.0129	1.6205	6.2370
	0.0752	0.0026	0.7174	3.1153
	0.0020	**0.0059**	**-0.0021**	**2.8990**
PEM (4m+1)	0.0820	0.0079	0.0108	7.0790
	0.0733	0.0024	0.0003	2.5730

relate to the inter-area mode (mode number 3). As predicted from the analysis of the moments, ***4m+1*** the PEM variant method good approximately matches the MC-based results.

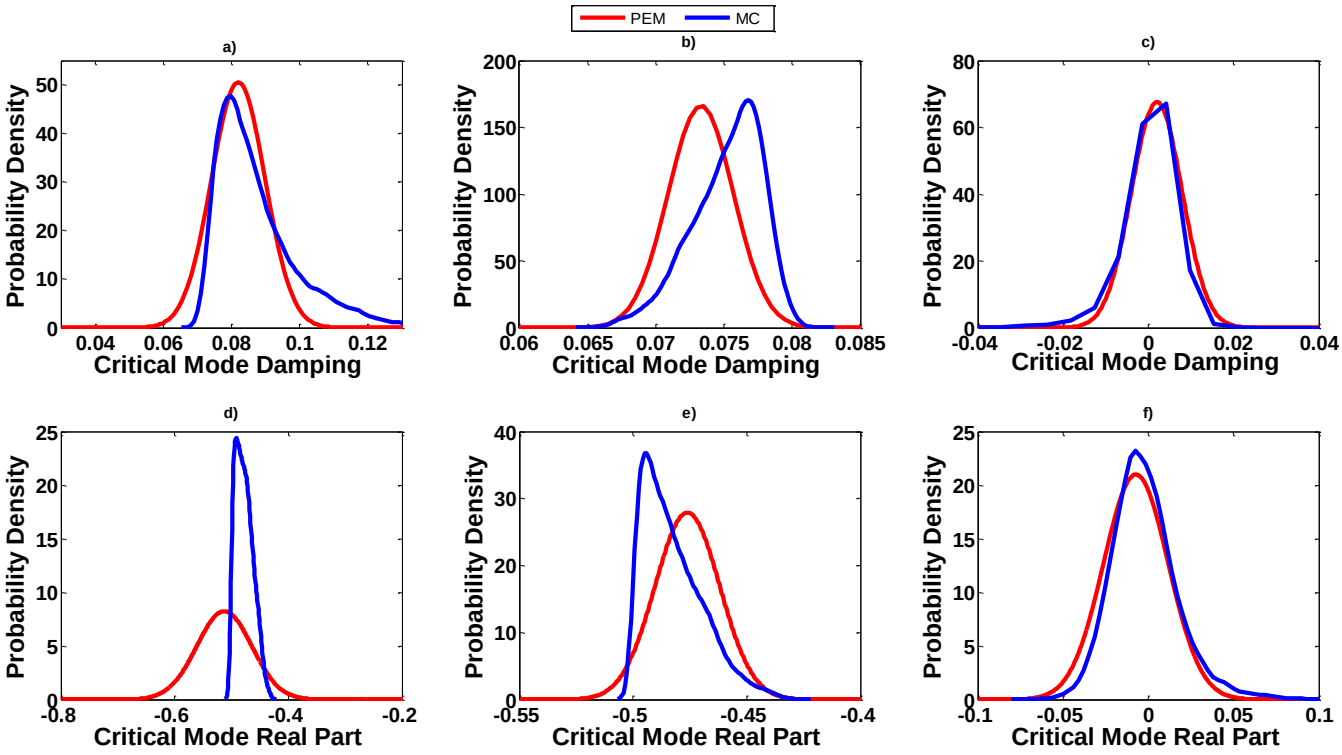

Figure 4.9 PDFs of σ_{crit} and ζ_{crit} Produced for 24% Input Certainty for Critical Mode Damping (Upper) and Real Part (Lower) for Modes Numbers 1, 2 and 3

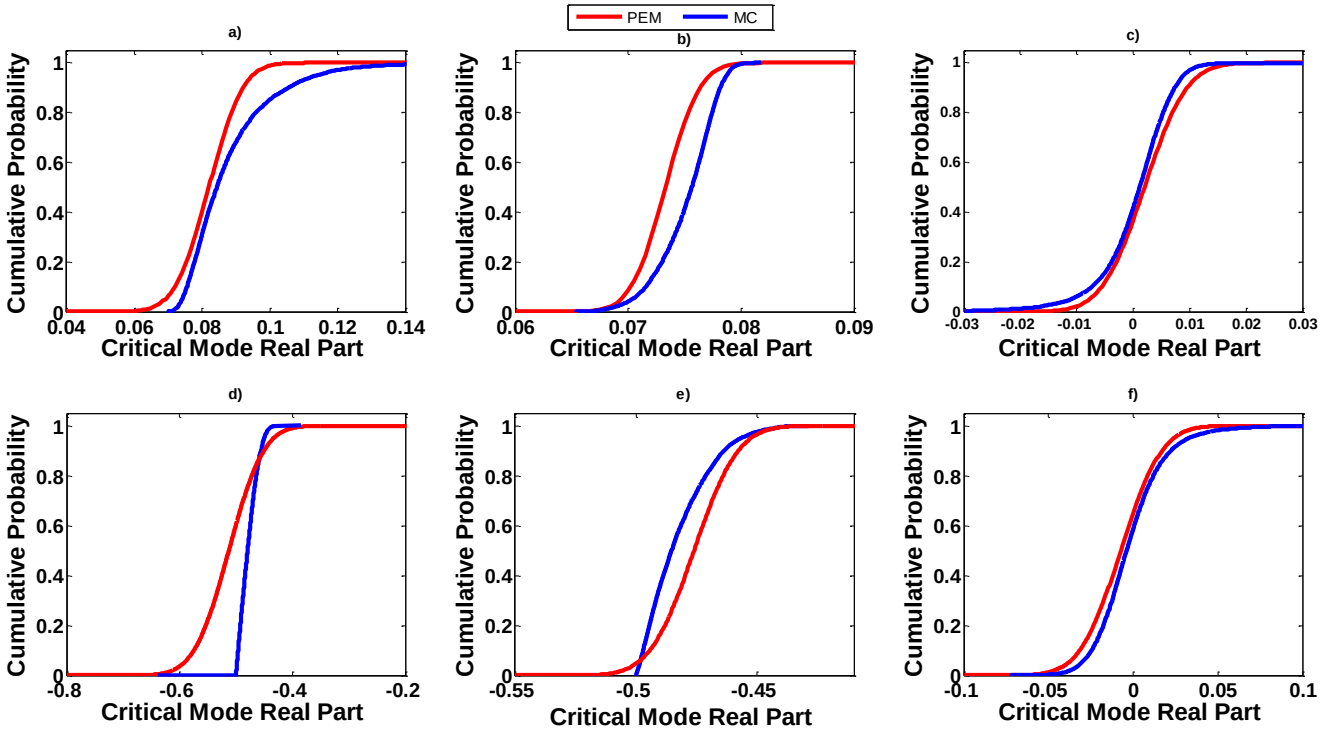

Figure 4.10 cdfs of σ_{crit} and ζ_{crit} Produced for 24% Input Certainty for Critical Mode Damping (Upper) and Real Part (Lower) for Modes Numbers1, 2 and 3

4.5 Concluding Remarks

This chapter has presented the fundamental modelling and analysis techniques which will be used throughout this thesis. The way in which non-linear power system models can be linearized in order to conduct small-disturbance stability analysis was then discussed. Finally, the test networks used throughout this research have been introduced.

Also this chapter presents stability analysis of the power system using of a probabilistic studies are completed to determine the most likely locations of critical oscillatory modes which are then incorporated into the linearized system model. A comparative investigation of a two of efficient estimation techniques (Point Estimated Method and Monte Carlo) was carried out in order to evaluate their suitability for probabilistic small-disturbance stability studies of the test system. This ensures that the probabilistic variation in critical system eigenvalues is more accurately accounted for.

.

Chapter 5

Damping Controller Design

5.1 Introduction

The majority of power system simulation packages do not provide the model of the system in a mathematical format to the users. Since the model of the system has to be available for supplementary controller's design, in this chapter, the application of a system identification method to obtain an equivalent model of it is studied. For the next step, the application of the design of the damping controllers is presented. The two controllers that have been use in this thesis are modal Linear Quadratic Gaussian Control (MLQG) and Modal Predictive Control (MPC). The most context of this chapter has been published in [175].

5.2 System Linearization and the System Identification Method

To implement both MPC and MLQG based supplementary POD controller schemes for an HVDC link, the model of the system has to be known in advance and for real power system networks, an accurate one is hard to obtain. Additionally, the majority of power system simulation packages do not provide the model of the system. To obtain a linearized model, system identification methods can be employed [176], [177]. This method involves constructing mathematical models of dynamic systems from measured input-output data. It also linearizes the nonlinear nature of the studied power system around an operation point.

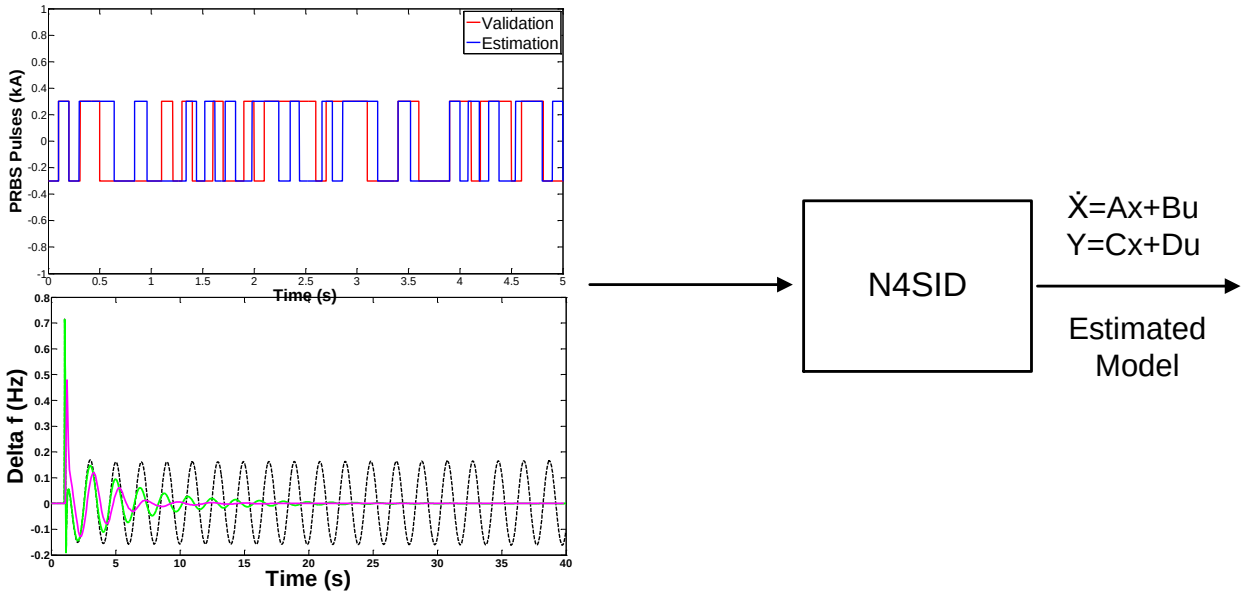

Figure 5.1. An Overview of the N4SID System Identification Process

In this research the dynamic model of the test system that has been described in Chapter 3, and simulations are performed in DIgSILENT/ PowerFactory. The system matrix ***A*** can be obtained directly from DIgSILENT, although this software cannot provide the input ***B*** and output ***C*** matrices of the linearized state-space directly. Therefore, a system identification technique was used to estimate the linear model from the simulated outputs in response to appropriate probing signals at the LCC HVDC control inputs. A numerical algorithm for the system identification (N4SID) was employed to identify system dynamics within this study, which was performed in a MATLAB environment and consequently, a link was needed between DIgSILENT and MATLAB. The details of this interfacing and linearization are shown in Figure 5.1.

5.3 Case Study

The simulated system is the well-known two area four machine system taken from Kundur [11] , the schematic of which is provided in Figure 5.2. Each generator is equipped with an AVR and governor. However, there is no PSS installed so as to illustrate better the inter area oscillation between two areas of the system. 100 MW of active power is transferred by the LCC HVDC link, which connects two areas of the network in a steady state operating condition. All details about this test system have been provided in Chapter 3.

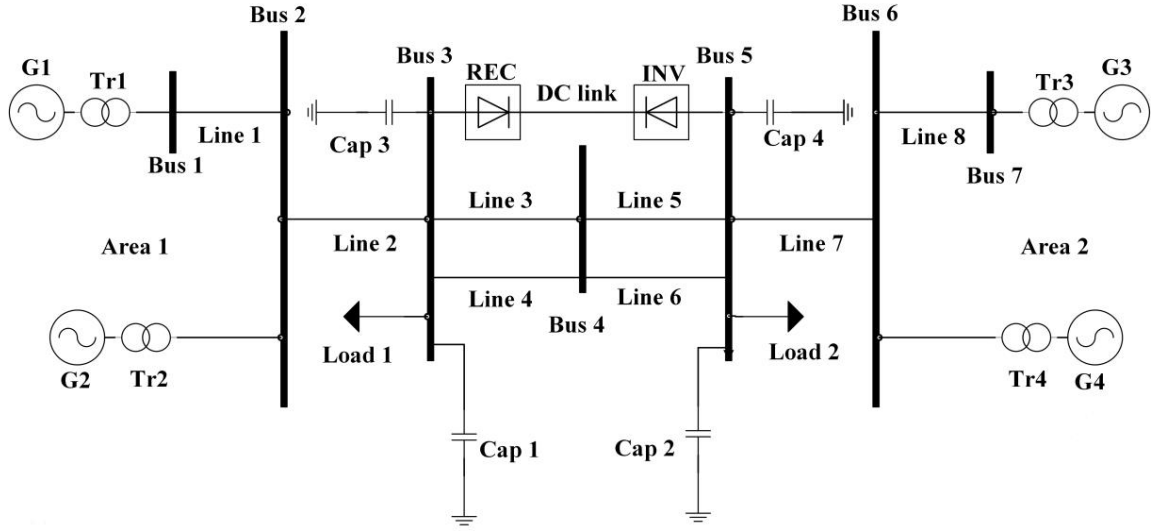

Figure 5.2 Schematic of the Two-area Four-machine System Connected with an HVDC Transmission Link [11].

5.3.1 Signal Selection and Probing

Selection of an appropriate probing signal is the most important part in system identification. In other words, in order to prepare the necessary data for system identification, appropriate inputs and outputs of the system have to be selected. Since the POD will be performed by modulation of the HVDC link's active power set-point, the HVDC's current order signal is considered as the system input signal in the present study.

Different methods for probing signals, such as repeated pulses, band-limited Gaussian white noise, Pseudo Random Binary Sequence (PRBS) signals and Fourier sequence, have been used in the literature [177] , [178] and [179]. In the current research the PRBS signal is employed as an input signal. In order to excite the critical modes sufficiently the signal amplitude has to be chosen high enough and this amplitude should be chosen carefully to keep the responses within the linearisable zone of the operating condition [168].

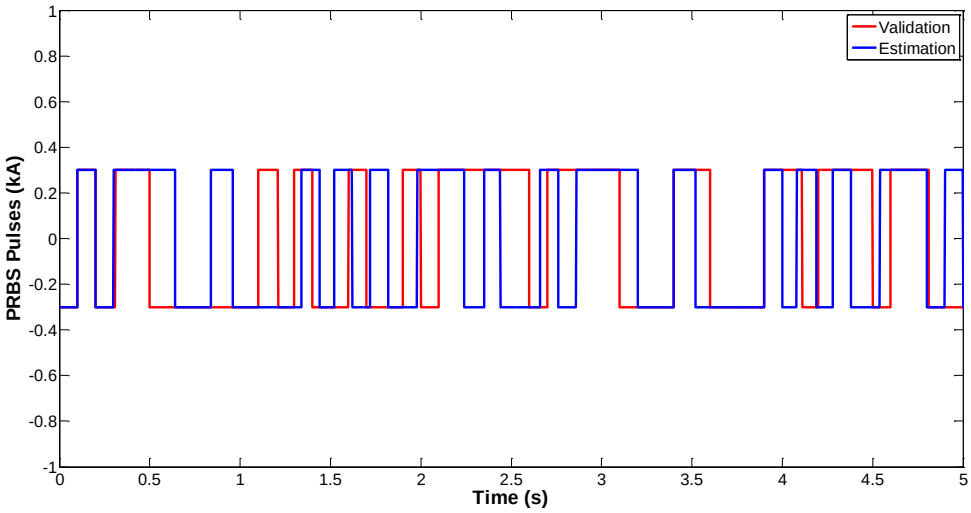

Figure 5.3 The Injected Signal for System Identification at the HVDC Current Set-point

The employed PRBS injection signals as inputs for the system identification are shown in Figure 5.3. In the present study, a PRBS signal with amplitude of 0.3 was injected into the system to create approximately 3 MW change in the output power. It should be noted that the main reason for such a minor change in the output of the HVDC is its relatively long response time [168]. The output signals can be selected from the state observability matrix of the system. These selected signals are limited in number to two, in part to reflect the expense and current scarcity of Phasor Measurement Units within a

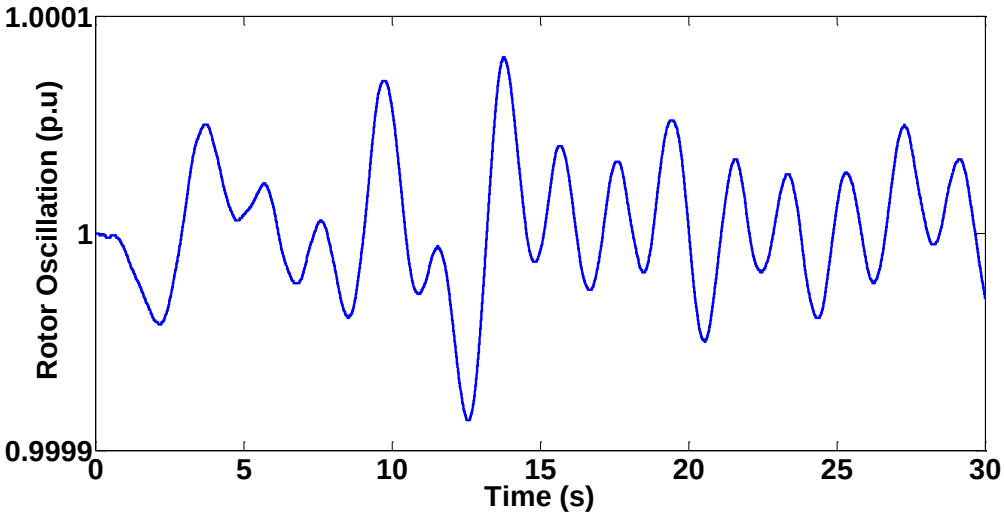

Figure 5.4 The Resulting Rotor Oscillations by Injecting a PRBS Signal

network and in part to decrease the controller complexity [10].

In small networks, suitable signals can also be determined by considering the nature of the problem. Since the inter area oscillation is related to the electrical torque of the generators in each area, any signal that relates to the electrical torque of the generators, i.e. the frequency, the generators rotor speed or the load angle of the voltages, can be considered. In addition, inter area oscillations will be strongly affected by the transferred active power between the areas. As a shown in Chapter 3, the tie lines active power flow, the angular speed of the contributing generators (perhaps more realistically the voltage phase angles of the local bus) or frequency difference between the areas give a high observability of the inter-area modes and therefore they can be selected as an output signal. However, the frequency difference is the better option since its value is independent of the system operating point and consequently, the estimated model will show more robustness [177]. Hence in this study, the frequency difference between two areas is chosen as the system output for system identification. Figure 5.4 shows the resulted rotor oscillations by injecting PRBS signal [168].

5.3.2 Order Selection

The system can be identified with different formats (state space, transfer function, polynomial model, etc.) and various model orders. The author adopted the state space format for system modelling [75],[76]. System identification provides model estimation with different orders. Two techniques are used for order selection in this study [168].

Table 5.1: Measured and Simulated Model Output Fitness (%)

Model Order	G2	G4	Power Line 5
20	-40.96	73.78	93.77
30	63.48	90.47	94.94
40	66.82	93.77	97.23
50	45.37	91.4	96.63
60	63.8	95.45	97.79

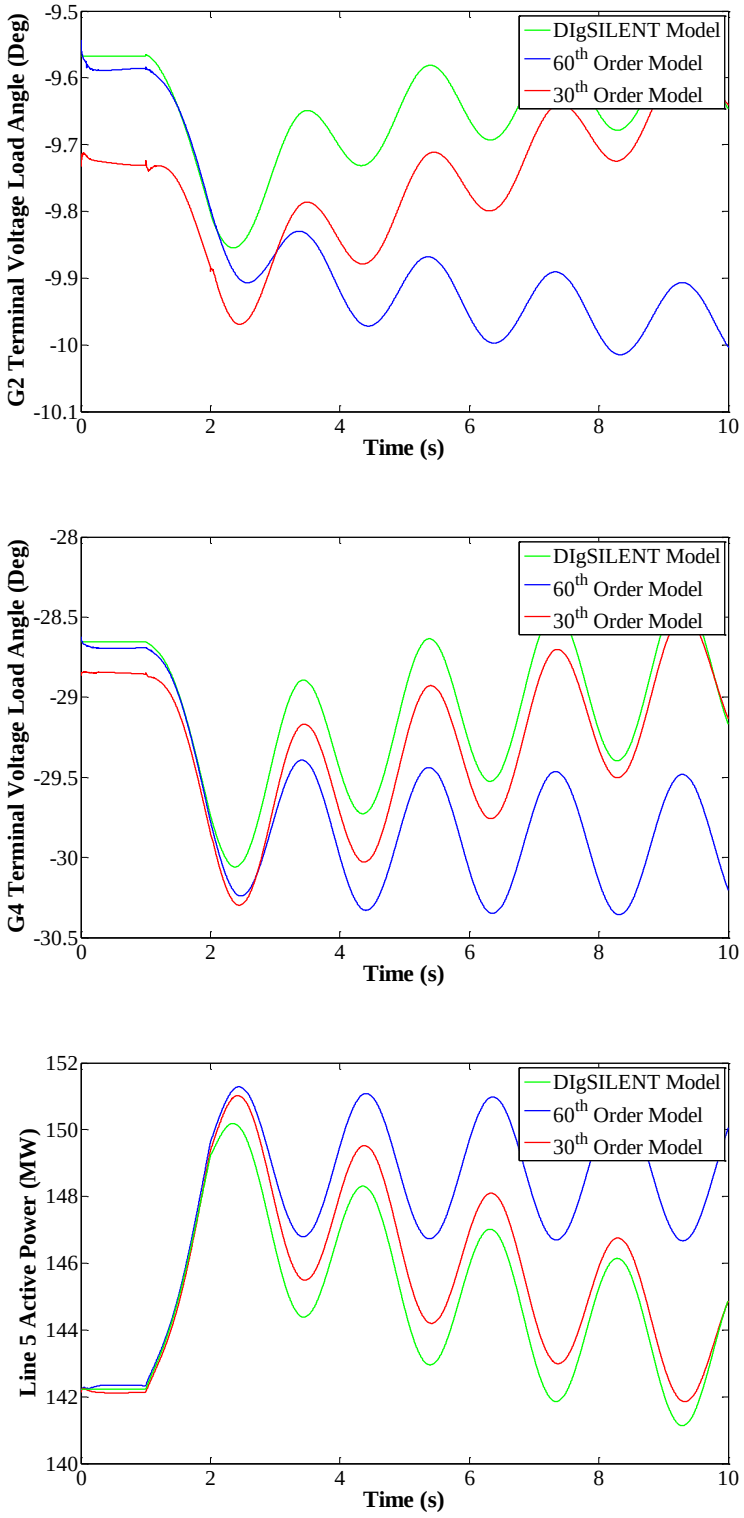

Figure 5.5 . Comparison of the Identified Models with the Original Model

1- In this method different orders have been tested and for each order the model output is compare with the actual system. The accurately of each model are shown in Table 5.1 The provided fitness value is used to choose the appropriate

models and one with less order as well as more accurate output will be preferable. As shown in Table 5.1, the model with 60th orders has the best accuracy, however, with a slight compromise in accuracy the 30th order model can also be a good candidate [168]. fitness value is calculated from equation (5. 1):

$$\overline{Y}_{fit} = 100\left[1 - \frac{|y - \hat{y}|}{|y - \bar{y}|}\right] \qquad \textbf{(5. 1)}$$

where, y is the measured output, $\hat{y}$ is the simulated output and $\bar{y}$ is the mean of y over the simulation period.

It is strongly recommended to compare the response of the actual and identified systems for the same event for validation. Figure 5.5 compares the response of the actual system and selected identified systems to a pulse change in the current set-point input of the HVDC current controller. As can be seen, although the higher order has more accurate initial condition, it fails to follow the same pattern of the actual system response. On the other hand, the 30th order model demonstrates a very low frequency oscillation and this low frequency mode in the identified model deviates its response [168].

2- As a second method, a log of singular values has been chosen to select the most suitable system order. The singular value related to order 'n' provides a measure for n^{th} component contribution of the state vector to the input-output

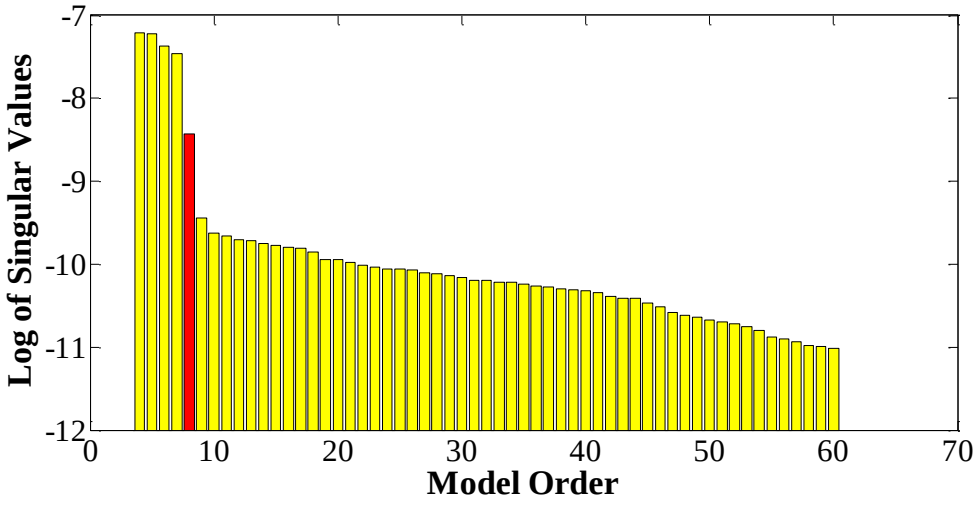

Figure 5.6 Model Order Selection

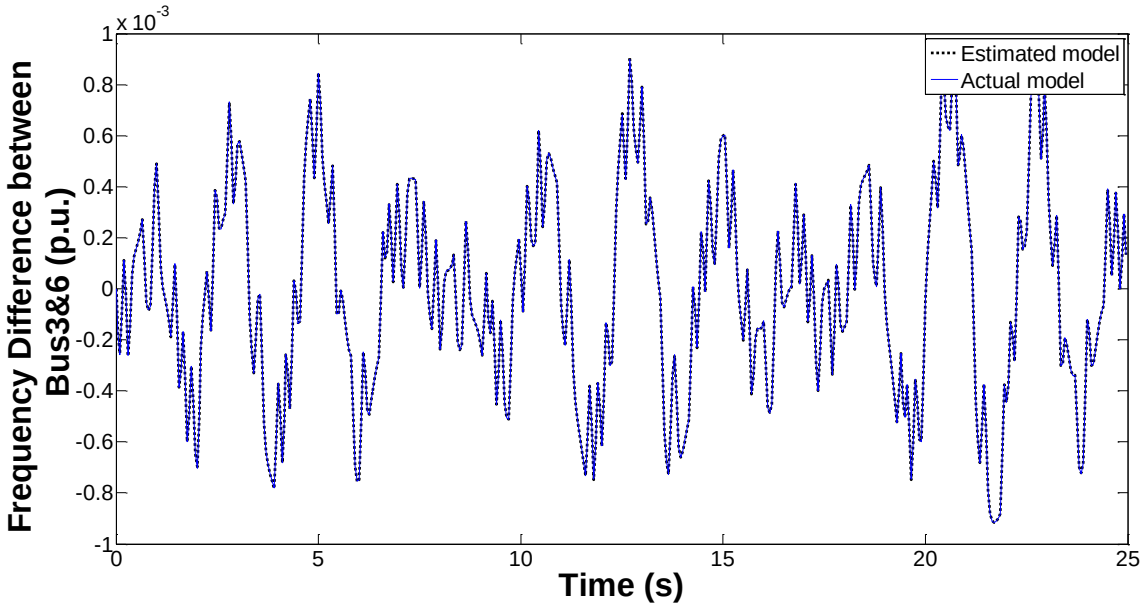

Figure 5.7 The Response of the Estimated and Actual Model

performance of the model. The selected model order '***n***' is one where the singular values to the right of n are small compared to those to the left [180]. Based on Hankel singular values chart (Figure 5.6) the order 8 satisfies this condition.

5.3.3 Model Validation and Reduction

In order to reduce the size of the controller, the identified system was further reduced to 6 orders.

To validate the identified model it was tested against a set of independent input-output data generated by DIgSILENT. Figure 5.3 shows the uncorrelated injected signal (red line) to produce the validation data. As can be seen in Figure 5.7, the adopted model can accurately estimate the obtained data with a fitness value of 99.62%. The fitness value is calculated from equation (5. 1).

In order to test the identified and reduced model the designed supplementary controller that will be presented in section 5-5 and 5-6, is tested. It has the same size of the provided system and for a high order model, especially in power networks; it is strongly recommended to reduce the order of the controller. This can be implemented through the following ways:

1) On the plant model prior to commencing the design procedure;

2) On the final controller design after completion of the design process;

3) Both on the plant model and the final controller design in order to minimize the final controller size.

The frequency responses of the 60th order and the reduced 6th order models are depicted in Figure 5.8 and the magnitude of both models shows a good match. Despite there being a dramatic change for the phase shift curves, the fact that each 360 degrees of phase shift is equivalent to no phase shift, means that the original and reduced models also exhibit a perfect match for the phase shift curves [168] .

5.4 Damping Controller Design

This section presents the application of the POD controller designs that have been used in this thesis. The two controllers which have been used in this thesis are Modal Linear Quadratic Gaussian control and Model Predictive Control. For both designed controllers, the optimal control theory defines the control signal of a dynamic system over a time horizon to minimize a cost function performance. It should be noted that these two control schemes were chosen from many other alternative schemes which

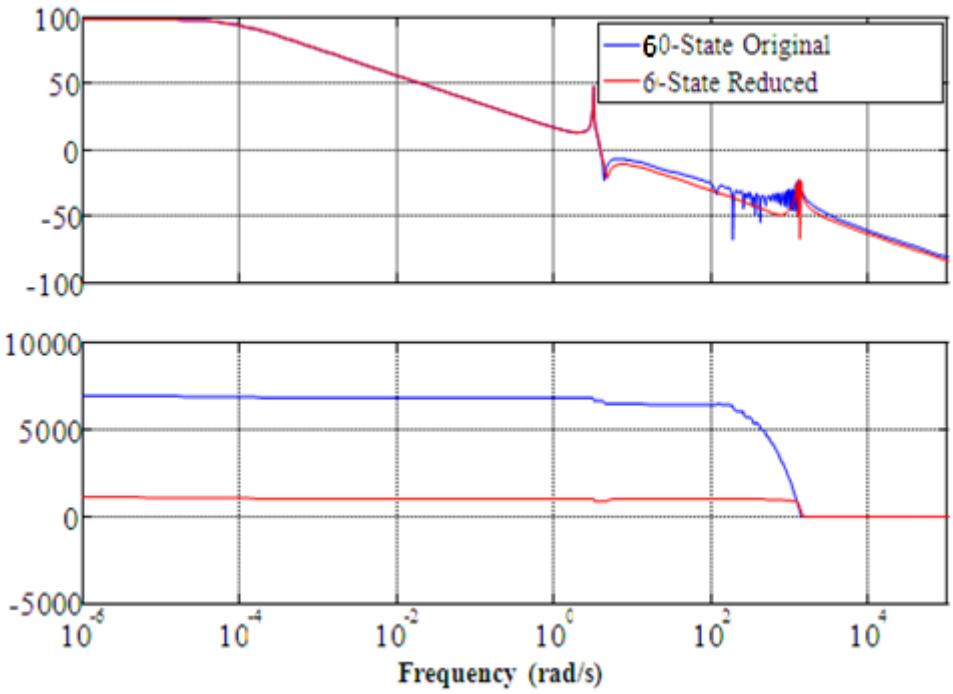

Figure 5.8 Frequency Response Comparison of the Original and Reduced Models

have been described in Chapter 2.

5.5 Modal Linear Quadratic Gaussian (MLQG) Method

Linear quadratic Gaussian (LQG) control is considered to be a foundation of modern optimal control theory [3]. The LQG scheme employs the following linearised state-space plant model in the power system [181]:

$$\dot{\boldsymbol{x}} = \boldsymbol{Ax} + \boldsymbol{Bu} + \boldsymbol{\Gamma w} \qquad \textbf{(5. 2)}$$

$$\boldsymbol{y} = \boldsymbol{Cx} + \boldsymbol{Du} + \boldsymbol{v} \qquad \textbf{(5. 3)}$$

where,

$\boldsymbol{w}$: process noise.

$\boldsymbol{v}$: measurement (sensor) noise.

The LQG scheme employs the linearized state space model of the system to find the control input ***u(t)*** signal that minimises the quadratic cost function in equation (5. 4):

$$\mathbf{J_k} = \lim_{\boldsymbol{\tau}\to\infty} \mathbf{E} \int_{\mathbf{0}}^{\boldsymbol{\tau}} (\mathbf{x^T Q x} + \mathbf{u^T R u})\mathbf{dt} \qquad \textbf{(5. 4)}$$

In this design the objective is to minimize the energy of the controlled output (states' deviation) and the energy of the input signal (control effort). The values of the diagonal elements of $\boldsymbol{Q}$ are selected to penalize the corresponding states when deviating from their steady-states values. Similarly, the values of the diagonal elements of $\boldsymbol{R}$ are set in order to penalize the corresponding system inputs [3].

For the LQR problem, the solution of equation (5. 4) can be written in the form of standard state feedback law presented in equation (5. 5). The LQR controller gain is computed by solving the associated Algebraic Riccati Equation (ARE) as shown in equation (5. 7) based on the cost function presented above [168], [177] .

$$\boldsymbol{u(t)} = -\boldsymbol{Kx(t)} \qquad \textbf{(5. 5)}$$

$$\boldsymbol{K} = \boldsymbol{R^{-1}B^T X} \qquad \textbf{(5. 6)}$$

where, $\boldsymbol{K}$ is a constant state feedback matrix and $\boldsymbol{X^T X \geq 0}$ is the unique positive semi-definite solution of the algebraic Riccati equation (5. 7):

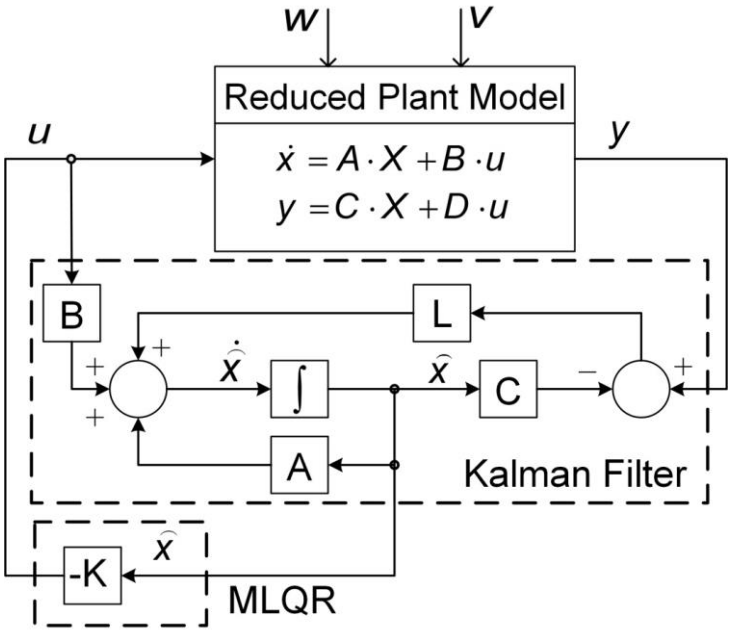

Figure 5.9 Standard MLQG Controller Structure

$$\boldsymbol{A^T X + XA - XBR^{-1}B^T X + Q = 0} \qquad \textbf{(5. 7)}$$

For solving the LQR problem all states must be measurable and since in most cases the states of the system are not available an observer is required to estimate the unavailable ones. Consequently, the LQG, as shown in Figure 5.9, is the combination of an optimal LQR state feedback gain with an optimal state estimator (Kalman filter) [168], [177].

The design of the LQG controller scheme is intricate, especially within large power systems. As the weighting factors are affecting states of the system, if these states are involved in modes that do not require altering, their damping can be adversely affected. Moreover, the indirect access to the targeted modes makes the controller tuning process prohibitively complex as the size of the system becomes larger [3, 10].

In order to provide direct alteration of the targeted modes without any adverse effect on the other modes a re-formulated LQR cost function in terms of modal variables is used in the MLQG controller scheme (Figure 5.9). The LQR control problem in the modal formulation is shown in equation (5. 8) [3, 10].

$$J_k = \lim_{\tau \to \infty} E \int_0^{\tau} (\mathbf{x}^{\mathbf{T}}(\mathbf{M}^{\mathbf{T}} \boldsymbol{Q_m} \mathbf{M})\mathbf{x} + \mathbf{u}^{\mathbf{T}}\mathbf{R}\mathbf{u})\mathbf{dt} \qquad \textbf{(5. 8)}$$

where, $\boldsymbol{Q_m}$ and $\boldsymbol{R}$ are appropriately chosen weighting matrices such that $\boldsymbol{M}$ is a real matrix that provides mapping between system modal variables z and state variables $\boldsymbol{x}$, as in equation (5. 9):

$$\boldsymbol{z(t) = Mx(t)} \qquad \textbf{(5. 9)}$$

The modal variables $\boldsymbol{z}$ are directly related to the system modes and the real transformation matrix M is associated with the matrix of right eigenvectors $\boldsymbol{\Phi}$ as $\boldsymbol{M = \Phi^{-1}}$. It should be mentioned that the weighting matrices $\boldsymbol{Q_m}$ and $\boldsymbol{R}$ are diagonal matrices. Similar to the LQG scheme, in matrix $\boldsymbol{R}$, the value of the diagonal elements should be set to penalize the corresponding controller's outputs. Each diagonal element of this matrix, ($\boldsymbol{Q_m}$), is directly related to a modal variable $\boldsymbol{z_i}$ and consequently, with the equivalent mode $\boldsymbol{e^{\lambda i t}}$. In the MLQG scheme, the controller solely affects the modes of interest, by shifting them to the left in the complex plane, while keeping the locations of other modes unchanged. Additionally, each mode can be moved independently only by tuning the value of the corresponding element in the $\boldsymbol{Q_m}$ matrix. In this research, the tuning process has been implemented using optimization method. Normally, each element is tuned to the lowest value which increases damping of the targeted mode within the required range and high gain values should be avoided [168], [177].

In order to design an MLQG controller, selection of the weighting matrices is a critical step. The corresponding weights in the $\boldsymbol{Q_m}$ matrix to the modes of interest are set to non-zero while keeping the other elements as zero. The non-zero elements will be tuned to achieve being the required range.

The standard LQG feedback control law can be written as:

$$\boldsymbol{u(t) = -K\hat{x}(t)} \qquad \textbf{(5. 10)}$$

where, $\boldsymbol{\hat{x}}$ is an estimate of the states $\boldsymbol{x}$ which can be calculated by (5. 11)

$$\boldsymbol{\dot{\hat{x}} = A\hat{x} + Bu + L(y - C\hat{x}) + Lv} \qquad \textbf{(5. 11)}$$

where, $\boldsymbol{L}$ is a constant estimation error feedback matrix, which is obtained by solving the Algebraic Riccati Equation (ARE) associated with the cost function described by equation (5. 12):

$$\boldsymbol{J_L = \lim_{T\to\infty} E\left\{\int_0^T (x^T W x + u^T V u)dt\right\}} \qquad \textbf{(5. 12)}$$

where, $\boldsymbol{W}$ and $\boldsymbol{V}$ are weighting matrices which, in this study, have been tuned using Loop Transfer Recovery (LTR) as described in the next section.

5.5.1 Application of Loop Transient Recovery (LTR)

As can be seen in Figure 5.9, the combination of an optimal LQR state feedback gain with an optimal state estimator (Kalman filter) is used in the LQG controller, which both have good individual robustness properties [3, 181, 182] . Nevertheless, by combining these two loops to form the LQG controller, individual robustness properties are lost [3]. A commonly used method to recover these robustness properties for designing of LQG is the loop transfer recovery (LTR) method. This recovery can be used at either plant input or output [3, 183]. The optimal choice of the matrix L in equation (5. 11) is calculated by solving the ARE associated with the cost function (5. 12). The weighting matrices W and V can be calculated as in equations (5. 13) and (5. 14) [177]:

$$\boldsymbol{W = \Gamma W_0 \Gamma^T + qB\theta B^T} \qquad \textbf{(5. 13)}$$

$$\boldsymbol{V = V_0} \qquad \textbf{(5. 14)}$$

where $\boldsymbol{W_0}$ and $\boldsymbol{V_0}$ are estimates of the nominal model noise, and $\boldsymbol{\theta}$ is any positive definite matrix.

5.6 Model Predictive Control Method

In MPC-based controller, the approach first achieves an estimate of the system model's dynamic state. The future behaviour of the system is then predicted and an appropriate HVDC power injection selected. To this end, an optimization problem is solved using a discrete time linear model of the system and the procedure is repeated at a fixed sampling rate [184]. The main difference between the MPC and other optimal control schemes, e.g. the MLQG approach, is its ability to take into account the system constraints. Moreover, the MPC optimization horizon is finite.

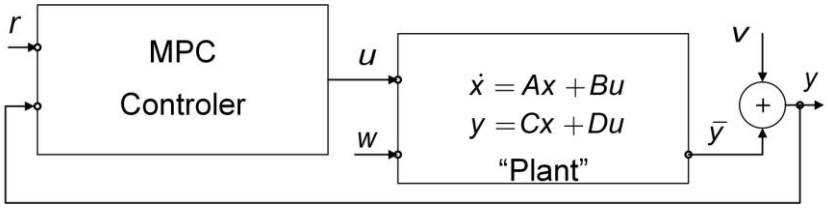

Figure 5. 10 Standard MPC Controller Structure

Figure 5. 10 represents the MPC block diagram, where, ***r***, ***u***, ***w***, ***v, y*** and $\bar{\boldsymbol{y}}$ represent the reference, control, process noise, measurement noise, measured output, and true value of the output (controlled variable) signals, respectively.

5.6.1 MPC Weight Tuning

The standard MPC Controller Structure is shown in Figure 5. 10. The critical step in its design is defining appropriate weights to the input and output variables as well as determining the MPC controller parameters. The weighting matrices control the trade-off between the tracking performance and control effort. Relating weights to the output variables determines the flexibility of the controller with regards to reference tracking of the weighted signal. Associating higher weights to outputs would result in severe tracking of the reference value [82],[168],[177].

5.6.2 MPC Parameterization

The initial step for MPC controller design is determining the value of the following parameters: control interval, prediction horizon (P), and control horizon (M). Choosing appropriate values for these parameters is a fundamental step in MPC control design, for one with ideal parameter values will have less computation effort with maximum performance [82]. The MPC controller executes both estimation and optimization algorithms. The former is performed to determine an approximate value of the states of the system. If all of the states are measured, the state estimation only considers the effect of noise on the measurement [82]. A discretized model of the system, equation (5. 15), is used by the MPC scheme [168], [177].

$$\boldsymbol{X(k+1) = Ax(k) + B_u u(k) + w(k)}$$
$$\boldsymbol{y(k) = Cx(k) + v(k)} \qquad \textbf{(5. 15)}$$

where, ***v(k)*** is the measurement noise assumed to be a zero- mean one.

The MPC controller estimates the future outputs using the past and present measurements. In the next step, the control moves will be calculated over the prediction horizon. This calculation has to be based on both the reference signals and pre-defined constraints. Subsequently, only the controller move at the present sampling time is applied to the system. And this procedure will be repeated for each sampling time. The MPC action at time is achieved by solving the optimization problem shown in equation (5. 16) [82], [168],[177]:

$$\Delta\mathbf{u}\sim(\mathbf{k}|\mathbf{k}),\dots.,\Delta\mathbf{u}(\mathbf{k}+\mathbf{M}-\mathbf{1}|\mathbf{k})\sum_{\mathbf{i}=\mathbf{0}}^{\mathbf{p}-\mathbf{1}}\left\{\sum_{\mathbf{j}=\mathbf{1}}^{\mathbf{n_y}}\mathbf{w}_{\mathbf{i}+\mathbf{1},\mathbf{j}}^{\mathbf{y}}\left(\mathbf{y_j}(\mathbf{k}+\mathbf{i}+\mathbf{1}|\mathbf{k})-\mathbf{r_j}(\mathbf{k}+\mathbf{i}+\mathbf{1})\right)^{\mathbf{2}}+\sum_{\mathbf{j}=\mathbf{1}}^{\mathbf{n_u}}\mathbf{w}_{\mathbf{i},\mathbf{j}}^{\Delta\mathbf{u}}\Delta\mathbf{u_j}(\mathbf{k}+\mathbf{i}|\mathbf{k})^{\mathbf{2}}\right\} \quad \textbf{(5. 16)}$$

$$\forall \boldsymbol{i}=\mathbf{0},\dots.,\boldsymbol{p}-\mathbf{1},\ \forall \boldsymbol{j}=\mathbf{1},\dots\dots.,\boldsymbol{n_y}\begin{cases}\boldsymbol{u_{jmin}}(\boldsymbol{i})\le\boldsymbol{u_j}(\boldsymbol{k}+\boldsymbol{i}|\boldsymbol{k})\le\boldsymbol{u_{jmax}}(\boldsymbol{i})\\ \Delta\boldsymbol{u_{jmin}}(\boldsymbol{i})\le\Delta\boldsymbol{u_j}(\boldsymbol{k}+\boldsymbol{i}|\boldsymbol{k})\le\Delta\boldsymbol{u_{jmax}}(\boldsymbol{i})\end{cases} \quad \textbf{(5. 17)}$$

$$\Delta\mathbf{u}(\boldsymbol{k}+\boldsymbol{h}|\boldsymbol{k})=\mathbf{0},\ \ \forall\boldsymbol{h}=\boldsymbol{M},\dots,\boldsymbol{P} \quad \textbf{(5. 18)}$$

where, $\boldsymbol{w}_{\boldsymbol{i}+\mathbf{1},\boldsymbol{j}}^{\boldsymbol{y}}$ is the weight for output $\boldsymbol{j}$, $\boldsymbol{w}_{\boldsymbol{i},\boldsymbol{j}}^{\Delta\boldsymbol{u}}$ is the rate weight for control signal j at $\boldsymbol{i}$ steps ahead from the current step, $\boldsymbol{r_j}(\boldsymbol{i})$ is the set-point at time step $\boldsymbol{i}$, $\boldsymbol{k}$ is the current step, and $\Delta\boldsymbol{u_j}(\boldsymbol{k}+\boldsymbol{i}\,|\,\boldsymbol{k})$ is the adjustment of the control signal $\boldsymbol{j}$ at time step $\boldsymbol{k}$+$\boldsymbol{i}$ based on the measurements at time step $\boldsymbol{k}$.

5.7 Concluding Remarks

The everyday increasing demand and consequent increase in transmission lines loading is pushing power systems towards the stability boundaries. As a counter measure, supplementary damping controllers have to be put in place for increasing the stability margin of the operating system. In order to enhance the system's transient and steady state stability, the MLQG and MPC based supplementary power modulation control strategies for the HVDC converter has been presented here. The HVDC supplementary controller is designed based on the model predictive control technique so as to provide improved damping and robust functionality for the system.

The design process of above mentioned controllers including the weight tuning and parameterization of the controller were explained within the chapter. Since the original simulation model was developed within DIgSILENT software, using the injected pulses

and measurement of the certain output data, an equivalent model was identified in Matlab by system identification toolbox.

The supplementary controllers were designed based on the identified model and the reduced order model. The provided controllers is a controller with the approximately the size of the network. Since the implementation of such controllers is not recommended in practice, the system was reduced using model reduction techniques by preserving the main characteristic of the original model. The reduced model was applied for controller design.

Chapter 6

Application of the Designed Controllers to a Test System

6.1 Introduction

To enhance the damping of inter-area oscillations in power systems, a model predictive control (MPC) scheme as an HVDC supplementary controller for improving AC system stability has been designed and implemented in this study. This chapter also compares the performance of MPC with other HVDC supplementary controller strategies for improving AC system stability, such as Modal Linear Quadratic Gaussian (MLQG) and State Feedback (SF). These three approaches are tested on a two area four machine system incorporating parallel HVDC/AC transmission and the results show the superior performance of MPC for damping oscillatory modes of the test system.

It should be noted that the design process including system identification, input and output signal selection, system order reduction (which have been presented in the previous chapter) and controller tuning for both schemes, has been provided within the presented study.

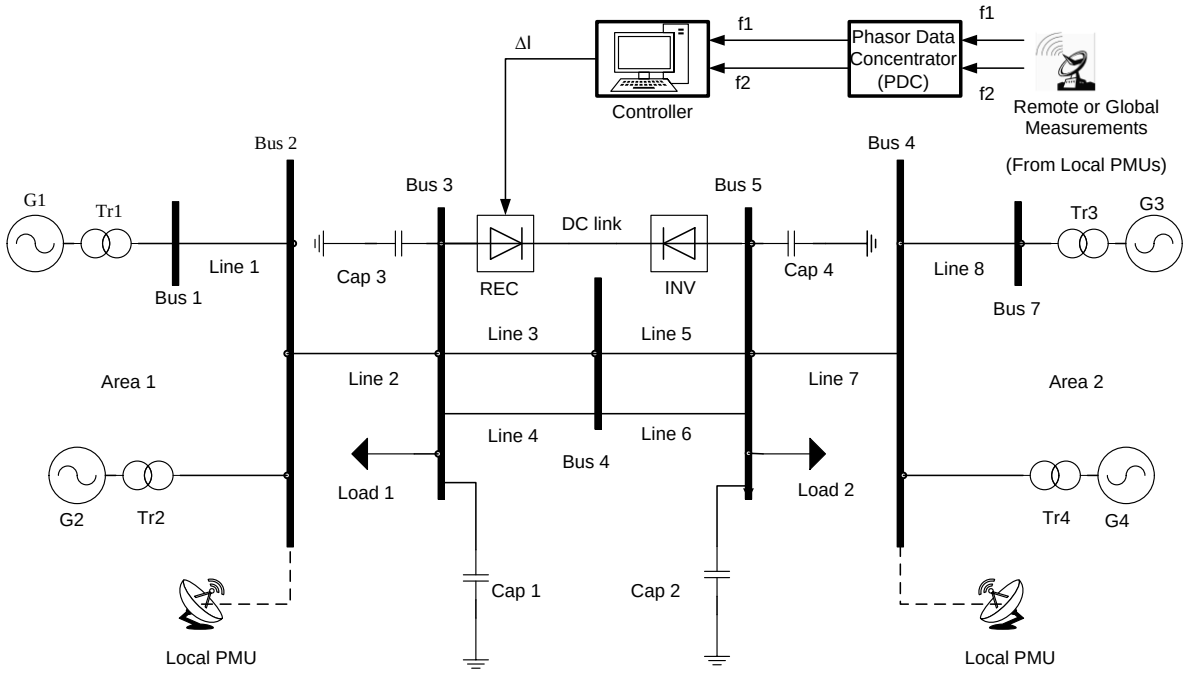

Figure 6.1 Schematic Diagram of the Two-area Four-machine System Connected with an HVDC Transmission Link

6.2 Test System

The test system presented in this study is the four-machine two area network, taken from Kundur, incorporated with an LCC-HVDC model, as shown in Figure 6.1. In the modified Kundor system an HVDC link has been added in parallel with an AC transmission corridor between two areas. In addition, each generator is equipped with an AVR and governor. However, no PSS is installed so as to better illustrate the inter-area oscillation between two areas of the system. The full set of the system parameters, i.e. the generator, transformer and transmission line parameters, as well as the controller settings of the Automatic Voltage Regulator (AVR) and Turbine Governor (TG), are given in Appendix A. 100 MW of active power is transferred by the LCC-HVDC link that connects two areas of the network in a steady state operating condition.

System analysis and controller design have been performed within the MATLAB environment and dynamic simulations carried out in DIgSILENT/PowerFactory. To observe the effect of the supplementary controller on the system, DIgSILENT has been linked to MATLAB.

The inter-area mode of the system is shown in Table 6.1. As can be seen, this mode is unstable and requires additional damping through the use of a supplementary POD controller. It is assumed the achieved damping will be adequate if $\zeta > 5\%$.

Table 6.1 Electromechanical Mode Properties for Two Area Test System with an Embedded LCC-HVDC Link

Mode	Description	Eigenvalue, $\lambda = \sigma \pm j\omega$	Frequency f (Hz)	Damping Factor (1/s)
Mode 1	Local mode	-0.54 ± j6.12	0.97	0.54
Mode 2	Local Mode	-0.54 ± j6.35	1.01	0.54
Mode3	Inter-area mode	0.039 ± j2.951	0.469	-0.0339

6.3 Power Oscillation Damping Control Design Approaches and Specification

For all the considered supplementary HVDC POD controller schemes, the controller output is chosen as the HVDC current order signal. This signal is added to the current reference set point at the converter station controller of the LCC-HVDC line. All controller schemes used in this research require a linearized model of the system to be known in advance. To estimate a linearized model of the system at the current operating scenario, system identification methods can be employed. The system identification method involves constructing a mathematical model of a dynamic system from measured input-output data [3].

As an initial step for the system identification, appropriate inputs and outputs of the system have to be selected. In the present study, the HVDC link current order is considered as the system input signal. For the output signal, the frequency difference between bus number 3 and 5 is selected to be employed by the system identification method. In addition, the PRBS signal is injected into the input point, which along with the consequent measured frequency difference is used to construct the system model by the system identification method. The calculated order of the system from system identification is 60. Since the size of the designed controller is at least equivalent to the size of the system, the high order models introduce design complications and consequently, practical implementation of such high order controllers is not recommended [14]. It is strongly recommended to reduce the order of the controller

before and/or prior to the design stage [3]. For the present study, a low order controller was designed by reducing the size of the system. Specifically, based on Hankel singular values chart, the Schur balanced model reduction [14] technique has been used to reduce the 60th order identified plant down to a 6th order equivalent system. The reduced model was validated against the original system using bode plots matching within the desired frequency range (below 100 Hz).

6.3.1 SF-Based Damping Controller

One of the schemes available to increase the damping performance of critical inter-area oscillations is the Sate Feedback (SF) controller [13], [14], which is employed in this research. This scheme places critical modes at a pre-determined location to ensure the settling time of inter-area oscillation modes within the desired value, which is typically 12-13s for power systems [13], [14], [15]. Because not all the states are available usually for a power system model, an observer is needed to estimate those of the system from measured outputs. The block diagram of the SF controller is shown in Figure 6.2.

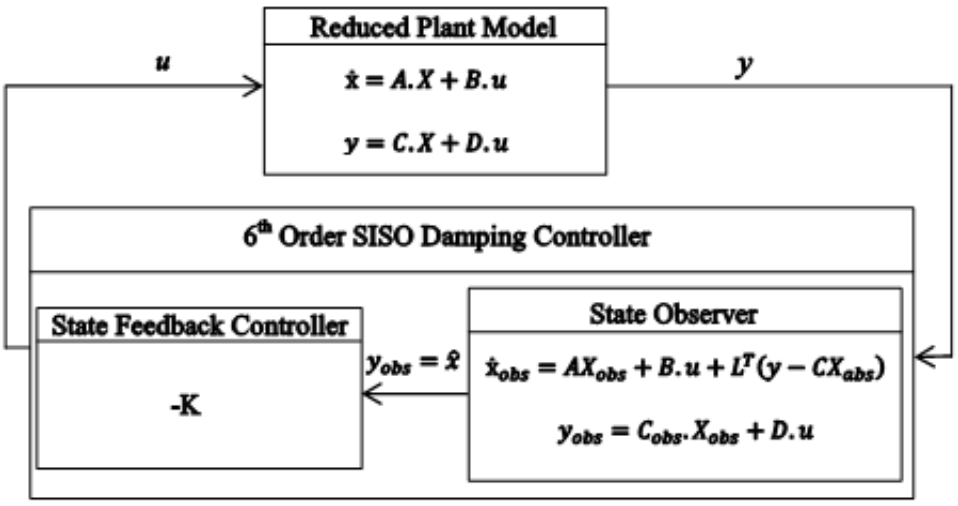

Figure 6.2 Feedback Control for Single Input

In this method, an approximate location of all poles of the system has to be determined as a first step and then the new locations have to be selected [75]. Using a ‘place’ command in MATLAB a gain matrix is designed to move the eigenvalues of the system to their new location.

In this study an observer-based SF controller has been designed for the aforementioned 6th order reduced plant model and two critical modes placed in pre-determined locations in order to enhance the damping performance. The "place" command in the Matlab Control System Toolbox has been used to compute the controller gain K [75, 76, 184], .

An observer has been employed to derive the states of the system from the measured output and the observer gain for this controller has been calculated to make the observer 10 times faster than the closed-loop system. The designed state feedback controller moves the inter-area lightly damped poles from 0.039+j2.951 (for the system without a POD controller) to the new location to provide satisfactory damping.

6.3.2 MLQG Damping Controller

The MLQG scheme directly alters the desired modes by assigning a non-zero value to the corresponding element within the Q_m matrix without the need for calculation of the participation factor matrix. The higher weighting value can lead to a larger displacement of the targeted mode. Very high values of Q_m elements have to be avoided as they create instability within the system. As only the ratio of the R and Q_m element is important for LQR tuning, the unity matrix is assigned to R and the elements of Q_m are adjusted. The Q_m and R are diagonal matrices. The parameters of the design are shown in Figure 6.3.

To make sure that the applied tuning for the MLQG controller provides the best damping performance, a multivariate search algorithm based on the fminunc function in Matlab is employed to find appropriate values of Q_m and q. The LTR procedure, which

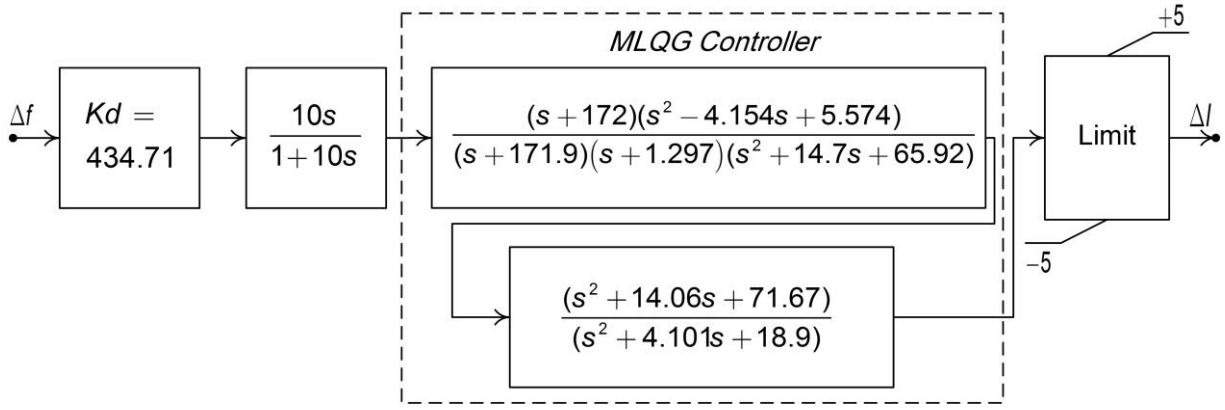

Figure 6.3 Parameters of the Designed MLQG

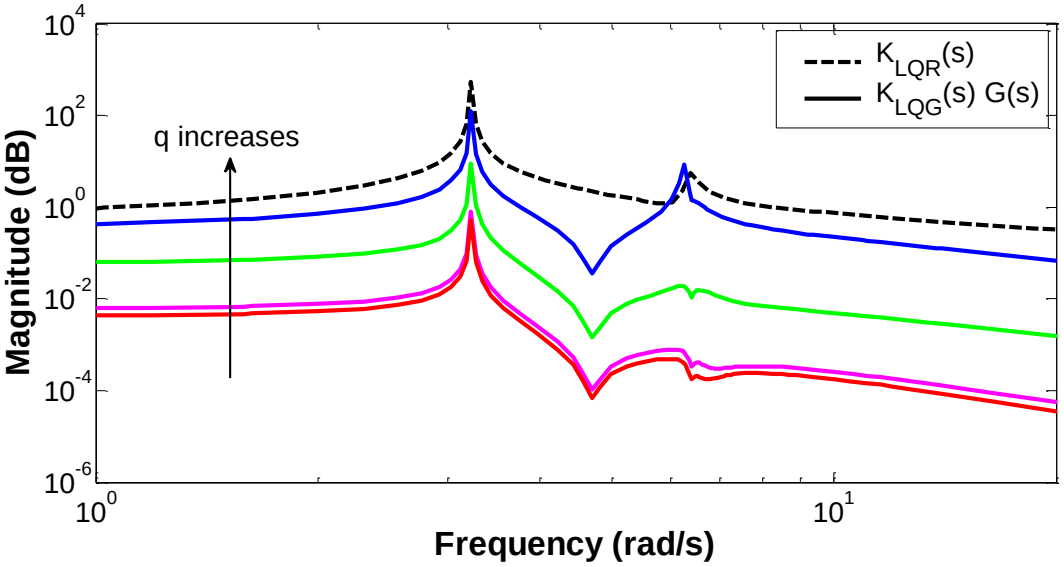

Figure 6.4 LTR Procedure at Plant Inputs with Various Values of q

was explained in the section 5.5.1, provides an initial guess for *q* and the designed Kalman Filter limits the performance of the LQR controller when they are combined together.

To achieve a close stabilizing effect of LQR the LTR method is used for optimum design of the Kalman filter. As mentioned before, despite the good individual robustness properties of both LQR and Kalman filter loops; a combined loop does not exhibit this. A widely acceptable method for the robustness recovery is the loop transfer recovery (LTR) procedure at either plant input or output [42]. And the former is used in this study. Figure 6.4 shows the LTR procedure for 0, 0.1, 1, 10. The measurement

Table 6.2 MLQG Controller Design Parameters

MLQG design parameters	
Washout time constant	10 s
Final controller size	6
WAC output limiter	±5
weight matrix of output deviations (Q)	1E5
Weight matrix of control inputs (R)	*I*

noise covariance is selected quite low (0.001) to reflect the characteristics of high quality PMUs. As shown in Figure 6.4, even for small values of q the LQG controller maintains LQR robustness around the desired frequency range of the inter-area modes.

The detail with regards to designing the MLQG controller is presented in Table 6.2.

6.3.3 MPC Damping Controller

For designing the MPC controller, it is recommended to select the control interval such that the plant's settling time is minimum 20–30 sampling periods [175]. To reduce the computational problem, a sampling time of 0.01 seconds is considered in this study. The value of the prediction horizon is 200 samples, and the selected value for the control horizon is 5 to set up the controller. The manipulated variable for the current set-point of the HVDC is constrained between -5 and 5 kA. Moreover, the measurement noise is modelled as white noise with 0.01×I amplitude, where I is the unity matrix. Table 6.3 shows the selected parameters for tuning the MPC controller, with the final controller parameters being illustrated in Figure 6.5. The shown transfer function for the MPC scheme is based under the assumption that there is no active constraint, only for presentation purposes. The applied controller is a constraint non-linear MPC.

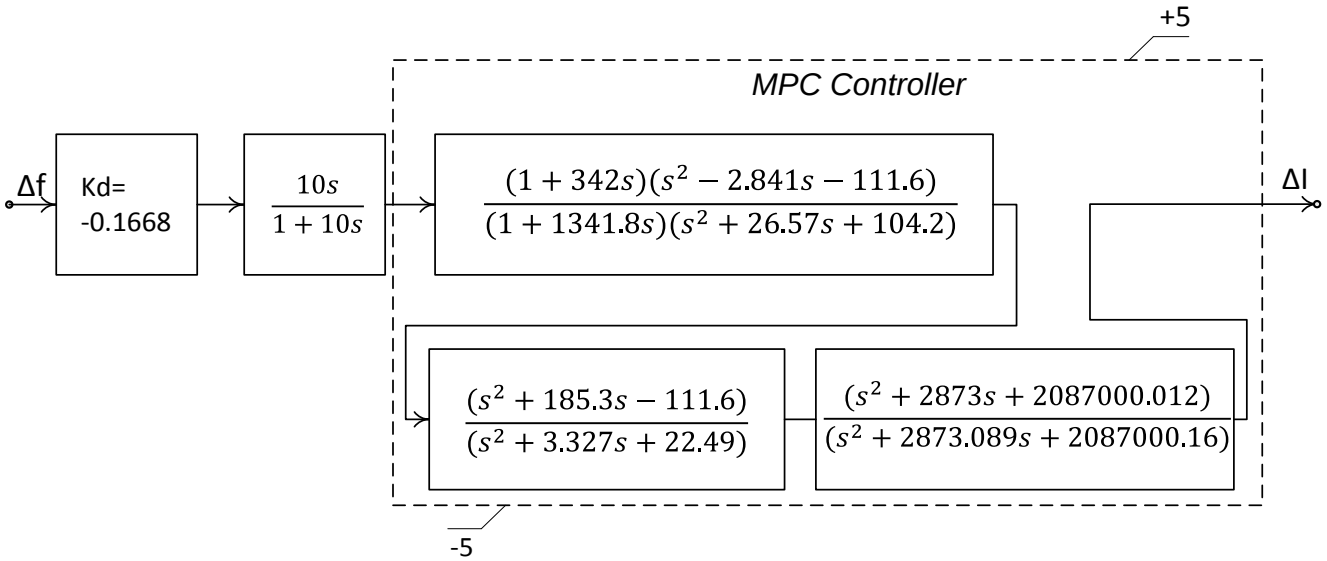

Figure 6.5 Parameters of the Designed MPC

Table 6.3 MPC Controller Design Parameters

MPC design parameters	
Prediction horizon	200
Control horizon	5
Sampling time	0.01
Output constraint	±5
Final controller size	7
Weights on manipulated variables	0
Weights on manipulated variable rates	0.04
Weights on the output signals	2.2

6.4 Nominal Performance of the Designed Controller

6.4.1 Small Signal Stability Performance of the Controllers

Eigenvalue analysis is used to compare the nominal performance of the controllers within this study. Since the MPC is a non-linear controller, it has been linearized around its operating point for assessment of its small signal performance. The achieved results from eigenvalue analysis as presented in Figure 6.6 show the MPC controller is more

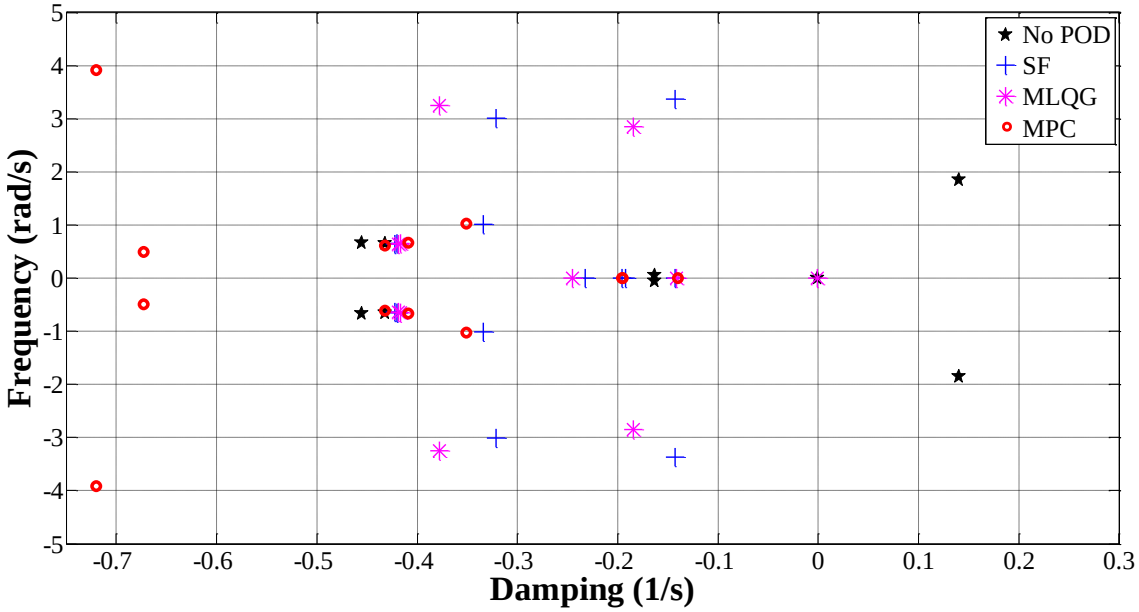

Figure 6.6 The System Poles with and without Controllers

effective in damping the inter-area mode in comparison with the MLQG and SF controller schemes. The damping factor is increased up to 15% for the MPC controller compared with 7.8% for the MLQG for the nominal condition.

6.4.2 Transient Performance of Controllers

In order to assess the transient performance of the supplementary MPC controller and to compare it with the MLQG and SF controllers, the following scenarios have been simulated: 1) without any supplementary controller in service (no control) 2) SF controller 3) MLQG controller and 4) MPC controller. For all these scenarios, the network was subjected to a 100 ms self-clearing three-phase fault at line 4 (large disturbance analysis). Simulated results for active power flow on the HVDC link and line 3, the speed of generators 2 and 4 as well as the input and output of the control system are shown, respectively, in Figure 6.7 to Figure 6.12.

Eigenvalue analysis is generally used to evaluate the performance of linear systems. However, since the closed-loop system of this study is nonlinear, the transfer function does not exist and eigenvalue analysis is not possible. Consequently, to address this issue and perform an eigenvalue analysis for all designed controller schemes for comparison, the linear state-space model of MPC has been created (assuming there is no constraint in the MPC). Clearly, as shown in Table 6.4, the inter-area mode for the test system is unstable and needs additional damping through the use of a supplementary POD controller.

Table 6.4 Electromechanical Mode Details for the Test System

Controller Type	Mode	Eigenvalue $\sigma \pm jw$	Damped Frequency f[Hz]	Damping Factor, σ(%)
No POD	Inter-area	0.04 ± j 2.95	0.47	-0.08
SF	Inter-area	-0.167± j 2.96	0.5355	6.5
MLQG	Inter-area	-0.1844± j 2.848	0.5381	7.8
MPC	Inter-area	-0.351 ± j 1.031	0.44	15

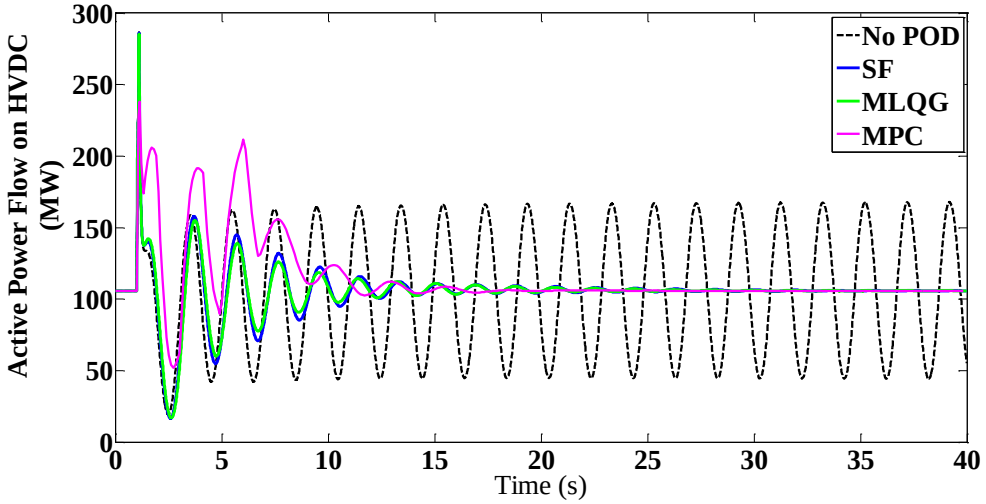

Figure 6.7 Active power Flow on HVDC Link

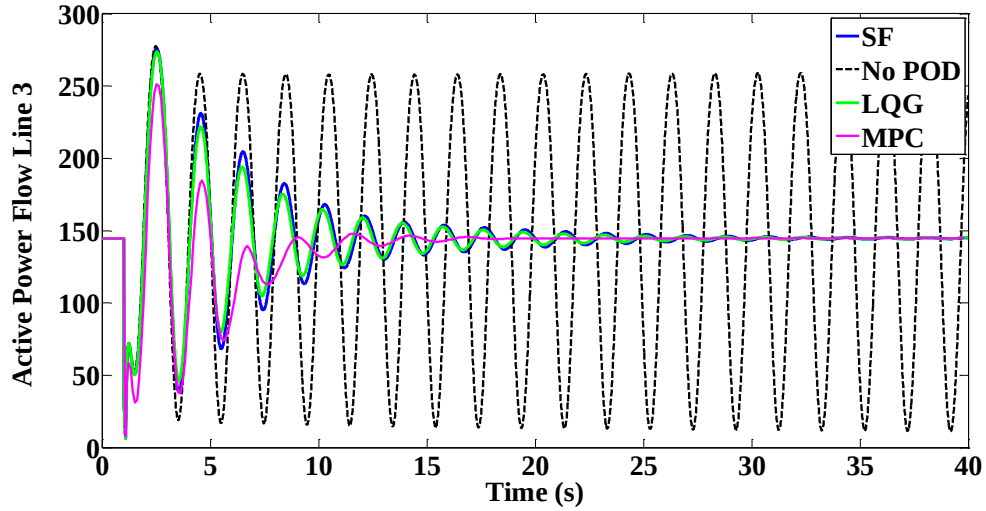

Figure 6.8 Active Power Flow on Line 3

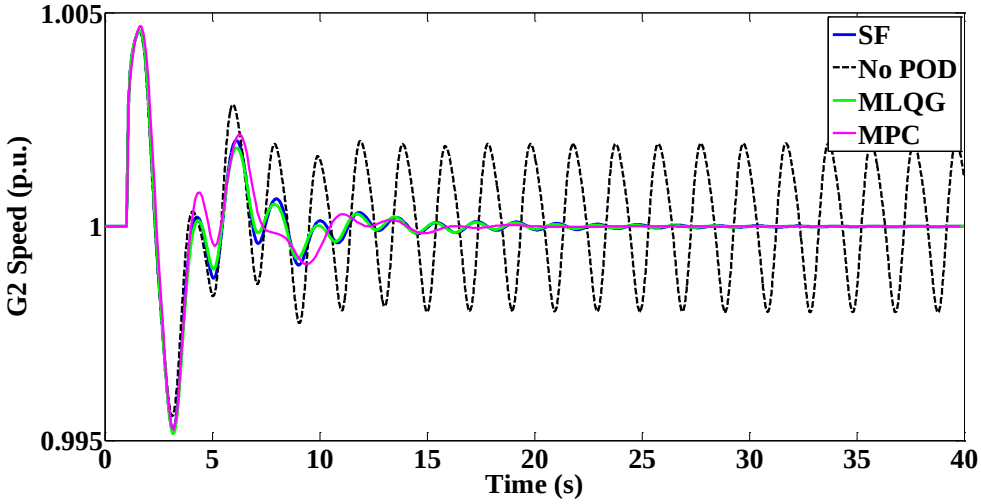

Figure 6.9 Generator2 Speed

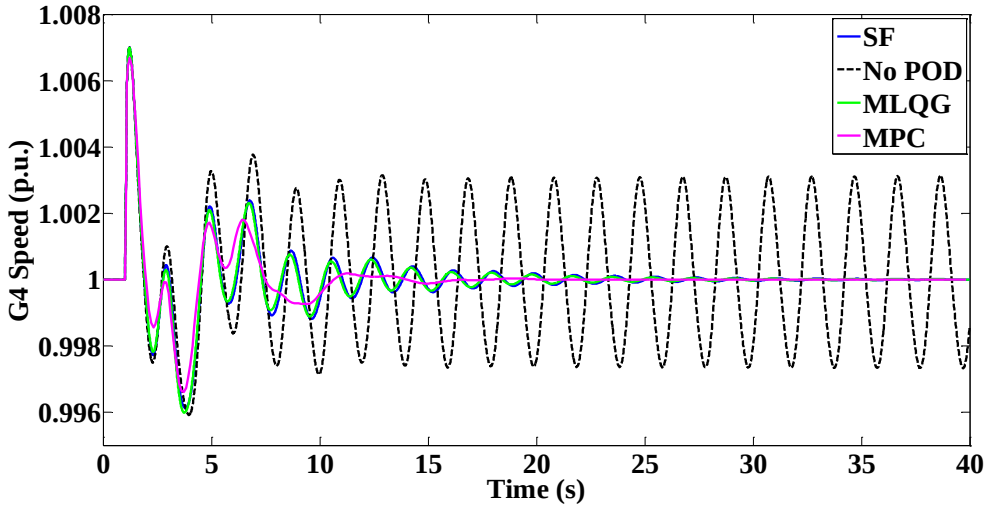

Figure 6.10 Generator4 Speed

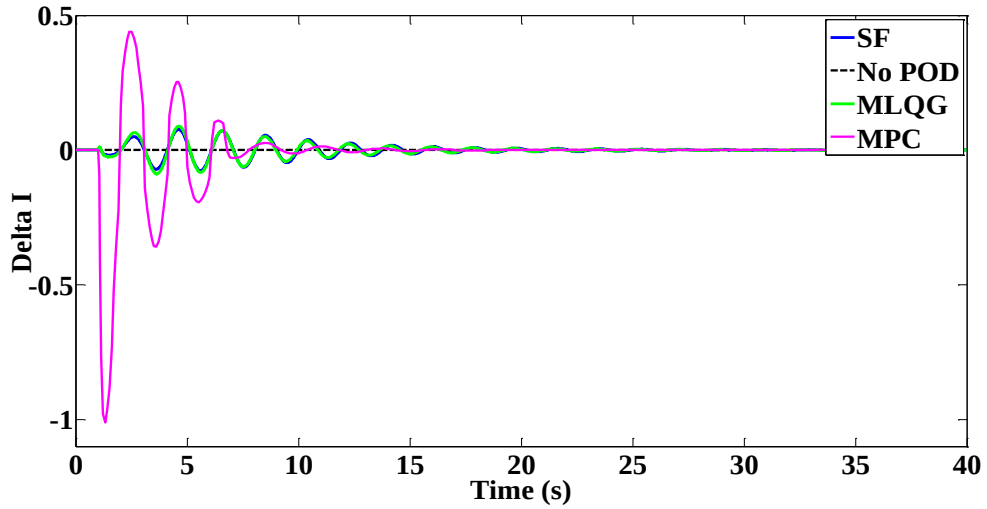

Figure 6.11 Output Control System Signal

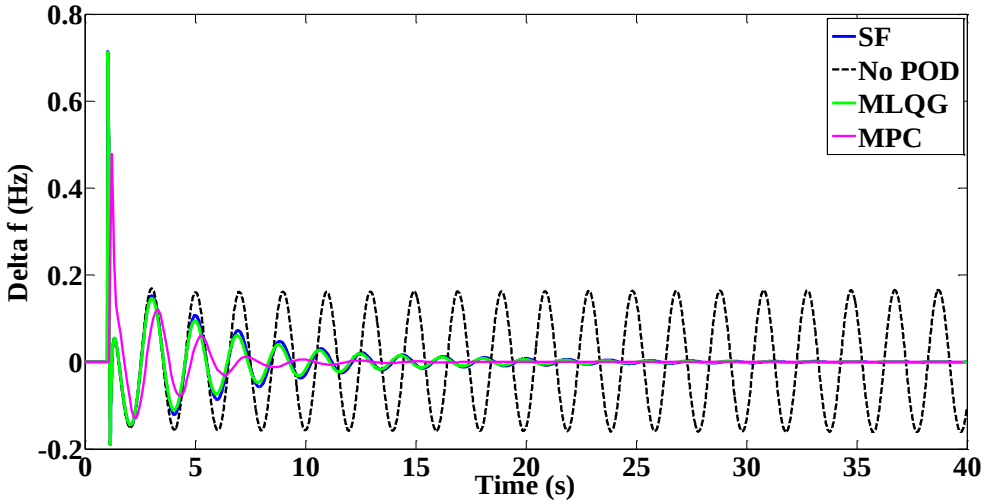

Figure 6.12 Input Control System Signal

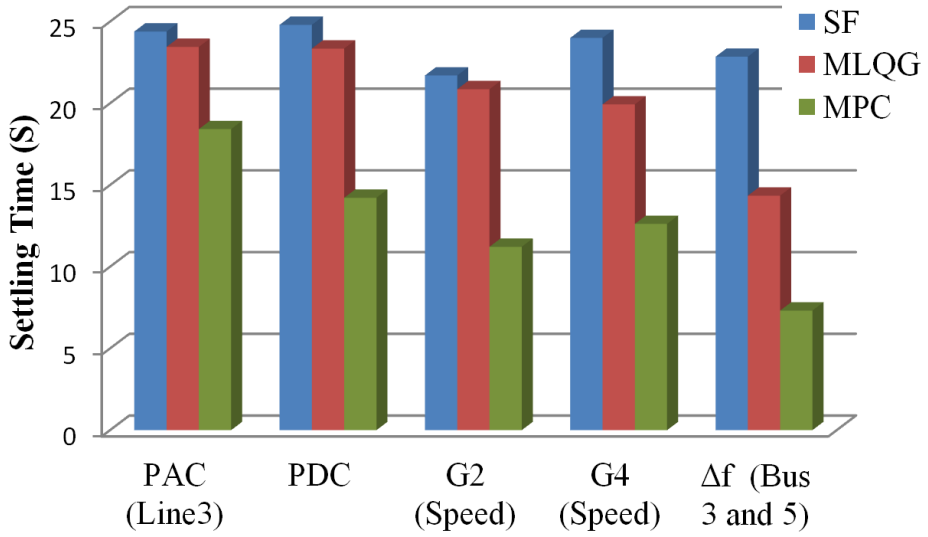

Figure 6.13 Settling Times for Two Area Test System

From the plots and the settling times shown (Table 6.5) it is evident that all the supplementary POD controllers are effective at damping oscillations for the test system. Furthermore, the MPC controller has the better performance and faster settling time for monitored active power flows and generator speeds. Plots of HVDC links (Figure 6.7) and the line 3 active power (Figure 6.8) are shown to demonstrate the controller effect on the transmitted power between the two areas. These figures show the SF controller is less effective at damping the oscillations for the test system at the operating conditions compared with MLQG and MPC controllers. As shown in Figure 6.13, the P_{AC} settling time for the SF controller is 24.39 and for P_{DC} it is 24.80. In comparison, for the MLQG controller the P_{AC} settling time is improved to 23.45 and P_{DC} to 23.35. These results are

Table 6.5 Settling Time for the Test System

Controller Type	Settling time(s)				
	P_{AC} (Line3)	**P_{DC}**	**G2 (Speed)**	**G4 (Speed)**	**Δf (Bus 3 and 5)**
No POD	--	--	--	--	--
SF	24.39	24.8	21.7	24	22.85
MLQG	23.45	23.35	20.86	19.93	14.35
MPC	18.42	14.22	11.22	12.62	7.318

further improved by using the MPC controller to 20.05 for P_{AC} and 22.15 for P_{DC}.

Furthermore, to verify the performance of the selected controllers on the stability of the system, the speed of the generators 2 and 4 of the test system, after the fault clearance, are shown in Figure 6.9 and Figure 6.10. The results show that with the MPC-based supplementary controller in service, faster damping is achieved compared to the MLQG and SF controllers. The reason for the better performance and fast damping of the MPC controller is its ability to optimize the objective function while considering the system constraints. The output and input signals of the control systems are shown in Figure 6.11 and Figure 6.12 respectively.

Figure 6.6 plots system poles with and without controllers. Clearly, adding a controller moves the inter-area modes more towards the left hand side of the imaginary axis, which is a sign of better stability. The achieved results from eigenvalue analysis show the MPC controller is more effective in damping the inter-area mode in comparison with the MLQG and SF controller schemes, with the damping factor being increased up to 15% for the MPC controller.

6.5 Assessing the Robustness of the Controllers

The uncertainty introduced by load and renewable energy variations can dramatically change the power system operating condition to the point that the linearized model is no longer valid. Consequently, performance of the designed wide area controller can be reduced or even introduce an adverse effect on system stability. This necessitates a thorough investigation of the controller's performance over a wide range of operating points. In this thesis, the Monte Carlo simulation method has been adopted to assess and compare the robustness of the designed wide area controllers [189].

To implement the Monte Carlo method the probabilistic distribution of system operating points must be defined. The considered uncertainties are composed of loads and HVDC active power. Loads follow a normal distribution with the nominal operating point assumed to represent 80% of maximum system loading and the full loading represents a $+3\sigma$ increase from the mean nominal values μ [185]. The active power of the HVDC is uniformly distributed between 100 and 300MW for this case study. Since in practical power systems the behaviour of various loads and generators can be correlated, an optimal power flow determines generator output [189].

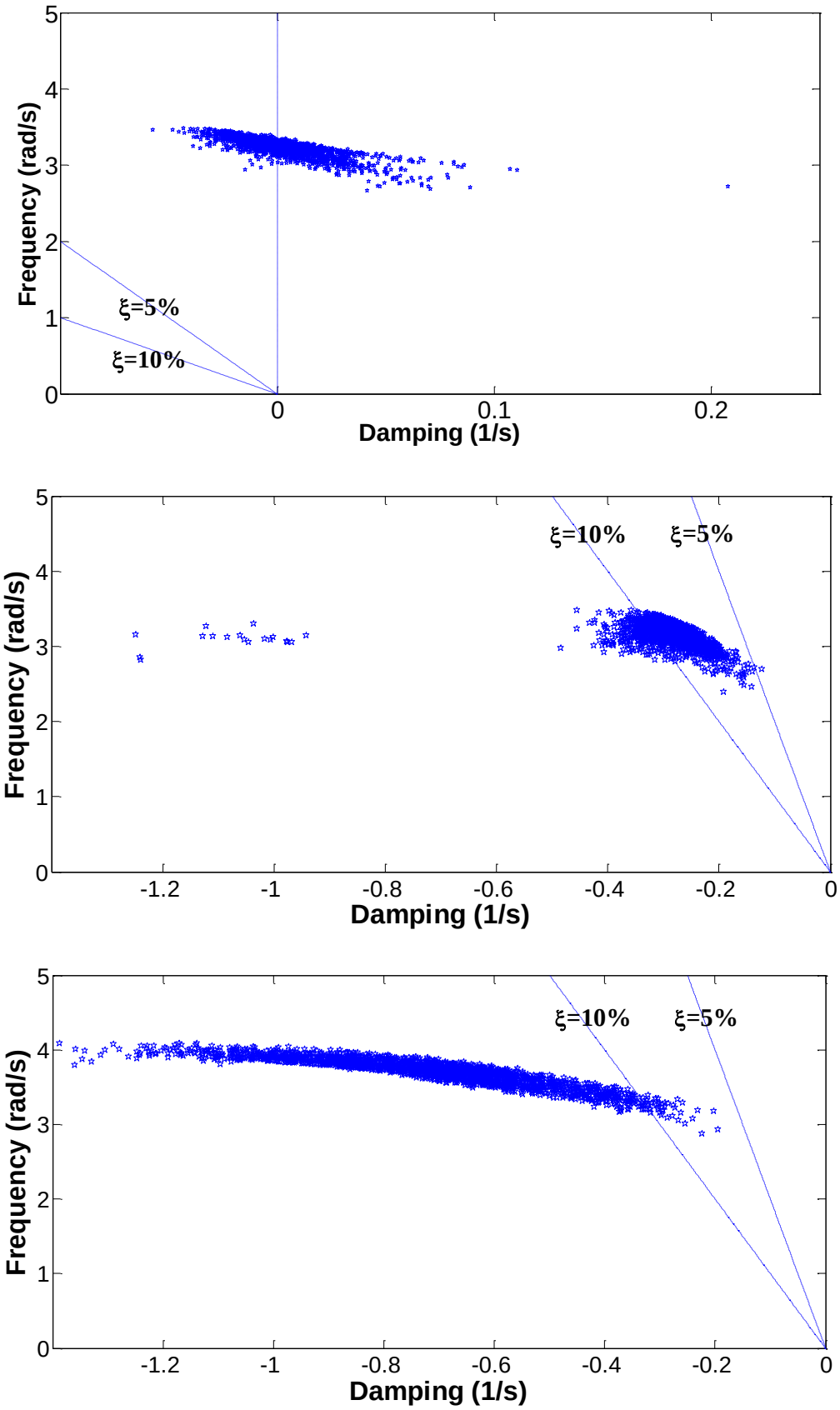

Figure 6.14 Probabilistic Inter-area Mode Locations for No POD Controller (top), MLQG Controller (middle), MPC Controller (bottom)

6.5.1 Eigenvalue Analysis

The robustness of controllers was evaluated by creating 2000 distinct operating points by the Monte Carlo method. Figure 6.14 shows the locations of the inter-area modes, respectively, for the system without WAC and as affected by the MLQG and MPC controllers. Almost for half of the scenarios the system is unstable [189]. Whilst the MLQG controller is able to shift the inter-area modes beyond the 5% damping line, most of the inter-area modes have been located further left to the 10% damping line, as can be seen in Figure 6.14.

6.5.2 Risk of Instability and General Comparison of the Controllers

In order to further investigate the probabilistic feature of the controllers a boxplot graph of the damping of the inter-area mode is provided in Figure 6.15. The tops and bottoms of each box are the 25th and 75th percentiles of the data samples, respectively. The line in the middle of each box is the sample median and the whiskers extend from the ends of the interquartile ranges to 1.5 times the height of the central box measured from the top or bottom of the box.

Despite both controllers achieve a target damping of 5% for the inter-area oscillation; the median damping obtained by MPC is almost twice that of MLQG meaning that for various operating points the former is likely to provide twice the amount of damping provided by the latter. The nonlinear effect of MPC is also observable within this graph as it provides various damping for different operating conditions. This is reflected in the

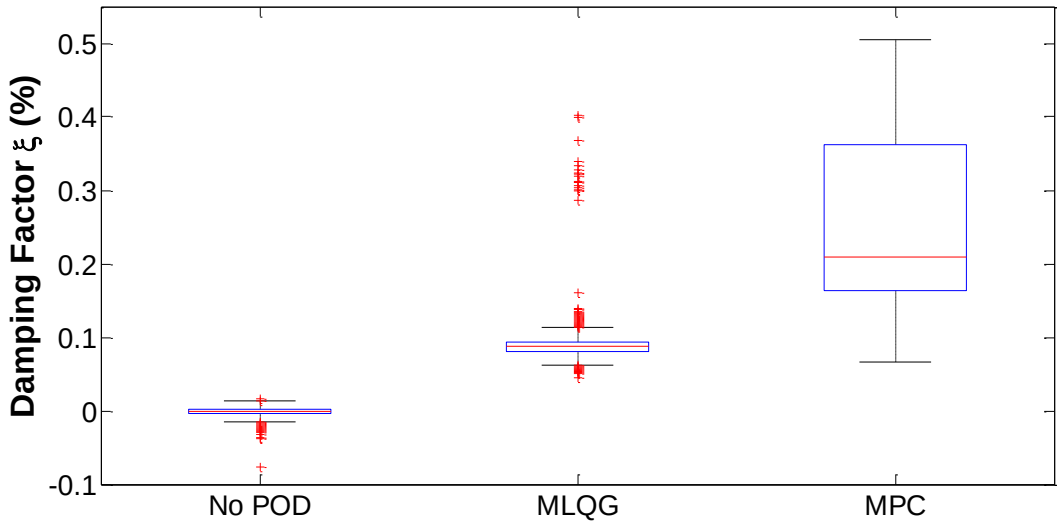

Figure 6.15 Boxplot for the Damping of the Inter-area Mode

interquartile range of the MPC boxplot, which is much larger, compared to the MLQG and no POD scenarios [189].

Also, it can be seen from Figure 6.15 that the risk of instability is down to approximately zero when controllers are in place. The risk of instability (ROI) is defined as follows:

$$\boldsymbol{ROI = P(\zeta < 0)} \qquad \textbf{(6.1)}$$

where, $\boldsymbol{\zeta}$ is the damping of the inter-area mode.

Table 6.6 provides more information about the extreme points for the damping spectrum for local and inter-area modes. The bold text relates to the inter-area mode, whereas the other two modes refer to the local modes for each area. Whilst the MLQG controller narrowly misses the target of 5% damping for the worst case, MPC can provide sufficient damping for all the simulated cases. Since the controller is designed mainly focused on damping the inter-area mode, the local modes have not been significantly displaced [189].

Table 6.6 Damping Ratio and Frequencies of Critical odes

Different Scenarios	No Controller		MLQG		MPC	
	ζ_1(%)	f_1(Hz)	ζ_1(%)	f_1(Hz)	ζ_1(%)	f_1(Hz)
Normal	**-0.08**	**0.5**	**7.8**	**0.5**	**15**	**0.44**
	7.7	1.0	7.8	1.0	8	1.0
	7.3	1.0	7.4	1.0	8	1.0
Best Damping	**1.7**	**0.6**	**40.3**	**0.6**	**50.5**	**0.6**
	15.6	1.0	15.5	1.0	15.0	1.0
	8.1	1.0	15.6	1.0	22.4	1.0
Worst Damping	**-7.6**	**0.4**	**4.5**	**0.4**	**6.6**	**0.4**
	7.1	0.9	7.4	0.9	7.0	0.9
	6.5	1.0	7.1	0.9	6.6	0.6

6.6 Concluding Remarks

This chapter has examined the performance of a wide area supplementary HVDC controller, based on the MPC scheme for damping inter-area oscillatory modes. The performance of the designed MPC controller was compared to the traditional MLQG and SF schemes. For the nominal operating point, the results show that the designed MPC controller provides improved damping of electromechanical oscillations when compared with the other two schemes. Due to the increasing penetration of renewable energy resources into the power system, future power networks will observe highly variable energy flows within the transmission network, thus resulting in a greater range of operating conditions. Hence, to design the new generation of controllers, the acceptable performance of the designed scheme not only needs to be guaranteed for the nominal operating point but also it has to be tested for other possible operating conditions.

To show the satisfactory performance and practical applicability over a wide range of operating points, a robustness assessment was also performed in this chapter at different operating points through employing the Monte Carlo method. The simulated results show that the proposed MPC controller significantly damps the critical inter-area mode under different operating conditions. From a comparison point of view, the MPC scheme not only provides considerably higher average damping among the tested operating conditions, but also it outperforms the MLQG scheme in every scenario.

Chapter 7

Conclusions and Future Work

7.1 Thesis Conclusions

This thesis has evaluated the improvements to small-disturbance stability that HVDC-based power oscillation damping control can achieve. In finalizing this research, probabilistic methods have been developed, which assess the performance of damping controllers and subsequently design controllers that are more robust to variable operating conditions.

It is concluded that:

1- What the review of past research revealed can be summarized as follows:
   - A comprehensive assessment of the robustness of LCC-HVDC POD controllers is currently lacking. Many nominally robust control schemes have been published, but these have not been thoroughly tested across the wide ranging operating conditions that are typical of modern power systems;
   - The Probabilistic Collocation Method requires development for implementation on large power systems in order to assess probabilistic power system small-disturbance stability with respect to uncertain operating conditions efficiently.

2- The fundamental modelling and analysis techniques used throughout this thesis were presented. The way in which non-linear power system models can be linearized in order to conduct small-disturbance stability analysis was then

discussed. Subsequently, the introduced modal analysis techniques formed the basis of the linear POD controller designs. The two controllers (MPC and MLQG) have been used throughout the thesis and their impact on system stability and performance in the presence of uncertainties assessed. Finally, the test networks used throughout this research were described.

3- The first contribution of this thesis is the stability analysis of power systems using a probabilistic approach being carried out to determine the most likely locations of critical oscillatory modes, which were then incorporated into the linearized system model. This ensured that the probabilistic variation in critical system eigenvalues was more accurately accounted for. Both the traditional MC approach and the efficient sampling of the PEM method were used to produce this probabilistic representation for a realistic power system.

4- In order to enhance the system's transient and steady state stability, MPC has gained preference over POD due to its functionality and robustness against noise and disturbances. However, there has been no research that has assessed its robust functionality. Consequently, as a second original contribution of this thesis, the robust characteristics of the MPC scheme on power oscillation damping were evaluated. To enhance the damping of inter-area oscillations in power systems, this researcher designed and implemented an MPC as a HVDC supplementary controller for improving AC system stability. Additionally, to evaluate the robustness of this method, statistical Monte Carlo simulation was employed. Moreover, the application of MPC has also been compared with the MLQG and SF schemes to provide a better insight into the robustness of the controller's functionality. For the nominal operating point, the results show that the designed MPC controller provides improved damping of electromechanical oscillations when compared with the MLQG and SF schemes. Also, the simulated results show that the proposed MPC controller significantly damps the critical inter-area mode under different operating conditions. From a comparison point of view, the MPC scheme not only provides considerably higher average damping among the tested operating conditions, but also, outperforms the MLQG scheme in every scenario.

5- The third and final original contribution of this thesis is developing of a reduced model of the GB transmission system within a PSACD/EMTDC platform. The performance of the developed system was compared and confirmed using a

DIgSILENT model, which was developed by the National Grid. The results show that both models respond similarly to the three phases of ground fault, although there are slight differences in the transient period and post-fault, which might be due to numerical solving issues in the control system that are related to the different solvers used in the two software tools. Nevertheless, the results show, in terms of active and reactive power flow, that both software tools provide similar results.

7.2 Future Work

The work presented in this thesis has achieved all of the research aims that were initially defined.

The performance of a wide area supplementary HVDC controller, based on the MPC scheme for damping inter-area oscillatory modes has been examined. Moreover, the performance of the designed MPC controller was compared to the traditional MLQG scheme. Regarding the nominal operating point, the results show that the designed MPC controller provides improved damping of electromechanical oscillations when compared with an MLQG scheme.

Due Owing to the increasing penetration of renewable energy resources into the power system, future power networks will experience highly variable energy flows within the transmission network, which will result in an increasing range of operating conditions. Hence, to design the new generation of controllers, the acceptable performance of the designed controller scheme not only needs to be guaranteed for the nominal operating point, but also, it has to be tested for other possible operating conditions.

To demonstrate satisfactory performance and practical applicability over a wide range of operating points, a robustness assessment was also performed at different operating points, obtained by the Monte Carlo method. The simulated results show that the proposed MPC controller significantly damps the critical inter-area mode under different operating conditions. From a comparison point of view, the MPC scheme not only provides considerably higher average damping among the tested operating conditions, but also, it outperforms the MLQG scheme in every scenario. Nevertheless there are a number of areas where this work could be extended in order to develop the ideas and methods that have been established further.

Further research proposed for continuation of this work includes the following:

- Developing of test system to the realistic system by adding the FACTS devises such as wind turbine
- Probabilistic analysis to investigate the impact of stochastic uncertainty of grid-connected wind generation on power system small-signal stability
- Investigating of online controller tuning using the PEM method
- Improving the reduced model of the GB system by adding the HVDC
- Investigating of a probabilistic analysis of small-signal stability on a reduced model of the GB system
- Investigating the performance of MLQG and MPC controllers on a reduced model of the GB system

References

[1] P. M. Ashton, "Exploiting Phasor Measurement Units for Enhanced Transmission Network Operation and Control", in Department of Electronic and Computer Engineering vol.Ph.D. Great London: Brunel University, 2014.

[2] S. K. Kerahroudi, F. Li, M. E. Bradley, Z. Ma, M. M. Alamuti, R. Rabbani, M. Abbod and G. Taylor, "Critical evaluation of power system stability enhancement in the future GB transmission using an embedded HVDC link," in *AC and DC Power Transmission, 11th IET International Conference On*, 2015, pp. 1-10.

[3] A. Almutairi, "Enhancement of Power System Stability using Wide Area Measurement System Based Damping Controller", in School of Electrical and Electronic Engineering. vol. Ph.D. Manchester: University of Manchester, 2010.

[4] D. Cai, "Wide area monitoring, protection and control in the future great Britain power system," in School of Electrical and Electronic Engineering. vol. Ph.D. Manchester: University of Manchester, 2012.

[5] C. Hor, J. Finn, G. Thumm and S. Mortimer, "Introducing series compensation in the UK transmission network," in *AC and DC Power Transmission, 2010. ACDC. 9th IET International Conference On*, 2010, pp. 1-5.

[6] A. Myles, "British system operation experience," in *IEE Proceedings C (Generation, Transmission and Distribution)*, 1988, pp. 233-237.

[7] P. Kundur and IEEE CIGRE Joint Task Force on Stability Terms and Definitions, "Definition and classification of power system stability," in 2003, .

[8] C. P. Steinmetz, "Power control and stability of electric generating stations," Transactions of the American Institute of Electrical Engineers, vol. 2, pp. 1215-1287, 1920.

[9] G. S. Vassell, "The Northeast Blackout of 1965," *Public Utilities Fortnightly;(United States)*, vol. 126, 1990.

[10] R. Preece, "A probabilistic approach to improving the stability of meshed power networks with embedded HVDC lines," in School of Electrical and Electronic Engineering. vol. Ph.D. Manchester: University of Manchester, 2013.

[11] P. Kundur, Power System Stability and Control. London: McGraw-Hill, Inc., 1994.

[12] G. Rogers, "Power System Oscillations, Norwell: Kluwer Academic Publishers 2000,".

[13] M. E. Aboul-Ela, A. Sallam, J. D. McCalley and A. Fouad, "Damping controller design for power system oscillations using global signals," *Power Systems, IEEE Transactions On*, vol. 11, pp. 767-773, 1996.

[14] I. Kamwa, R. Grondin and Y. Hébert, "Wide-area measurement based stabilizing control of large power systems-a decentralized/hierarchical approach," *Power Systems, IEEE Transactions On*, vol. 16, pp. 136-153, 2001.

[15] S. P. Azad, "Small-Signal Dynamic Stability Enhancement of A DC-Segmented AC Power System", in Department of Electronic and Computer Engineering vol.Ph.D. University of Toronto 2014.

[16] C. Kim, V. K. Sood, G. Jang, S. Lim and S. Lee, "HVDC Transmission: Power Conversion Applications in Power Systems". John Wiley & Sons, 2009.

[17] "*ABB Reference Projects"*, E. A. AB. (2015, Aug.19). [Online]. Available: http://www.abb.com/hvdc.

[18] O. A. Mousavi, L. Bizumic and R. Cherkaoui, "Assessment of HVDC grid segmentation for reducing the risk of cascading outages and blackouts," in Bulk Power System Dynamics and Control-IX Optimization, Security and Control of the Emerging Power Grid (IREP), 2013 IREP Symposium, 2013, pp. 1-10.

[19] H. Clark and D. Woodford, "Segmentation of the power system with DC links," in IEEE HVDC-FACTS Subcommittee Meeting, Las Vegas, NV, 2006, .

[20] H. K. Clark, M. M. El-Gasseir, H. K. Epp and A. Edris, "The application of segmentation and grid shock absorber concept for reliable power grids," in Power System Conference, 2008. MEPCON 2008. 12th International Middle-East, 2008, pp. 34-38.

[21] B. Van Eeckhout, "The economic value of VSC HVDC compared to HVAC for offshore wind farms," Offshore (Conroe, TX), 2008.

[22] L. Weimers. "Bulk Power Transmission at + 800 kV DC" [Online]. Available: www.abb.com.

[23] G. Asplund, K. Eriksson and K. Svensson, "DC transmission based on voltage source converters," in CIGRE SC14 Colloquium, South Africa, 1997, pp. 1-7.

[24] R. Rabbani, M. Mohammadi, S. K. Kerahroudi, A. F. Zobaa and G. Taylor, "Modelling of reduced GB transmission system in PSCAD/EMTDC," in Power Engineering Conference (UPEC), 2014 49th International Universities, 2014, pp. 1-6.

[25] L. P. Kunjumuhammed, B. C. Pal and N. F. Thornhill, "A test system model for stability studies of UK power grid," in PowerTech (POWERTECH), 2013 IEEE Grenoble, 2013, pp. 1-6.

[26] D. Novosel, "Final Project Report Phasor Measurement Application Study," *University of California, Prepared for CIEE*, 2007.

[27] *RenewableUK* - "UK Wind Energy Database (UKWED"). (Feb 2015). [Online] Available: www.bwea.com.

[28] "*Energy & Infrastructure Outlook offshore wind, The Crown Estate"*. (2014) [Online].Available: http://www.thecrownestate.co.uk/energy-and-infrastructure/.

[29] National Grid, " Electricity ten year statement_,", 2013. [Online]. Available: www2.nationalgrid.com/uk/.

[30] L. Livermore, C. E. Ugalde-Loo, Q. Mu, J. Liang, J. B. Ekanayake and N. Jenkins, "Damping of subsynchronous resonance using a voltage source converter-based high-voltage direct-current link in a series-compensated Great Britain transmission network," *Generation, Transmission & Distribution, IET,* vol. 8, pp. 542-551, 2014.

[31] M. Belivanis and K. R. Bell, "Use of phase-shifting transformers on the transmission network in great britain," in 45th International Universities Power Engineering Conference UPEC2010, 2010, .

[32] S. Chondrogiannis, M. Barnes, M. Aten and P. Cartwright, "Modelling and GB grid code compliance studies of offshore wind farms with doubly-fed induction generators," 2006.

[33] C. Spallarossa, Y. Pipelzadeh, B. Chaudhuri and T. Green, "Assessment of disturbance propagation between AC grids through VSC HVDC links using reduced Great Britain model," 2012.

[34] K. Bell, "Test system requirements for modelling future power systems," in *Power and Energy Society General Meeting, 2010 IEEE,* 2010, pp. 1-8.

[35] M. Belivanis and K. Bell, "Representative Model of the GB Transmission System," *Thinking Network, System Operation,* 2011.

[36] R. Eriksson, V. Knazkins and L. Söder, "Coordinated control of multiple HVDC links using input–output exact linearization," *Electr. Power Syst. Res.,* vol. 80, pp. 1406-1412, 12, 2010.

[37] B. Chaudhuri, R. Majumder and B. C. Pal, "Wide-area measurement-based stabilizing control of power system considering signal transmission delay," *Power Systems, IEEE Transactions On,* vol. 19, pp. 1971-1979, 2004.

[38] B. Chaudhuri, B. C. Pal, A. C. Zolotas, I. M. Jaimoukha and T. C. Green, "Mixed-sensitivity approach to H∞ control of power system oscillations employing multiple facts devices," *Power Systems, IEEE Transactions On,* vol. 18, pp. 1149-1156, 2003.

[39] B. Chaudhuri and B. C. Pal, "Robust damping of multiple swing modes employing global stabilizing signals with a TCSC," *Power Systems, IEEE Transactions On,* vol. 19, pp. 499-506, 2004.

[40] M. Zarghami, M. L. Crow and S. Jagannathan, "Nonlinear control of FACTS controllers for damping interarea oscillations in power systems," *Power Delivery, IEEE Transactions On,* vol. 25, pp. 3113-3121, 2010.

[41] P. Dash, S. Mishra and G. Panda, "Damping multimodal power system oscillation using a hybrid fuzzy controller for series connected FACTS devices," *Power Systems, IEEE Transactions On,* vol. 15, pp. 1360-1366, 2000.

[42] A. C. Zolotas, B. Chaudhuri, I. M. Jaimoukha and P. Korba, "A study on LQG/LTR control for damping inter-area oscillations in power systems," *Control Systems Technology, IEEE Transactions On,* vol. 15, pp. 151-160, 2007.

[43] X. Lei, D. Jiang and D. Retzmann, "Stability improvement in power systems with non-linear TCSC control strategies," *European Transactions on Electrical Power,* vol. 10, pp. 339-345, 2000.

[44] E. Lerch, D. Povh and L. Xu, "Advanced SVC control for damping power system oscillations," *Power Systems, IEEE Transactions On,* vol. 6, pp. 524-535, 1991.

[45] G. N. Taranto, J. Shiau, J. H. Chow and H. Othman, "Robust decentralised design for multiple FACTS damping controllers," *IEE Proceedings-Generation, Transmission and Distribution,* vol. 144, pp. 61-67, 1997.

[46] M. Klein, L. Le, G. Rogers, S. Farrokhpay, N. Balu, I. KAMWA and R. GRONDIN, "H∞ damping controller design in large power systems. Discussion. Author's reply," *IEEE Trans. Power Syst.,* vol. 10, pp. 158-166, 1995.

[47] J. J. Sanchez-Gasca and J. H. Chow, "Power system reduction to simplify the design of damping controllers for interarea oscillations," *Power Systems, IEEE Transactions On,* vol. 11, pp. 1342-1349, 1996.

[48] M. Noroozian, M. Ghandhari, G. Andersson, J. Gronquist and I. Hiskens, "A robust control strategy for shunt and series reactive compensators to damp electromechanical oscillations," *Power Delivery, IEEE Transactions On,* vol. 16, pp. 812-817, 2001.

[49] M. Ghandhari, G. Andersson and I. A. Hiskens, "Control Lyapunov functions for controllable series devices," *Power Systems, IEEE Transactions On,* vol. 16, pp. 689-694, 2001.

[50] N. Yang, Q. Liu and J. D. McCalley, "TCSC controller design for damping interarea oscillations," *Power Systems, IEEE Transactions On,* vol. 13, pp. 1304-1310, 1998.

[51] K. M. Son and J. K. Park, "On the robust LQG control of TCSC for damping power system oscillations," *Power Systems, IEEE Transactions On,* vol. 15, pp. 1306-1312, 2000.

[52] A. Kulkarni and K. Padiyar, "Damping of power swings using series facts controllers," *International Journal of Electrical Power & Energy Systems,* vol. 21, pp. 475-495, 1999.

[53] M. Noroozian, L. Angquist, M. Ghandhari and G. Andersson, "Improving power system dynamics by series-connected FACTS devices," *Power Delivery, IEEE Transactions On,* vol. 12, pp. 1635-1641, 1997.

[54] R. Rouco and F. Pagola, "An eigenvalue sensitivity approach to location and controller design of controllable series capacitors for damping power system oscillations," *Power Systems, IEEE Transactions On,* vol. 12, pp. 1660-1666, 1997.

[55] N. Martins, H. Pinto and J. J. Paserba, "Using a TCSC for line power scheduling and system oscillation damping–small-signal and transient stability studies," in *Proceedings of IEEE PES Winter Meeting,* 2000, pp. 1455-1461.

[56] Z. Huang, Y. Ni, C. Shen, F. F. Wu, S. Chen and B. Zhang, "Application of unified power flow controller in interconnected power systems-modeling, interface, control strategy, and case study," *Power Systems, IEEE Transactions On,* vol. 15, pp. 817-824, 2000.

[57] S. Jiang, U. Annakkage and A. Gole, "A platform for validation of FACTS models," *Power Delivery, IEEE Transactions On,* vol. 21, pp. 484-491, 2006.

[58] S. Arabi, G. Rogers, D. Wong, P. Kundur and M. Lauby, "Small signal stability program analysis of SVC and HVDC in AC power systems," *Power Systems, IEEE Transactions On,* vol. 6, pp. 1147-1153, 1991.

[59] I. Kamwa, J. Beland, G. Trudel, R. Grondin, C. Lafond and D. McNabb, "Wide-area monitoring and control at hydro-québec: Past, present and future," in *Power Engineering Society General Meeting, 2006. IEEE,* 2006, pp. 12 pp.

[60] M. Iravani, P. L. Dandeno, K. Nguyen, D. Zhu and D. Maratukulam, "Applications of static phase shifters in power systems," *Power Delivery, IEEE Transactions On,* vol. 9, pp. 1600-1608, 1994.

[61] K. Patil, J. Senthil, J. Jiang and R. Mathur, "Application of STATCOM for damping torsional oscillations in series compensated AC systems," *Energy Conversion, IEEE Transactions On,* vol. 13, pp. 237-243, 1998.

[62] E. V. Larsen, J. J. Sanchez-Gasca and J. H. Chow, "Concepts for design of FACTS controllers to damp power swings," *Power Systems, IEEE Transactions On,* vol. 10, pp. 948-956, 1995.

[63] M. Farsangi, Y. Song and K. Y. Lee, "Choice of FACTS device control inputs for damping interarea oscillations," *Power Systems, IEEE Transactions On,* vol. 19, pp. 1135-1143, 2004.

[64] H. Wang, "Selection of robust installing locations and feedback signals of FACTS-based stabilizers in multi-machine power systems," *Power Systems, IEEE Transactions On,* vol. 14, pp. 569-574, 1999.

[65] J. Machowski, P. Kacejko, Ł Nogal and M. Wancerz, "Power system stability enhancement by WAMS-based supplementary control of multi-terminal HVDC networks," *Control Eng. Pract.,* vol. 21, pp. 583-592, 2013.

[66] R. Eriksson, "Coordinated Control of Multiterminal DC Grid Power Injections for Improved Rotor-Angle Stability Based on Lyapunov Theory," .

[67] R. Eriksson, "On the centralized nonlinear control of HVDC systems using lyapunov theory," *IEEE Trans. Power Del.,* vol. 28, pp. 1156-1163, 2013.

[68] D. Simfukwe, B. Pal, R. Jabr and N. Martins, "Robust and low-order design of flexible ac transmission systems and power system stabilisers for oscillation damping," *Generation, Transmission & Distribution, IET,* vol. 6, pp. 445-452, 2012.

[69] X. Lei, E. N. Lerch and D. Povh, "Optimization and coordination of damping controls for improving system dynamic performance," *Power Systems, IEEE Transactions On,* vol. 16, pp. 473-480, 2001.

[70] L. Cai and I. Erlich, "Simultaneous coordinated tuning of PSS and FACTS damping controllers in large power systems," Power Systems, IEEE Transactions On, vol. 20, pp. 294-300, 2005.

[71] P. Pourbeik and M. J. Gibbard, "Simultaneous coordination of power system stabilizers and FACTS device stabilizers in a multimachine power system for enhancing dynamic performance," Power Systems, IEEE Transactions On, vol. 13, pp. 473-479, 1998.

[72] T. Nguyen and R. Gianto, "Optimisation-based control coordination of PSSs and FACTS devices for optimal oscillations damping in multi-machine power system," IET Generation, Transmission & Distribution, vol. 1, pp. 564-573, 2007.

[73] A. L. Do Bomfim, G. N. Taranto and D. M. Falcao, "Simultaneous tuning of power system damping controllers using genetic algorithms," Power Systems, IEEE Transactions On, vol. 15, pp. 163-169, 2000.

[74] R. A. Jabr, B. C. Pal and N. Martins, "A sequential conic programming approach for the coordinated and robust design of power system stabilizers," Power Systems, IEEE Transactions On, vol. 25, pp. 1627-1637, 2010.

[75] Y. Pipelzadeh, B. Chaudhuri and T. C. Green, "Stability improvement through HVDC upgrade in the australian equivalent system," in Universities Power Engineering Conference (UPEC), 2010 45th International, 2010, pp. 1-6.

[76] Y. Pipelzadeh, B. Chaudhuri and T. Green, "Wide-area power oscillation damping control through HVDC: A case study on australian equivalent system," in Power and Energy Society General Meeting, 2010 IEEE, 2010, pp. 1-7.

[77] M. Abido, "Optimal design of power-system stabilizers using particle swarm optimization," Energy Conversion, IEEE Transactions On, vol. 17, pp. 406-413, 2002.

[78] Y. Abdel-Magid and M. Abido, "Optimal multiobjective design of robust power system stabilizers using genetic algorithms," Power Systems, IEEE Transactions On, vol. 18, pp. 1125-1132, 2003.

[79] Y. Abdel-Magid, M. Abido, S. Al-Baiyat and A. Mantawy, "Simultaneous stabilization of multimachine power systems via genetic algorithms," *Power Systems, IEEE Transactions On,* vol. 14, pp. 1428-1439, 1999.

[80] R. A. Ramos, L. F. Alberto and N. G. Bretas, "A new methodology for the coordinated design of robust decentralized power system damping controllers," *Power Systems, IEEE Transactions On,* vol. 19, pp. 444-454, 2004.

[81] D. Trudnowski, J. Smith, T. Short and D. Pierre, "An application of Prony methods in PSS design for multimachine systems," *Power Systems, IEEE Transactions On,* vol. 6, pp. 118-126, 1991.

[82] S. P. Azad, R. Iravani and J. E. Tate, "Damping inter-area oscillations based on a model predictive control (MPC) HVDC supplementary controller," *Power Systems, IEEE Transactions On,* vol. 28, pp. 3174-3183, 2013.

[83] A. Fuchs, M. Imhof, T. Demiray and M. Morari, "Stabilization of Large Power Systems Using VSC–HVDC and Model Predictive Control," 2013.

[84] Y. Pipelzadeh, B. Chaudhuri and T. C. Green, "Control coordination within a VSC HVDC link for power oscillation damping: A robust decentralized approach using homotopy," *Control Systems Technology, IEEE Transactions On,* vol. 21, pp. 1270-1279, 2013.

[85] C. Karawita and U. D. Annakkage, "Multi-infeed HVDC interaction studies using small-signal stability assessment," Power Delivery, IEEE Transactions On, vol. 24, pp. 910-918, 2009.

[86] R. Pandey, "Stability analysis of AC/DC system with multirate discrete-time HVDC converter model," Power Delivery, IEEE Transactions On, vol. 23, pp. 311-318, 2008.

[87] C. Osauskas and A. Wood, "Small-signal dynamic modeling of HVDC systems," Power Delivery, IEEE Transactions On, vol. 18, pp. 220-225, 2003.

[88] D. Jovcic, N. Pahalawaththa and M. Zavahir, "Small signal analysis of HVDC-HVAC interactions," Power Delivery, IEEE Transactions On, vol. 14, pp. 525-530, 1999.

[89] S. Cole and R. Belmans, "A proposal for standard VSC HVDC dynamic models in power system stability studies," Electr. Power Syst. Res., vol. 81, pp. 967-973, 2011.

[90] V. Lukic, A. Prole and S. Gruber, "Perturbation approach to optimal connection of HVDC to AC power systems," International Journal of Electrical Power & Energy Systems, vol. 4, pp. 100-110, 1982.

[91] V. Lukic and A. Prole, "Optimal connection of controlled HVDC to AC power system," International Journal of Electrical Power & Energy Systems, vol. 6, pp. 150-160, 1984.

[92] H. S. Ramadan, H. Siguerdidjane, M. Petit and R. Kaczmarek, "Performance enhancement and robustness assessment of VSC–HVDC transmission systems controllers under uncertainties," International Journal of Electrical Power & Energy Systems, vol. 35, pp. 34-46, 2012.

[93] H. Weng and Z. Xu, "WAMS based robust HVDC control considering model imprecision for AC/DC power systems using sliding mode control," Electr. Power Syst. Res., vol. 95, pp. 38-46, 2013.

[94] L. Wang and M. Thi, "Stability analysis of four PMSG-based offshore wind farms fed to an SG-based power system through an LCC-HVDC link," IEEE Trans. Ind. Electron., pp. 2392-2400, 2013.

[95] L. Wang and M. N. Thi, "Stability enhancement of a PMSG-based offshore wind farm fed to a multi-machine system through an LCC-HVDC link," Power Systems, IEEE Transactions On, vol. 28, pp. 3327-3334, 2013.

[96] Z. Miao, L. Fan, D. Osborn and S. Yuvarajan, "Wind farms with HVDC delivery in inertial response and primary frequency control," Energy Conversion, IEEE Transactions On, vol. 25, pp. 1171-1178, 2010.

[97] R. L. Cresap and W. A. Mittelstadt, "Small-signal modulation of the Pacific HVDC intertie," Power Apparatus and Systems, IEEE Transactions On, vol. 95, pp. 536-541, 1976.

[98] R. Cresap, W. Mittelstadt, D. Scott and C. Taylor, "Operating experience with modulation of the Pacific HVDC Intertie," Power Apparatus and Systems, IEEE Transactions On, pp. 1053-1059, 1978.

[99] H. Peiris, U. Annakkage and N. Pahalawaththa, "Frequency regulation of rectifier side AC system of an HVDC scheme using coordinated fuzzy logic control," *Electr. Power Syst. Res.*, vol. 48, pp. 89-95, 1998.

[100] P. Dash, A. Liew and A. Routray, "Design of robust controllers for HVDC links in AC-DC power systems," *Electr. Power Syst. Res.*, vol. 33, pp. 201-209, 1995.

[101] H. Cai, Z. Qu and D. Gan, "A nonlinear robust HVDC control for a parallel AC/DC power system," *Comput. Electr. Eng.*, vol. 29, pp. 135-150, 2003.

[102] T. Smed and G. Andersson, "Utilizing HVDC to damp power oscillations," *Power Delivery, IEEE Transactions On,* vol. 8, pp. 620-627, 1993.

[103] G. Liu, Z. Xu, Y. Huang and W. Pan, "Analysis of inter-area oscillations in the South China interconnected power system," *Electr. Power Syst. Res.*, vol. 70, pp. 38-45, 2004.

[104] J. He, C. Lu, X. Wu, P. Li and J. Wu, "Design and experiment of wide area HVDC supplementary damping controller considering time delay in China southern power grid," *Generation, Transmission & Distribution, IET,* vol. 3, pp. 17-25, 2009.

[105] M. Xiao-Ming, Z. Yao, G. Lin and W. Xiao-Chen, "Coordinated control of interarea oscillation in the China Southern power grid," *Power Systems, IEEE Transactions On,* vol. 21, pp. 845-852, 2006.

[106] J. He, C. Lu, X. Wu, J. Wu and T. Bi, "Design and experiment of heuristic adaptive HVDC supplementary damping controller based on online prony analysis," in *Power Engineering Society General Meeting, 2007. IEEE,* 2007, pp. 1-7.

[107] H. F. Latorre, M. Ghandhari and L. Soder, "Use of local and remote information in POD control of a VSC-HVDC," in *PowerTech, 2009 IEEE Bucharest,* 2009, pp. 1-6.

[108] J. Zhu, C. D. Booth, G. P. Adam, A. J. Roscoe and C. G. Bright, "Inertia emulation control strategy for VSC-HVDC transmission systems," *Power Systems, IEEE Transactions On,* vol. 28, pp. 1277-1287, 2013.

[109] J. Hazra, Y. Phulpin and D. Ernst, "HVDC control strategies to improve transient stability in interconnected power systems," in *PowerTech, 2009 IEEE Bucharest*, 2009, pp. 1-6.

[110] Y. Liu and Z. Chen, "A Flexible Power Control Method of VSC-HVDC Link for the Enhancement of Effective Short-Circuit Ratio in a Hybrid Multi-Infeed HVDC System," *Power Systems, IEEE Transactions On*, vol. 28, pp. 1568-1581, 2013.

[111] R. Eriksson and L. Söder, "Coordinated control design of multiple HVDC links based on model identification," *Comput. Math. Appl.*, vol. 60, pp. 944-953, 2010.

[112] R. Eriksson and L. Söder, "On the coordinated control of multiple HVDC links using input–output exact linearization in large power systems," *International Journal of Electrical Power & Energy Systems*, vol. 43, pp. 118-125, 2012.

[113] D. Dotta and I. Decker, "Wide-area measurements-based two-level control design considering signal transmission delay," *Power Systems, IEEE Transactions On*, vol. 24, pp. 208-216, 2009.

[114] J. Ford, G. Ledwich and Z. Y. Dong, "Efficient and robust model predictive control for first swing transient stability of power systems using flexible AC transmission systems devices," *Generation, Transmission & Distribution, IET*, vol. 2, pp. 731-742, 2008.

[115] G. C. Zweigle and V. Venkatasubramanian, "Wide-area Optimal Control of Electric Power Systems with Application to Transient Stability for Higher Order Contingencies," *IEEE Trans. Power Syst.*, vol. 28, pp. 2313-2320, 2013.

[116] H. F. Latorre, M. Ghandhari and L. Söder, "Active and reactive power control of a VSC-HVdc," Electr. Power Syst. Res., vol. 78, pp. 1756-1763, 2008.

[117] Y. Li, C. Rehtanz, D. Yang, S. Rüberg and U. Häger, "Robust high-voltage direct current stabilising control using wide-area measurement and taking transmission time delay into consideration," IET Generation, Transmission & Distribution, vol. 5, pp. 289-297, 2011.

[118] W. Juanjuan, F. Chuang and Z. Yao, "Design of WAMS-based multiple HVDC damping control system," Smart Grid, IEEE Transactions On, vol. 2, pp. 363-374, 2011.

[119] J. Slootweg and W. Kling, "The impact of large scale wind power generation on power system oscillations," Electr. Power Syst. Res., vol. 67, pp. 9-20, 2003.

[120] J. Sanchez-Gasca, N. Miller and W. Price, "A modal analysis of a two-area system with significant wind power penetration," in Power Systems Conference and Exposition, 2004. IEEE PES, 2004, pp. 1148-1152.

[121] D. Gautam and V. Vittal, "Impact of DFIG based wind turbine generators on transient and small signal stability of power systems," in Power & Energy Society General Meeting, 2009. PES'09. IEEE, 2009, pp. 1-6.

[122] E. Hinrichsen and P. Nolan, "Dynamics and stability of wind turbine generators," Power Apparatus and Systems, IEEE Transactions On, pp. 2640-2648, 1982.

[123] S. Bu, W. Du, H. Wang, Z. Chen, L. Xiao and H. Li, "Probabilistic analysis of small-signal stability of large-scale power systems as affected by penetration of wind generation," Power Systems, IEEE Transactions On, vol. 27, pp. 762-770, 2012.

[124] R. C. Burchett and G. Heydt, "Probabilistic methods for power system dynamic stability studies," Power Apparatus and Systems, IEEE Transactions On, pp. 695-702, 1978.

[125] B. Borkowska, "Probabilistic load flow," IEEE Transactions on Power Apparatus and Systems, vol. 93, pp. 752-759, 1974.

[126] R. Allan, B. Borkowska and C. Grigg, "Probabilistic analysis of power flows," *Electrical Engineers, Proceedings of the Institution Of,* vol. 121, pp. 1551-1556, 1974.

[127] R. Allan and M. Al-Shakarchi, "Probabilistic ac load flow," in *Proceedings of the Institutio*n of Electrical Engineers, 1976, pp. 531-536.

[128] J. C. Helton and F. J. Davis, "Latin hypercube sampling and the propagation of uncertainty in analyses of complex systems," Reliab. Eng. Syst. Saf., vol. 81, pp. 23-69, 7, 2003.

[129] Z. Xu, Z. Dong and P. Zhang, "Probabilistic small signal analysis using monte carlo simulation," in Power Engineering Society General Meeting, 2005. IEEE, 2005, pp. 1658-1664.

[130] C. Wang, L. Shi, L. Yao, L. Wang, Y. Ni and M. Bazargan, "Modelling analysis in power system small signal stability considering uncertainty of wind generation," in Power and Energy Society General Meeting, 2010 IEEE, 2010, pp. 1-7.

[131] J. L. Rueda and D. G. Colomé, "Probabilistic performance indexes for small signal stability enhancement in weak wind-hydro-thermal power systems," IET Generation, Transmission & Distribution, vol. 3, pp. 733-747, 2009.

[132] J. L. Rueda, D. G. Colomé and I. Erlich, "Assessment and enhancement of small signal stability considering uncertainties," Power Systems, IEEE Transactions On, vol. 24, pp. 198-207, 2009.

[133] C. Pans, Z. Dong, P. Zhang and X. Yin, "Probabilistic analysis of power system small signal stability region," in Control and Automation, 2005. ICCA'05. International Conference On, 2005, pp. 503-509.

[134] F. B. Alhasawi and J. V. Milanović, "Correlation between uncertainties in system model parameters and distribution of critical electromechanical modes," in Power Generation, Transmission, Distribution and Energy Conversion (MedPower 2010), 7th Mediterranean Conference and Exhibition On, 2010, pp. 1-6.

[135] S. Bu, W. Du and H. Wang, "Investigation on Probabilistic Small-Signal Stability of Power Systems as Affected by Offshore Wind Generation," .

[136] N. R. Chaudhuri, R. Majumder, B. Chaudhuri, J. Pan and R. Nuqui, "Modeling and stability analysis of MTDC grids for offshore wind farms: A case study on the north sea benchmark system," in Power and Energy Society General Meeting, 2011 IEEE, 2011, pp. 1-7.

[137] M. G. Kendall, "The advanced theory of statistics." The Advanced Theory of Statistics., 1946.

[138] G. Sinden, "Characteristics of the UK wind resource: Long-term patterns and relationship to electricity demand," Energy Policy, vol. 35, pp. 112-127, 2007.

[139] A. Beluco, P. K. de Souza and A. Krenzinger, "A dimensionless index evaluating the time complementarity between solar and hydraulic energies," Renewable Energy, vol. 33, pp. 2157-2165, 2008.

[140] K. Wang, C. Chung, C. Tse and K. Tsang, "Improved probabilistic method for power system dynamic stability studies," in Generation, Transmission and Distribution, IEE Proceedings-, 2000, pp. 37-43.

[141] R. Preece, K. Huang and J. V. Milanovic, "Comparison of point estimate and cumulant techniques for efficient estimation of critical oscillatory modes," in PES General Meeting| Conference & Exposition, 2014 IEEE, 2014, pp. 1-5.

[142] S. Bu, W. Du and H. Wang, "Probabilistic analysis of small-signal rotor angle/voltage stability of large-scale AC/DC power systems as affected by grid-connected offshore wind generation," Power Systems, IEEE Transactions On, vol. 28, pp. 3712-3719, 2013.

[143] X. Xu, T. Lin and X. Zha, "Probabilistic analysis of small signal stability of microgrid using point estimate method," in Sustainable Power Generation and Supply, 2009. SUPERGEN'09. International Conference On, 2009, pp. 1-6.

[144] A. Alabduljabbar, J. Milanovic and E. Al-Eid, "Low discrepancy sequences based optimization algorithm for tuning PSSs," in Probabilistic Methods Applied to Power Systems, 2008. PMAPS'08. Proceedings of the 10th International Conference On, 2008, pp. 1-9.

[145] H. Yu, C. Chung, K. Wong, H. Lee and J. Zhang, "Probabilistic load flow evaluation with hybrid latin hypercube sampling and cholesky decomposition," *Power Systems, IEEE Transactions On*, vol. 24, pp. 661-667, 2009.

[146] "PSCAD", VersionV45, [Online]. Available at: https://hvdc.ca/pscad.

[147] K. Kaberere, K. Folly, M. Ntombela and A. Petroianu, "Comparative analysis and numerical validation of industrial-grade power system simulation tools: Application to small-signal stability," in Proceedings of the 15th Power Systems Computation Conference, 2005, pp. 32-33.

[148] H. Teng, C. Liu, M. Han, S. Ma and X. Guo, "IEEE9 buses system simulation and modeling in PSCAD," in Power and Energy Engineering Conference (APPEEC), 2010 Asia-Pacific, 2010, pp. 1-4.

[149] O. K. Mokoka and K. O. Awodele, "Reliability evaluation of distribution networks using NEPLAN & DIgSILENT power factory," in AFRICON, 2013, 2013, pp. 1-5.

[150] K. Kaberere, K. Folly and A. Petroianu, "Assessment of commercially available software tools for transient stability: Experience gained in an academic environment," in AFRICON, 2004. 7th AFRICON Conference in Africa, 2004, pp. 711-716.

[151] Chapter 3, "modelling of power system in PSCAD/EMTDC" [online], Available: Programhttp://archive.lib.cmu.ac.th/full/T/2009/enel0109tk_ch3.pdf .

[152] PowerFactory,Version14.0.522.[Online].Available at: www.digsilent.com.

[153] F. Gonzalez-Longatt and J. L. Rueda, "PowerFactory Applications for Power System Analysis". Springer, 2015.

[154] A. Gole and A. Daneshpooy, "Towards open systems: A PSCAD/EMTDC to MATLAB interface," in International Conference on Power System Transients, IPST, 1997, pp. 22-26.

[155] S. K. Kerahroudi, G. Taylor, F. Li and M. Bradley, "Initial development of a novel stability control system for the future GB transmission system operation," in Power Engineering Conference (UPEC), 2013 48th International Universities', 2013, pp. 1-6.

[156] Francisco M. Gonzalez-Longatt , José Luis Rueda, PowerFactory Applications for Power System Analysis. Springer, 2014.

[157] "IEEE Recommended Practice for Excitation System Models for Power System Stability Studies" IEEE Power Engineering Society, IEEE Std 421.5-2005 (Revision of IEEE Std 421.5-1992), 2006.

[158] G. Andersson, P. Donalek, R. Farmer, N. Hatziargyriou, I. Kamwa, P. Kundur, N. Martins, J. Paserba, P. Pourbeik and J. Sanchez-Gasca, "Causes of the 2003 major grid blackouts in North America and Europe, and recommended means to improve system dynamic performance," *Power Systems, IEEE Transactions On*, vol. 20, pp. 1922-1928, 2005.

[159] E. Ruiz, J. Morataya and J. Castillo, "Stability analysis for the electrical integration of ecuador, colombia and panama," in *Transmission & Distribution Conference and Exposition: Latin America, 2006. TDC'06. IEEE/PES*, 2006, pp. 1-7.

[160] S. Teeuwsen, I. Erlich and M. El-Sharkawi, "Small-signal stability assessment for large power systems using computational intelligence," in Power Engineering Society General Meeting, 2005. IEEE, 2005, pp. 2661-2668

[161] V. Vittal, "Consequence and impact of electric utility industry restructuring on transient stability and small-signal stability analysis," Proc IEEE, vol. 88, pp. 196-207, 2000.

[162] H. Yi, Y. Hou, S. Cheng, H. Zhou and G. Chen, "Power system probabilistic small signal stability analysis using two point estimation method," in Universities Power Engineering Conference, 2007. UPEC 2007. 42nd International, 2007, pp. 402-407.

[163] G. Rogers, "Power system structure and oscillations," Springer, 2000, pp. 101-119.

[164] R. SadikoviC, *Use of FACTS Devices for Power Flow Control and Damping of Oscillations in Power Systems,* 2006.

[165] G. Verghese and F. Schweppe, "Selective modal analysis with applications to electric power systems, Part I: Heuristic introduction," *Power Apparatus and Systems, IEEE Transactions On,* pp. 3117-3125, 1982.

[166] M. B. Beck, "Water quality modeling: a review of the analysis of uncertainty," Water Resour. Res., vol. 23, pp. 1393-1442, 1987.

[167] R. Preece, K. Huang and J. V. Milanovic, "Probabilistic Small-Disturbance Stability Assessment of Uncertain Power Systems Using Efficient Estimation Methods," Power Systems, IEEE Transactions On, vol. 29, pp. 2509-2517, 2014.

[168] G. Verbič and C. Canizares, "Probabilistic optimal power flow in electricity markets based on a two-point estimate method," Power Systems, IEEE Transactions On, vol. 21, pp. 1883-1893, 2006.

[169] A. Papoulis and S. U. Pillai, Probability, Random Variables, and Stochastic Processes. Tata McGraw-Hill Education, 2002.

[170] G. Tsourakis, B. Nomikos and C. Vournas, "Effect of wind parks with doubly fed asynchronous generators on small-signal stability," Electr. Power Syst. Res., vol. 79, pp. 190-200, 2009.

[171] H. Hong, "An efficient point estimate method for probabilistic analysis," Reliab. Eng. Syst. Saf., vol. 59, pp. 261-267, 1998.

[172] J. M. Morales and J. Perez-Ruiz, "Point estimate schemes to solve the probabilistic power flow," Power Systems, IEEE Transactions On, vol. 22, pp. 1594-1601, 2007.

[173] K. Li, "Point-estimate method for calculating statistical moments," J. Eng. Mech., vol. 118, pp. 1506-1511, 1992.

[174] J. M. Morales, L. Baringo, A. J. Conejo and R. Mínguez, "Probabilistic power flow with correlated wind sources," IET Generation, Transmission & Distribution, vol. 4, pp. 641-651, 2010.

[175] M. M. Alamuti, R. Rabbani, S. K. Kerahroudi and G. Taylor, "System stability improvement through HVDC supplementary model predictive control," in Power Engineering Conference (UPEC), 2014 49th International Universities, 2014, pp. 1-5.

[176] P. Zhang, D. Yang, K. W. Chan and G. Cai, "Adaptive wide-area damping control scheme with stochastic subspace identification and signal time delay compensation," IET Generation, Transmission & Distribution, vol. 6, pp. 844-852, 2012.

[177] R. Eriksson and L. Söder, "Wide-area measurement system-based subspace identification for obtaining linear models to centrally coordinate controllable devices," Power Delivery, IEEE Transactions On, vol. 26, pp. 988-997, 2011.

[178] Y. Pipelzadeh, N. R. Chaudhuri, B. Chaudhuri and T. C. Green, "System stability improvement through optimal control allocation in voltage source converter-based high-voltage direct current links," IET Generation, Transmission & Distribution, vol. 6, pp. 811-821, 2012.

[179] J. F. Hauer, W. A. Mittelstadt, K. E. Martin, J. W. Burns, H. Lee, J. W. Pierre and D. J. Trudnowski, "Use of the WECC WAMS in wide-area probing tests for validation of system performance and modeling," Power Systems, IEEE Transactions On, vol. 24, pp. 250-257, 2009.

[180] Pai. M. A. and Stankovic.A, "Robust Control in Power Systems", New York: Springer Inc., 2005.

[181] J. M. Maciejowski, "Multivariable feedback design," Electronic Systems Engineering Series, Wokingham, England: Addison-Wesley,| c1989, vol. 1, 1989.

[182] S. Skogestad, "Control structure design for complete chemical plants," *Comput. Chem. Eng.*, vol. 28, pp. 219-234, 2004.

[183] J. C. Doyle and G. Stein, "Robustness with Observers", MASSACHUSETTS INST OF TECH CAMBRIDGE DEPT OF ELECTRICAL ENGINEERING AND COMPUTER SCIENCE 1979.

[184] M. M. Alamuti, R. Rabbani, S. K. Kerahroudi, G. Taylor, Y. Liu and J. Liu, "A critical evaluation of the application of HVDC supplementary control for system stability improvement," in Power System Technology (POWERCON), 2014 International Conference On, 2014, pp. 1172-1177.

[185] R. Preece, N. C. Woolley and J. V. Milanovic, "The probabilistic collocation method for power-system damping and voltage collapse studies in the presence of uncertainties," Power Systems, IEEE Transactions On, vol. 28, pp. 2253-2262, 2013.

[186] Energy and Strategy Policy, National Grid. (July 2015). UK Future Energy Scenarios [Online]. Available: www.nationalgridconnecting.com.

[187] Mohsen M. Alamuti, Ronak Rabbani, Shadi Khaleghi, Ahmen F. Zobaa and Gareth A. Taylor “Probabilistic Evaluation of Power System Stability Enhancement

Using Supplementary Controller Schemes for an Embedded HVDC link “ Submitted on 28th August to *IEEE Transactions on Power System, 2015.*

Appendix A

The Generator, Transformer and Transmission Line Parameters of the Two-area Test System

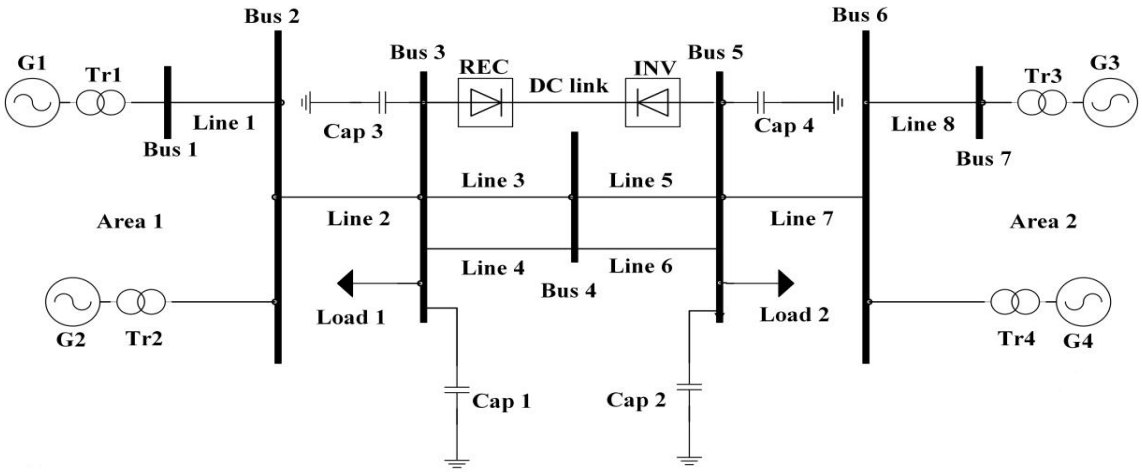

Figure A. 1 Schematic of the Two-area Four-machine System Connected with an HVDC Transmission Link.

A.1 Generators Parameter:

Table A. 1 Synchronous Machine Parameters of G1, G2 and G3 and G4 *

No. of Generator	1	2	3	4
Rotor type	Round Rotor	Round Rotor	Round Rotor	Round Rotor
Inertia time constant H (rated to Sgn)	6.5	6.5	6.5	6.5
Mechanical damping	0	0	0	0
Stator resistance r_a	0.0025	0.0025	0.0025	0.0025
Stator leakage reactance x_l	0.2	0.2	0.2	0.2
Synchronous reactance x_d d-axis	1.8	1.8	1.8	1.8
Synchronous reactance x_q q-axis	1.7	1.7	1.7	1.7
Transient reactance x_d' d-axis	0.3	0.3	0.3	0.3
Transient reactance x_q' q-axis	0.55	0.55	0.55	0.55
Sub-transient reactance x_d'' d-axis	0.25	0.25	0.25	0.25
Sub-transient reactance x_q'' q-axis	0.25	0.25	0.25	0.25
Transient time constant T_{d0}' d-axis	8	8	8	8
Transient time constant T_{q0}' q-axis	0.4	0.4	0.4	0.4
Sub-transient time constant T_{d0}'' d-axis	0.03	0.03	0.03	0.03
Sub-transient time constant T_{q0}'' q-axis	0.05	0.05	0.05	0.05

*P. Kundur, Power System Stability and Control. London: McGraw-Hill, Inc., 1994.

Table A. 2 Power Generation Conditions of G1, G2 and G3 and G4.

Gen	Bus type	Rated power (MVA)	Nominal voltage (L-L kV)	Active power output	Reactive power output	Terminal voltage (p.u.)
1	SL	900	20	750	185	1.03
2	PV	900	20	700	235	1.01
3	PV	900	20	719	176	1.03
4	PV	900	20	700	202	1.01

A.2 DC exciter

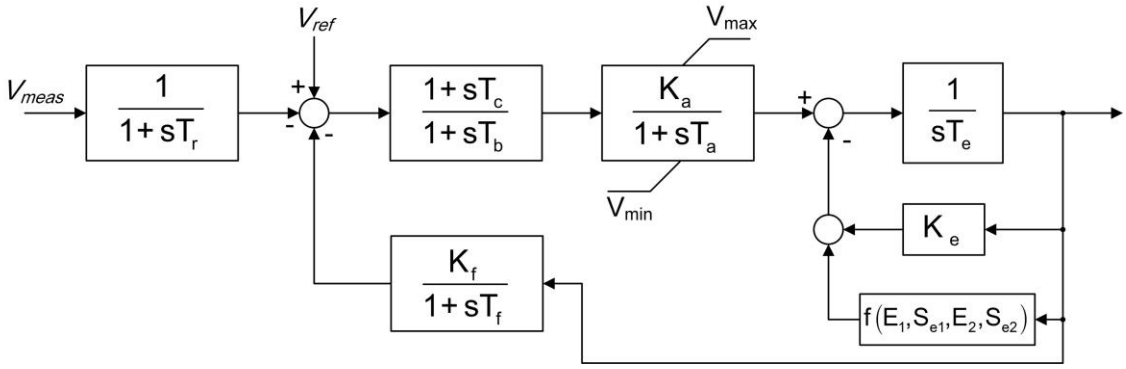

Figure A. 2 Block Diagram of DC Exciter of G1, G3 and G4

Table A. 3 Parameters of DC Exciter.

1	Transducer filter time constant T_r	0.02	second
2	Voltage regulator gain K_a	20	p.u.
3	Voltage regulator time constant T_a	0.005	second
4	Filter derivative time constant T_c	3.1	second
5	Filter delay time constant T_b	40	second
6	Exciter time constant T_e	0.05	second
7	Exciter constant K_e	0.5	p.u.
8	Stabilization path gain K_f	0.01	p.u.
9	Stabilization path time constant T_f	0.3	second
10	Saturation factor 1E1	3.9	p.u.
11	Saturation factor 2Se1	0.0001	p.u.
12	Saturation factor 3E2	5.2	p.u.
13	Saturation factor 4Se2	0.001	p.u.
14	Maximum voltage regulator output V_{max}	5	p.u.
15	Minimum voltage regulator output V_{min}	-5	p.u.

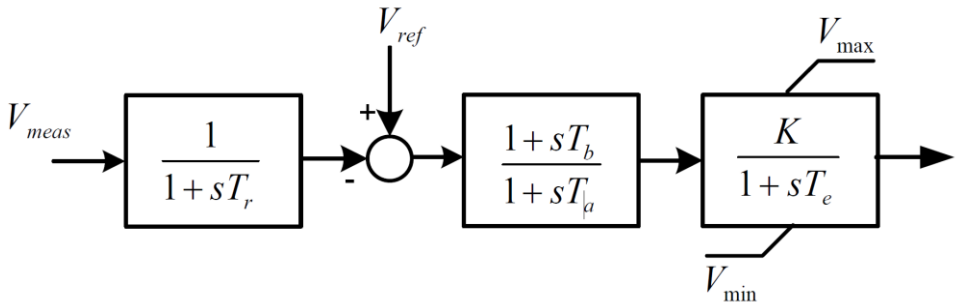

Figure A. 3 Block Diagram of Static Exciter of G2.

Table A. 4 Parameters of Static Exciter.

1	Transducer filter time constant T_r	0.01	second
2	Voltage regulator gain K	200	p.u.
3	Voltage regulator time constant T_e	0.05	second
4	Transient gain reduction time constant T_a	1	second
5	Transient gain reduction time constant T_b	10	second
6	Maximum voltage regulator output V_{max}	3	p.u.
7	Minimum voltage output V_{min}	-3	p.u.

A.3 Governor Parameter

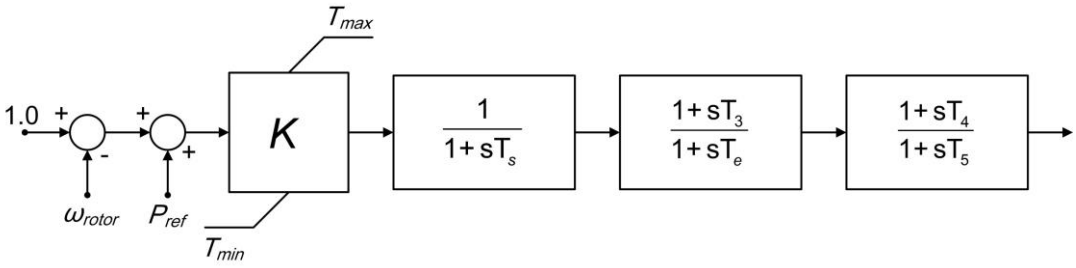

Figure A. 4 Block Diagram of Speed Governor of G1, G2, G3 and G4.

Table A. 5 Parameters of Speed Governor.

1	Governor gain K	50	p.u.
2	Servo time constant T_s	0.1	second
3	Transient gain time constant T_3	0	second
4	HP turbine time constant T_c	0.5	second
5	Time constant to set HP ratio T_4	1.25	second
6	Reheat time constant T_5	5	second
7	Maximum power P_{max}	1	p.u.
8	Minimum power P_{min}	0	p.u.

A.4 Transformer

Table A. 6 Transformer Parameters.

No. of Generator	1	2	3	4
Rated power (MVA)	900	900	900	900
Rated voltage (HV)	230	230	230	230
Rated voltage (LV)	20	20	20	20
Short circuit voltage (positive Sequence %)	15	15	15	15
Short circuit voltage (zero Sequence %)	3	3	3	3
Winding connection (HV)	YN	YN	YN	YN
Winding connection (LV)	YN	YN	YN	YN

A.5 Transmission line

Table A. 7 AC Transmission Line Parameters.

No. of line	1	2	3	4	5	6	7	8
Rated voltage (L-L kV)	230	230	230	230	230	230	230	230
Length (km)	25	10	110	110	110	110	10	25
Resistance (Ohm/km)	0.0529	0.0529	0.0529	0.0529	0.0529	0.0529	0.0529	0.0529
Reactance (Ohm/km)	0. 529	0. 529	0. 529	0. 529	0. 529	0. 529	0. 529	0. 529
Susceptance (μs/km)	3.3075	3.3075	3.3075	3.3075	3.3075	3.3075	3.3075	3.3075

Table A. 8 DC Transmission Line Parameters.

Dc transmission line 1	
Rated DC voltage (kV)	56
Rated current (kA)	3.6
Length (km)	200
Line type	Overhead line
Resistance (Ohm/km)	0.0075
Inductance (mH/km)	1

A.6 Rectifier control

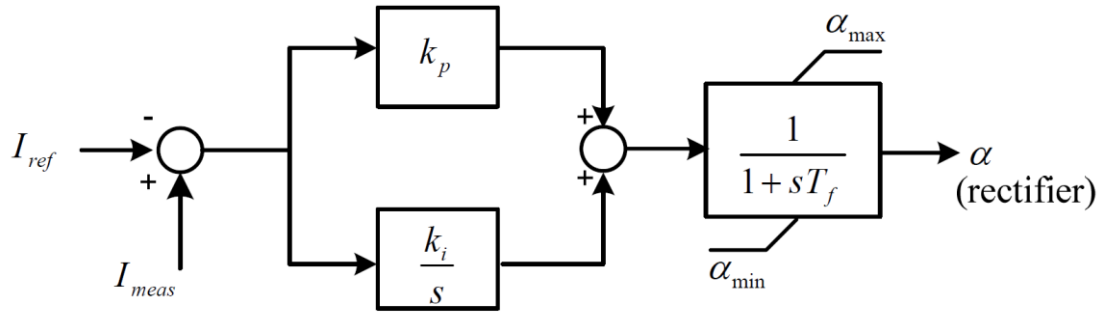

Figure A. 5 Rectifier's α Control for Constant Current.

Table A. 9 Parameters of Rectifier Control.

1	Current reference for current control	1.8	kA
2	Proportional gain K_p	0.001	p.u.
3	Output gain K_o	1.0	p.u.
4	Rectifier time constant T_f	0.001	Second
5	Integral gain K_i	0.01	p.u.
6	Minimum firing angle α_{min}	5	degree
	Maximum firing angle α_{max}	90	degree

A.7 Inverter control

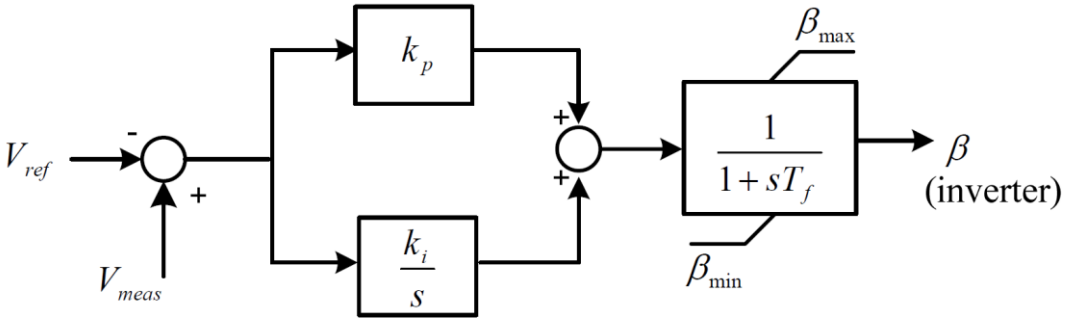

Figure A. 6 Inverter's β Control for Constant Voltage.

Table A. 10 Parameters of Inverter Control.

1	Voltage reference for voltage control	1.0	p.u.
2	Proportional gain K_p	0.001	p.u.
3	Output gain K_o	1	p.u.
4	Rectifier time constant T_f	0.001	Second
5	Integral gain K_i	0.01	p.u.
6	Minimum advance firing angle β_{min}	30	degree
7	Maximum advance firing angle β_{max}	90	degree

A.8 Load

Table A. 11 Load Data.

Load	Active power (MW)	Reactive power (MVar)
Load 1	967	100
Load 2	1667	100
The active load is modeled as 50% constant and 50% constant impedance. The reactive load is modeled as constant impedance.		

Table A. 12 Shunt Capacitors.

No. of Capacitor	Nominal voltage (kV)	Connected bus	Reactive power output (MVar)	Minimum output (MVar)	Maximum output (MVar)
1	230	3	189.88	100	600
2	230	5	341.61	50	500
3	230	Rectifier AC terminal	118.67	0	125
4	230	Rectifier AC terminal	122.00	0	125